The Substrate Binding Sites of Lignin Peroxidase and Manganese Peroxidase

Maarten D. Sollewijn Gelpke
B.S., Wageningen Agricultural University, 1993

A dissertation submitted to the faculty of the
OGI School of Science and Engineering
at Oregon Health & Science University
in partial fulfillment of the requirements
for the degree
Doctor of Philosophy
in
Biochemistry and Molecular Biology

March 2002

The dissertation "The Substrate Binding Sites of Lignin Peroxidase and Manganese Peroxidase" by Maarten D. Sollewijn Gelpke has been examined and approved by the following Examination Committee:

Michael H. Gold, Advisor
Professor

Thomas M. Loehr
Professor

V. Renganathan
Associate Professor

David R. Boone
Professor
Portland State University

ACKNOWLEDGEMENTS

I want to thank my advisor, Dr. Michael H. Gold, for the opportunity to obtain my doctoral degree at OGI, and for his guidance and support throughout the course of my research. I want to thank Drs. Thomas M. Loehr, V. Renganathan, and David R. Boone for sitting on my committee.

I also want to thank Heather, Frederick, Vijay, Mary, Biao, Dongmei, Jessica, Lakshmi, Sheng, Katsu, Ning, Suman, Barry, James, Jooyoung, Pauline, Joan and Geoff, who have all worked in the Gold lab during my stay and helped me to obtain my degree. Thanks to Nancy Christie and Terrie Hadfield for their assistance.

Special thanks to Heleen and my family.

TABLE OF CONTENTS

LIST OF TABLES

LIST OF FIGURES

Abstract

The Substrate Binding Sites of
Lignin Peroxidase and Manganese Peroxidase
Maarten D. Sollewijn Gelpke, B.S.

Ph.D., OGI School of Science and Engineering
March 2002
Thesis Advisor: Michael H. Gold

The lignin-degrading fungus, *Phanerochaete chrysosporium*, secretes two families of extracellular peroxidases, lignin peroxidase (LiP) and manganese peroxidase (MnP), which are major enzymatic components of its extracellular lignin degradation system.

The role of amino acid Arg177 in the binding and oxidation of Mn^{II} by MnP was investigated by constructing several site-directed mutant enzymes. These variant proteins were analyzed by UV-vis and resonance Raman spectroscopy, and steady-state and transient-state kinetics. Altered kinetic characteristics strongly suggest that Arg177 is important in Mn^{II} oxidation, orienting the Mn^{II} ligand Glu35 for efficient Mn^{II} binding.

A homologous expression system was developed for LiP in order to study structure-function relationships in this enzyme via site-directed mutagenesis. The expression vector contained the *Schizophyllum commune ura1* gene as a selectable marker and the coding regions of the *lipH8* or *lipH2* genes, which were placed under the control of the glyceraldehyde-3-phosphate dehydrogenase gene (*gpd*) promoter. Transformants of *P. chrysosporium* were selected for the production of extracellular, active recombinant LiP enzymes. Spectral and kinetic properties of the recombinant

enzymes are essentially identical to the respective LiPH8 and LiPH2 wild-type enzymes.

Recombinant LiPH2 was used, together with wild-type LiPH2 and LiPH8, to investigate claims that LiP is able to oxidize Mn^{II}. Spectral and kinetic analysis of purified enzyme preparations reveal that LiP is unable to use Mn^{II} as a productive substrate.

Mutant LiPH8 enzymes were produced to investigate the site for veratryl alcohol (VA) oxidation in LiP. Analysis of the site-directed mutations, H82A and Q222A, suggests that the heme access channel is an unlikely VA binding site in LiP. Analysis of the W171A and F267L mutant enzymes demonstrated that Trp171 is essential for VA oxidation and indicated that F267 affects VA binding, confirming that the Trp171 site is the productive site for VA oxidation.

CHAPTER 1
INTRODUCTION

1.1 Lignin as a Substrate for Fungi

1.1.1 Lignin

All the cells of plants have primary cell walls containing cellulose. As the plant grows, the cell walls become thickened by secondary deposits of cellulose, hemicellulose, and lignin, called lignocellulose. Lignocellulose is rich in carbon, with a carbon:nitrogen ratio of up to 500:1, but is poor in most other essential nutrients [Eriksson et al., 1990; Carlile and Watkinson, 1994]. Lignin is the second most abundant carbon source on earth, after cellulose, and it is the most abundant renewable aromatic resource on earth [Crawford, 1981]. It comprises 15–36% of the total lignocellulosic material in wood, and it provides strength to the cell wall. Lignin is a complex, heterogeneous, and random phenylpropanoid polymer which comprises three kinds of aromatic alcohols: *p*-coumaryl alcohol, and its methoxylated derivatives, coniferyl alcohol, and sinapyl alcohol (Fig. 1.1).

These substructures are commonly called *p*-coumaryl, guaiacyl, and syringyl nuclei, respectively. The proportions of these nuclei are different between plants. A typical softwood (gymnosperm) lignin contains mainly coniferyl alcohol, some *p*-coumaryl alcohol, but no sinapyl alcohol. Hardwood (angiosperm) contains guaiacyl-syringyl lignin, which is derived from approximately equal amounts of coniferyl and sinapyl alcohols. Grass and bamboo lignins are composed of all three alcohols [Eriksson et al., 1990]. Free-radical condensation of these alcohols, initiated by plant cell wall peroxidases or laccases [Harkin and Obst, 1973], results in the formation of a heterogeneous, amorphous, optically inactive, random, highly branched, three-dimensional polymer (Fig. 1.1), joined by many different bonds. The major

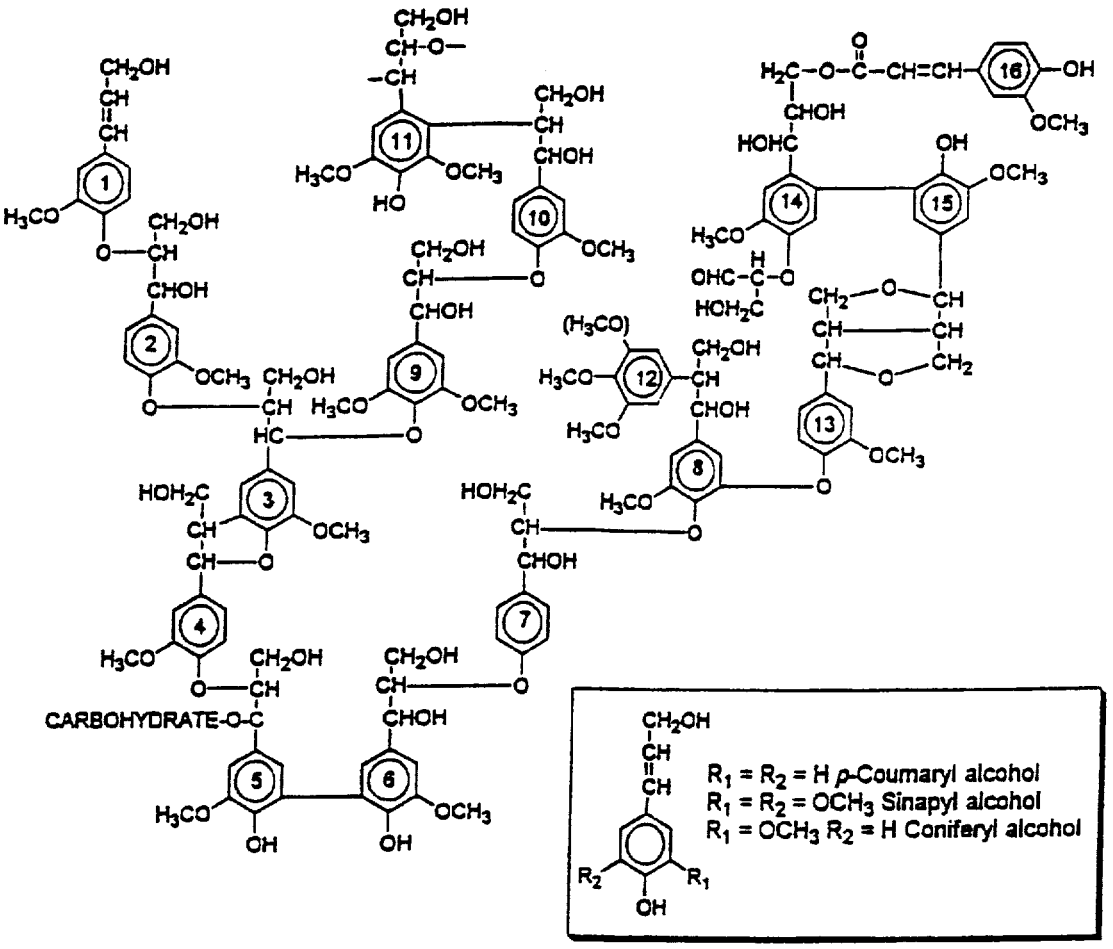

Fig. 1.1 Schematic structure of spruce lignin [Adler, 1977]. The inset shows the three lignin precursor alcohols.

functional groups in lignin consist of phenolic hydroxyl, benzylic hydroxyl, and carbonyl groups.

1.1.2 Lignin-Degrading Fungi

Wood-rotting fungi are the major class of microorganisms responsible for wood decay. They are capable of decomposing the three major structural components of wood: cellulose, hemicellulose, and lignin [Kirk and Farrell, 1987]. Wood-rotting fungi have been classified in three categories: soft-rot, white-rot, and brown-rot [Kirk and Cowling, 1984; Blanchette, 1991].

The brown-rot fungi are predominantly Basidiomycetes and usually decompose cellulose and hemicellulose, but do not degrade lignin. The effect of brown-rot is that the wood loses it strength and shrinks, developing cracks, breaking the wood into dark brown cubical crumbs. The brown-rotted lignin has a decreased methoxy content [Kirk and Adler, 1970; Kirk, 1975] and has a significant amount of introduced phenolic hydroxyl groups [Kirk, 1975; Crawford, 1981; Jin et al., 1990]. The dark brown color is due to the formation of additional quinones and conjugated carbonyl groups in the modified lignin [Kirk, 1975]. It appears that cellulose is degraded away from the hypae by cellulase enzymes, which are released from the hypae and diffuse freely into the wood. Loss of extracellular enzymes is possibly reduced by the existence of a polysaccharide-containing sheath around the growing hypae [Beguin, 1990].

Soft-rot fungi attack moist wood, degrading cellulose in the surface layers of wood which come in contact with the soil, resulting in the softening of the surface of the wood [Blanchette, 1991]. Most of the soft-rot fungi are Ascomycetes and Deuteromycetes. Common soft-rot fungi, which include species of *Chaetomium* and *Fusarium* are common fungi in soil, and are not true wood-inhabiting fungi [Carlile and Watkinson, 1994]. Soft-rot fungi are able to mineralize lignin-related phenolic compounds [Ander and Eriksson, 1984; Ander et al., 1988]. However, due to the difficulties in growing these fungi in the laboratory, little is known about the enzymes which are involved in the degradation of wood by these species.

Almost all white-rot fungi belong to the class of Basidiomycetes, and they are more numerous than brown-rot fungi. More than 1500 strains of white-rot fungi have been identified so far. Most white-rot fungi degrade both the lignin and cellulose of wood. However, some strains remove lignin selectively leaving the cellulose. When decaying wood, white-rot fungi grow many hyphae, eroding channels in the woody cell walls. Scanning electron microscopy reveals degradation of the lignified layers in wood. White-rot fungi are the most efficient ligninolytic microorganisms and are commonly found on the hardwood of angiosperms.

1.1.3 Biodegradation of Lignin by White-Rot Fungi

White-rot Basidiomycetes are primarily responsible for the initiation of lignin decomposition in wood [Crawford, 1981; Buswell and Odier, 1987; Kirk and Farrell, 1987; Gold et al., 1989]. The study of lignin biodegradation in white-rot fungi was initiated following the elucidation of the lignin structure in the 1960s. The biodegradation of lignin promised possible applications in pulping, bleaching, conversion of straw into animal feed, and lignin conversion into other products. Lignin degradation products provided evidence that the initial attack on this substrate is oxidative. White-rotted lignin contains decreased amounts of methoxy groups, an increase in carbonyl and carboxy groups, and a generally higher oxygen content than lignin from sound wood. Product analysis of released fragments indicates that lignin degradation mainly occurs through C_α–C_β cleavage of the propyl side chains and through aryl-ether cleavage followed by modification of side chains and aromatic ring fission [Kirk and Chang, 1974, 1975; Chen and Chang, 1982; Higuchi, 1990]. However, detailed studies of lignin degradation are hampered by the complex and heterogeneous structure of lignin. Therefore, various lignin model compounds have been used to investigate the mechanisms of lignin degradation.

The white-rot fungus, *Phanerochaete chrysosporium*, has served as a model organism for the biodegradation of lignin. Much of the knowledge about the biochemistry and molecular biology of lignin degradation has been obtained from studies with *P. chrysosporium*. Advantages of using this fungus as a model organism are that it can degrade both lignin and cellulose efficiently, it is thermotolerant, it can

be grown easily in the laboratory, and it produces sexual basidiospores and asexual conidia spores, which are essential for genetic manipulations [Burdsall and Eslyn, 1974; Gold and Cheng, 1978]. The ligninolytic activity of *P. chrysosporium* is triggered by the onset of secondary metabolic growth (idiophase) when nutrient carbon, sulfur, or nitrogen is depleted and the primary growth of the organism is halted. It is unusual for a mechanism that degrades a carbon substrate, like lignin, to be sensitive to control by nitrogen compounds. When addressed in the physiological context, nitrogen or carbon starvation triggers ligninolysis, and removal of a lignin layer possibly exposes fresh cellulose and nitrogen sources which will be used up before the ligninolytic mechanism is activated again.

1.2 Enzymes Involved in Lignin Degradation by White-Rot Fungi

To use lignin as a carbon source, white-rot fungi must degrade this random aromatic polymer into smaller units which can be taken up by the cell prior to mineralization to CO_2 and H_2O. Enzymes involved in lignin depolymerization are extracellular, relatively nonspecific, and oxidative. Extracellular phenol oxidation activity was observed in cultures of white-rot fungi in the 1920s. Two distinct types of enzymes have been considered as extracellular phenol oxidases: laccases and peroxidases [Ander and Eriksson, 1976].

The extracellular phenol oxidase, laccase (benzenediol:oxygen oxidoreductase, EC 1.10.3.2), is a copper-containing enzyme from the family of blue copper oxidases and is produced by nearly all white-rot fungi (Table 1.1). Fungal laccases are glycoproteins with 11–25% carbohydrate content and display a broad specificity for the reducing substrate, catalyzing the oxidation of a wide variety of aromatic, notably phenolic, and inorganic substrates [Xu, 1996]. Laccases are enzymes that catalyze the oxidation of phenolic compounds by abstracting one electron and one proton from phenolic hydroxyl groups to generate phenoxy radicals. Laccases use oxygen as the electron acceptor, which is ultimately reduced to water.

Two families of heme peroxidases, lignin peroxidase and manganese peroxidase, have been purified from *P. chrysosporium* and many other white-rot fungi

Table 1.1

The Production of Extracellular Oxidative Enzymes
by White-Rot Basidiomycetous Fungi*

Fungus	LiP	MnP	Lac	Glox	AAO
Armillaria mellea	-	+	+		
Armillaria ostoyae	-	+	+		
Bjerkandera adusta	+	+	+/-	+	+
Bjerkandera sp. BOS55	+	+	+/-	+	+
Ceriporiopsis subvermispora	-	+	+	-	
Coriolopsis occidentalis	+	+			
Daedaleopsis confragosa	-	+	+	-	-
Dichomitus squalens	-	+	+		-
Ganoderma australis		+			
Inonotus weirii	-	-			
Junghuhnia seperabilima	+		+		
Lentinula edodes	+/-	+	+		
Merulius (Phlebia) tremellosus	+/-	+	+		
Panus tigrinus	-	+	+		
Phanerochaete chrysosporium	+	+	-	+	-
Phanerochaete flavido alba	+	+			
Phanerochaete magnolia	+	+			
Phlebia brevispora	+	+	+	+	
Phlebia ochraceofulva	+	-	+		
Phlebia radiata	+	+	+	+	
Phlebia subserialis	-	+			
Phellinus igniarius	-	-	+		
Phellinus pini	+	+			
Pleurotus ostreatus	-	+	+		+

Table 1.1 (continued)

Fungus	LiP	MnP	Lac	Glox	AAO
Pleurotus sajor-caju	-	+	+		+
Pycoporus cinnabarinus	-	-	+		
Stereum hirsutum	-	+	+		
Trametes gibbosa	+	+	+		
Trametes hirsuta	+	+	+		
Trametes versicolor	+	+	+	+	+
Trametes villosa	-	+	+	+	-

* de Jong et al. [1994]; Hatakka, [1994]

LiP, lignin peroxidase; MnP, manganese peroxidase; Lac, laccase; Glox, glyoxal oxidase; AAO, aryl alcohol oxidase; +, enzyme produced; -, enzyme not produced.

(Table 1.1). These peroxidases and peroxide-generating enzymes are thought to be the major extracellular components of the lignin degrading system of these fungi. The extracellular lignin-degrading enzymes produced by some white-rot fungi are summarized in Table 1.1. Lignin peroxidase (LiP, EC 1.11.1.14) from *P. chrysosporium* was discovered as a hydrogen peroxide-requiring enzyme involved in lignin degradation [Glenn et al., 1983; Tien and Kirk, 1983; Gold et al., 1984]. Later, a second hydrogen peroxide-requiring enzyme involved in lignin degradation, manganese peroxidase (MnP, EC 1.11.1.13), was discovered and purified [Kuwahara et al., 1984; Glenn and Gold, 1985]. Each enzyme exists as a series of isozymes, which are encoded by multiple related genes [Kirk and Farrell, 1987; Leisola et al., 1987; Stewart et al., 1992; Gold and Alic, 1993; Cullen, 1997]. MnP is found in almost all white-rot fungi known to degrade lignin; however, LiP is only found in certain lignin-degrading white-rot fungi (Table 1.1) [Orth et al., 1993; de Jong et al., 1994; Hatakka, 1994]. The major isozymes of LiP and MnP have been isolated and purified from the extracellular medium of *P. chrysosporium* and have been characterized extensively [Gold and Alic, 1993; Cullen, 1997; Gold et al., 2000]. The properties of MnP and LiP are discussed in more detail in Sections 1.5 and 1.6, respectively.

White-rot fungi produce multiple intracellular and extracellular H_2O_2-generating oxidases which have been proposed as a source of H_2O_2 for peroxidase reactions. Of these enzymes, glyoxal oxidase (Glox) is the only oxidase secreted under standard ligninolytic conditions [Kersten and Kirk, 1987; Kirk and Farrell, 1987]. Glox is produced by several white-rot fungi [Orth et al., 1993], and two isozyme forms have been detected in *P. chrysosporium*. Substrates for Glox include glyoxal, methylglyoxal, and several other α-hydroxycarbonyl and dicarbonyl compounds. Both glyoxal and methylglyoxal have been identified in the extracellular medium of *P. chrysosporium* under ligninolytic conditions [Kirk and Farrell, 1987].

1.3 Recombinant Expression of Peroxidases

The recombinant expression of proteins is the production of a specific protein outside its wild-type expression context. In essence, a gene encoding the protein of interest is isolated, placed under the control of an expression promoter, and is transformed into a host organism. Growing the transformed host organism under promoter induction conditions results in the production of the recombinant protein. A widespread use for recombinant enzyme expression in fundamental research is the production of modified or mutated enzymes to study enzyme functions and mechanisms. Along with crystallographic and spectroscopic studies, site-directed mutagenesis is a powerful tool for understanding the roles and functions of potentially important amino acids of an enzyme. Multiple expression systems have been reported for the production of recombinant peroxidases, including lignin peroxidase and manganese peroxidase (LiP and MnP) from *P. chrysosporium*, horseradish peroxidase (HRP), *Coprinus cinereus* peroxidase (CiP), and cytochrome *c* peroxidase (CcP) from yeast.

1.3.1 Recombinant Expression of Heme Peroxidases in *Escherichia coli*

The recombinant expression of peroxidases in *E. coli* has several advantages but also has serious disadvantages. *E. coli* is a very well-studied prokaryote, and molecular biology and fermentation methods for this host organism are well established. However, *E. coli* does not possess the protein excretion pathways which exist in eukaryotes and which are essential for the correct folding and post-translational processing of many extracellular enzymes, including plant and fungal peroxidases.

To date, CcP from yeast has been the peroxidase which is best suited for site-directed mutagenesis studies. CcP is an intracellular peroxidase which does not require formation of disulfide bridges, glycosylation, or other post-translational processing to obtain active enzyme. In *E. coli*, CcP is produced as the apoenzyme, completely folded but lacking the heme cofactor; however, the CcP holoprotein can easily be reconstituted [Fishel et al., 1987]. The crystal structures and spectral

properties of recombinant and wild-type CcP enzymes are indistinguishable [Wang et al., 1990], demonstrating that the expression of CcP in *E. coli* and reconstitution of the recombinant holoenzyme is an excellent system to use for conducting site-directed mutagenesis studies on CcP.

The recombinant expression of other peroxidases in *E. coli* presents serious problems. Active, wild-type plant and fungal peroxidases all have several disulfide bonds, are glycosylated, contain metal ions, and have a heme cofactor [Poulos et al., 1993; Sundaramoorthy et al., 1994; Limongi et al., 1995; Schuller et al., 1996; Gajhede et al., 1997]. As mentioned, *E. coli* is unable to introduce these structural characteristics into these peroxidase apoproteins, leading to the formation of intracellular insoluble inclusion bodies in which the excess, unfolded peroxidase polypeptides are deposited. The inclusion bodies can easily be isolated from *E. coli* but require complete denaturation, followed by enzyme reconstitution to obtain active recombinant enzyme.

Smith et al. [1990] were the first to report the production of an active recombinant plant or fungal peroxidase from the *E. coli* expression system. Recombinant HRP isozyme C was reconstituted from inclusion bodies by denaturing the apoprotein in urea, followed by refolding in the presence of Ca^{II}, heme, and oxidized glutathione [Smith et al., 1990]. However, the yield of active HRP C isolated from *E. coli* is only 3−4% of the inclusion body material [Smith et al., 1990]. It was demonstrated that Ca^{II} is essential for the folding of HRP C [Smith et al., 1990], and it was shown recently that HRP contains two Ca^{II} ions with important structural roles [Gajhede et al., 1997].

Similar strategies have been used to express LiP [Doyle and Smith, 1996] and MnP [Whitwam et al., 1995; Whitwam and Tien, 1996] in *E. coli* with yields of $<1\%$ conversion of inclusion body protein to active enzyme. The integrity of the heme binding site in recombinant LiP was confirmed using one- and two-dimensional ^1H NMR spectroscopy [Doyle et al., 1998]. However, neither detailed spectroscopic nor crystallographic studies of recombinant MnP have been reported to demonstrate that reconstituted wild-type or mutant recombinant MnP from the *E. coli* expression system is correctly folded. Kinetic analysis of both recombinant LiP and MnP

suggested that the various kinetic parameters for substrate oxidation by the recombinant enzymes were similar to those of the respective enzymes from natural sources [Whitwam and Tien, 1996]. The *E. coli* expression system has been used to produce and study several site-directed mutant lignin peroxidases [Ambert-Balay et al., 1998; Doyle et al., 1998] and manganese peroxidases [Whitwam et al., 1997; Timofeevski et al., 1999, 2000].

1.3.2 Fungal Expression Systems for Heme Peroxidases

The recombinant expression of heme peroxidases in fungal systems also has advantages and disadvantages. Expression of enzymes which require extensive post-translational processing, contain enzyme cofactors, or appear difficult to fold into the active conformation is more likely to succeed in eukaryotes than prokaryotes. On the other hand, fungal expression systems are not as well characterized as the *E. coli* system.

1.3.2.1 Homologous Expression in **P. chrysosporium.** A different approach to obtaining recombinant enzyme is the expression of the enzyme in its natural host, homologous expression. Essential for the production and isolation of recombinant enzyme by homologous expression is the ability to express and produce the recombinant enzyme separate from the wild-type enzyme. The wild-type lignin peroxidases and manganese peroxidases are expressed in *P. chrysosporium* only during secondary (idiophasic) growth, which is triggered by nutrient nitrogen depletion [Kirk and Farrell, 1987; Gold and Alic, 1993]. Placing the peroxidase gene under the control of a primary metabolic promoter results in the expression of the recombinant protein during primary metabolic growth in the presence of high nitrogen levels [Mayfield et al., 1994b]. For the homologous expression of recombinant MnP, the expression construct contained the primary metabolic promoter of the glyceraldehyde-3-phosphate dehydrogenase (*gpd*) gene, fused to the coding region of the *mnp* gene. The expression construct, which also contains the *ade5* marker gene, was used to transform protoplasts of the adenine auxotrophic *P. chrysosporium* (Ade^-) strain to prototrophy. Subsequent screening of transformants and basidiospore

purification resulted in the isolation of the *P. chrysosporium* recombinant MnP (rMnP) expression strain, which is able to produce rMnP in the extracellular medium under nitrogen-sufficient conditions [Mayfield et al., 1994b]. This expression system yields sufficient enzyme (1−3 mg of enzyme per liter of culture) for biochemical and spectroscopic studies, which show that the produced rMnP is very similar to wild-type MnP, suggesting proper folding, heme insertion, and essentially identical post-translational modification [Mayfield et al., 1994b; Sundaramoorthy et al., 1997]. This expression system has been used for several site-directed mutagenesis studies designed to elucidate the role of specific amino acids in the catalytic mechanism of MnP [Kusters-van Someren et al., 1995; Kishi et al., 1996, 1997].

1.3.2.2 Heterologous Expression in Fungi. CiP has been expressed in *Aspergillus oryzae* very successfully [Petersen et al., 1993, 1994]. Recombinant CiP (rCiP), expressed in the *Aspergillus* system, is identical to the wild-type CiP in all respects, including sites of glycosylation and N-terminal processing [Kjalke et al., 1992; Baunsgaard et al., 1993; Petersen et al., 1994; Limongi et al., 1995]. Several site-directed mutagenesis studies have been performed using the *A. oryzae* expression system [Veitch et al., 1994; Smulevich et al., 1996; Neri et al., 1998, 1999]. Recently it was reported that recombinant wild-type and mutant CiPs were expressed in *Saccharomyces cerevisiae,* yielding active enzymes [Cherry et al., 1999]. Newly developed techniques for directed evolution of the enzyme towards more thermal and oxidative stability and a higher pH optimum were performed. Site-directed and random mutagenesis of the CiP cDNA followed by the *in vivo* shuffling of point mutations from a large number of selected transformants resulted in the isolation of recombinant mutant CiP in which thermal stability increased by 174-fold and the oxidative stability increased by 100-fold relative to wild-type CiP [Cherry et al., 1999].

The expression of rMnP in *A. oryzae* was not as successful as that of CiP. Active, glycosylated enzyme was produced in yields comparable to that of the homologous expression system. However, the addition of heme to the cultures was required to obtain active enzyme, which may lead to adventitiously bound heme.

Furthermore, the only rMnP produced in the *Aspergillus* system to date has Mn^{II} oxidation kinetics which are significantly lower than for the wild-type enzyme [Stewart et al., 1996].

1.4 Plant and Fungal Heme Peroxidases

1.4.1 Classification of Heme Peroxidases

The heme peroxidases can be divided into two relatively well-defined superfamilies and a third indistinct family that includes chloroperoxidase and the di-heme cytochrome *c* peroxidases. The plant peroxidase superfamily contains peroxidases from plants, fungi, and bacteria [Welinder, 1992]. The second superfamily includes mammalian peroxidases such as lactoperoxidase, myeloperoxidase, and prostaglandin H synthase which have important functional and structural differences that were reviewed previously [English and Tsaprailis, 1995] but are not discussed here.

The plant peroxidase superfamily has been divided into three classes on the basis of amino acid sequence comparison data, which was confirmed by more recent crystal structure data [Welinder, 1992]. Yeast cytochrome *c* peroxidase (CcP) is a useful model for the classification of all plant peroxidases [Welinder, 1992]. CcP has a structure of 10 α-helices which are connected by random coil amino acid chains. These α-helical structures are conserved within the plant peroxidase superfamily, but the connecting chains are not. Class I includes peroxidases such as CcP, chloroplast and cytosol ascorbate peroxidases (APXs), and gene-duplicated bacterial catalase-peroxidases. Class II is composed of the fungal peroxidases, including LiP and MnP from white-rot fungi like *P. chrysosporium*, and *C. cinereus* peroxidase (CiP). Class III includes plant peroxidases, such as horseradish peroxidase (HRP), peanut peroxidase, and turnip peroxidase.

An important function of the various peroxidases is to oxidize substrate molecules at the expense of H_2O_2. The substrates for peroxidases range from compounds with low molecular mass, such as phenolic and non-phenolic compounds and halide ions, to compounds with a molecular mass >10 kDa, such as

ferrocytochrome *c* and lignin. Peroxidases in plants are thought to contribute to biological pathways of cell wall synthesis, metabolism of plant hormones, such as indole-3-acetic acid, stress responses, and fatty acid metabolism [Grisebach, 1981; Higuchi, 1989].

1.4.2 The Heme Peroxidase Catalytic Cycle

The active site for plant and fungal peroxidases is the heme prosthetic group, which is ferriprotoporphyrin IX in nearly all heme peroxidases. The heme is attached to the apoprotein by an amino acid side chain which is coordinated to the fifth coordination position of the heme iron. The propionate side chains of the heme form hydrogen bonds with protein residues, and weak hydrophobic forces complete the binding of the heme to the protein. The native state of these peroxidases contains a heme iron in the 3+ oxidation state (Fe^{III}), as determined by several spectroscopic studies [Spiro et al., 1979; Kobayashi et al., 1980; La Mar et al., 1988].

The catalytic cycle of most plant and fungal peroxidases are similar and involve the two-electron oxidation of the enzyme by hydrogen peroxide, followed by two one-electron reductions of the oxidized intermediates by the reducing substrate, thus completing the cycle (Scheme 1). This reaction mechanism is described as a modified or peroxidase bi-bi ping-pong mechanism [Dunford, 1982].

SCHEME 1:

Native enzyme + H_2O_2 → Compound I + H_2O

Compound I + substrate → Compound II + oxidized substrate

Compound II + substrate → Native enzyme + oxidized substrate + H_2O

Chemical studies have shown that the compound I oxidized intermediate contains two oxidizing equivalents over the native state of the enzyme. Therefore, the heme iron of compound I has a formal oxidation state of +5. Compound II is formed by the one-electron reduction of compound I by a reducing substrate. Thus, the heme iron of compound II has a formal oxidation state of +4. A variety of spectroscopic studies, including Mössbauer [Schultz et al., 1984], NMR [La Mar et al., 1983], X-

ray absorption [Chance et al., 1984], ENDOR [Roberts et al., 1981a], and resonance Raman spectroscopy [Sitter et al., 1985; Hashimoto et al., 1986] demonstrated that the heme peroxidases have a common compound II structure in which the single oxidizing equivalent is stored as an oxoferryl ($Fe^{IV}=O$) species. However, the same oxoferryl species is known to be present in the compound I state, which has one oxidizing equivalent over compound II [Chance et al., 1984; Schultz et al., 1984; Penner-Hahn et al., 1986; Edwards et al., 1987]. Therefore, the extra oxidizing equivalent must be located at a position other than the heme iron. Using EPR studies on a model compound, it was demonstrated that in HRP the second oxidizing equivalent in compound I occurs as a porphyrin-π-cation radical [Dolphin et al., 1971]. Presence of the porphyrin-π-cation radical was confirmed by NMR [La Mar et al., 1981], ENDOR [Roberts et al., 1981b] and resonance Raman spectroscopy [Felton et al., 1976]. The HRP compound I structure and, as was shown later, the compound I structures of almost all plant and fungal peroxidases can be described as $Fe^{IV}=O$, $P^{+\bullet}$, or oxoferryl porphyrin-π-cation radical. A remarkable exception with respect to the location of the second oxidizing equivalent of the two-electron oxidized enzyme intermediate is CcP, where the second oxidizing equivalent is located on the Trp191 amino acid on the proximal side of the heme of CcP [Goodin et al., 1986; Fishel et al., 1987, 1991; Mauro et al., 1988].

The reduction of peroxidase compound I to the ferric native enzyme by the reducing substrate usually occurs via compound II formation, involving two sequential one-electron reductions. Compound II reduction is the rate-limiting step in the peroxidase catalytic cycle and is 10- to 100-fold slower than compound I reduction [Critchlow and Dunford, 1972a,b; Dunford and Stillman, 1976; Wariishi et al., 1991a]. The energy for reorganization of the heme environment may contribute to the different reduction rates for compound I and II. The reduction of compound II involves the release of H_2O and a change in the coordination (hexa- to penta-coordinate) and spin state (low to high spin) of the iron center, whereas essentially no change of heme geometry is involved in compound I reduction. The higher reactivity of compound I may also result from exposure of the porphyrin π-cation radical at a

peripheral site, thus reducing the distance to the reducing substrate [Ator and Ortiz de Montellano, 1987; Ortiz-de-Montellano, 1992].

1.4.3 Amino Acids Involved in the Heme Peroxidase Catalytic Cycle

Multiple studies have helped to resolve the catalytic mechanism of the various heme peroxidases. Structure-function studies, using crystal structure and site-directed mutagenesis data, have increased the understanding of the role of specific amino acids in the catalytic cycle. The crystal structures for several heme peroxidases are available, including those of HRP [Gajhede et al., 1997], CcP [Finzel et al., 1984], LiP [Piontek et al., 1993; Poulos et al., 1993; Choinowski et al., 1999], MnP [Sundaramoorthy et al., 1994], CiP [Kunishima et al., 1994; Petersen et al., 1994], peanut peroxidase [Schuller et al., 1996] and barley grain peroxidase [Henriksen et al., 1998b]. Amino acid sequence alignments and crystal structure data show that multiple amino acids in the heme environment are identical among the heme peroxidases (Fig. 1.2). These amino acids have been excellent targets for elucidating the mechanisms of O–O cleavage, stabilizing the $Fe^{IV}=O$ intermediate and controlling the heme iron redox potential. In addition, these studies are being conducted to identify the role of specific amino acids in substrate binding and electron transfer.

1.4.3.1 Residues on the Distal Side of the Heme. The formation of peroxidase compound I involves the cleavage of the O–O bond of hydrogen peroxide [Poulos and Kraut, 1980; Dawson, 1988]. The original mechanism of Poulos and Kraut [1980] was based on the crystal structure of CcP (Fig. 1.3). Two essential steps in the formation of compound I are the acid-base catalysis by a distal His, where the distal His acts as a proton acceptor from peroxide upon its binding, and the stabilization of the charge of a precursor enzyme–substrate complex by the distal Arg. One peroxide oxygen binds to the heme iron and the distal Arg hydrogen bonds to the other peroxide oxygen, thus forming the so-called ferric hydroperoxyl anion [Poulos and Kraut, 1980]. The subsequent heterolytic cleavage of the O–O bond of peroxide, through acid-base catalysis at the heme distal site, is described by the "push-pull" mechanism [Dawson, 1988].

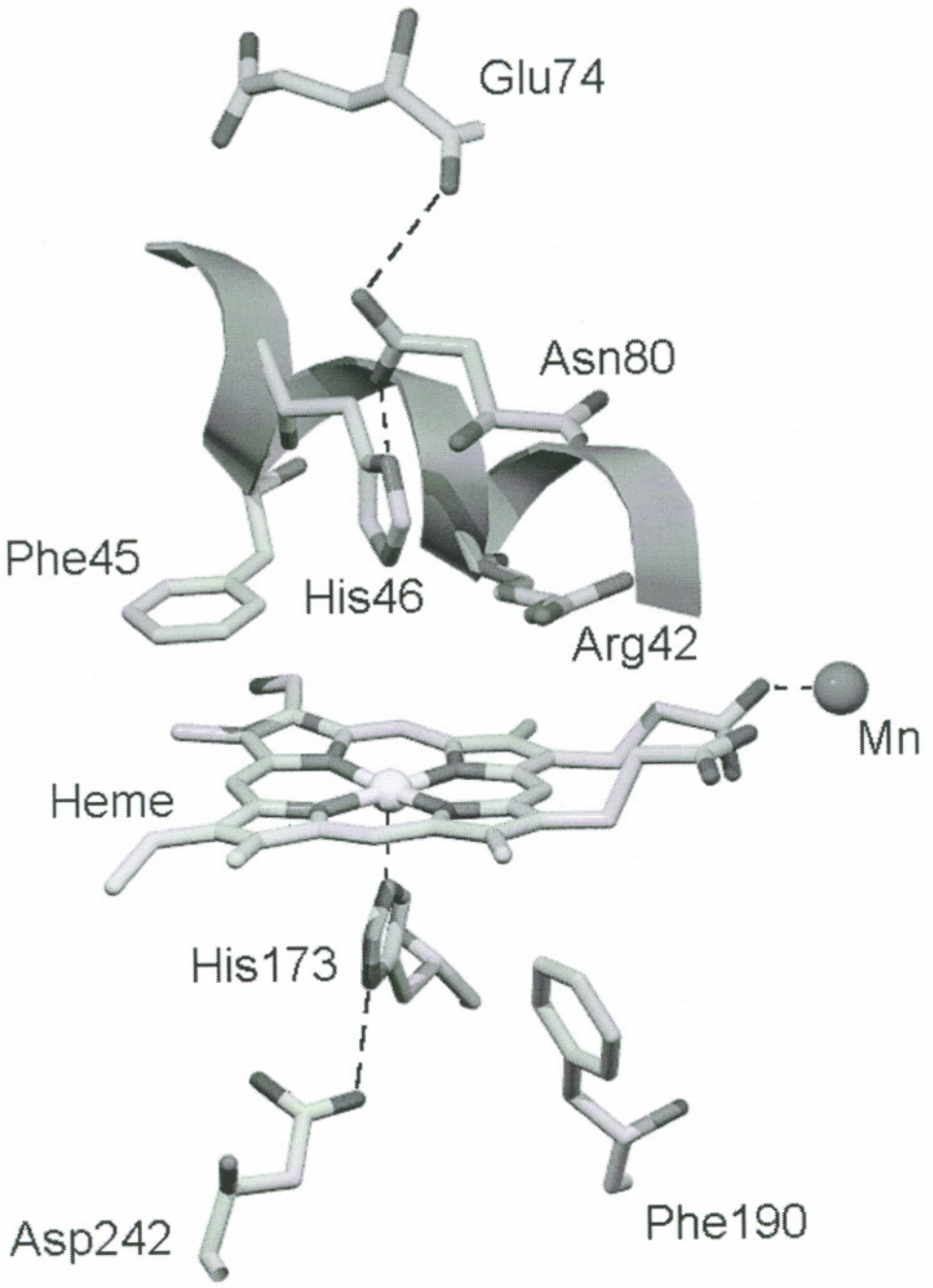

Fig. 1.2 A view of the heme environment of MnP [Sundaramoorthy et al., 1994]. Key residues for compound I formation and compound I and II stabilization are shown. The architecture of this site is essentially identical for other heme peroxidases.

Originally published as Fig. 8 in: Sundaramoorthy, M., Kishi, K., Gold, M. H., and Poulos, T. L. (1994) The crystal structure of manganese peroxidase from *Phanerochaete chrysosporium* at 2.06-Å resolution. *J. Biol. Chem.* **269**, 32759–32767. Used with permission of the *Journal of Biological Chemistry*.

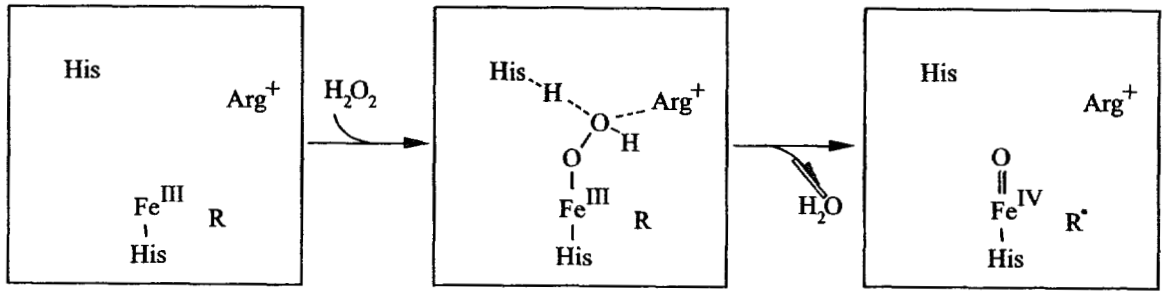

Fig. 1.3 Schematic diagram of the mechanism of compound I formation [Poulos and Fenna, 1994].

Originally published as a scheme in: Poulos, T. L., and Fenna, R. E. (1994) Peroxidases: structure, function, and engineering. In *Metals Ions in Biological Systems, Vol. 30: Metalloenzymes Involving Amino Acid-Residue and Related Radicals* (H. Sigel and A. Sigel, Eds.). Marcel Dekker, New York, pp. 25–75. Used with permission of Marcel Dekker.

Electron donation by the proximal ligand promotes the O−O bond cleavage ("push"). At the same time, the distal His now serves as a proton donor and works together with a charged residue, the distal Arg in most peroxidases, to give the distal side a polar character and to "pull" apart the O−O bond of the peroxide by stabilizing the separating charge. This results in the formation of the $Fe^{IV}=O$ porphyrin-π-cation radical intermediate of compound I and the release of a H_2O molecule [Poulos and Fenna, 1994].

Mutations of the distal His in HRP and CcP result in decreased compound I formation rates of around 10^6-fold [Erman et al., 1993; Newmyer and Ortiz de Montellano, 1995; Smith and Veitch, 1998], indicating that the distal His of heme peroxidases is essential for catalytic activity. Mutation of the distal Arg in HRP and CcP results in decreased compound I formation rates of around 10^2-fold [Vitello et al., 1993; Smith and Veitch, 1998], which suggests that the distal Arg contributes to but is not as essential for catalytic activity as the distal His.

The distal histidine forms a hydrogen bonding network with other amino acids at the distal side of the enzyme, which are conserved in all plant and fungal peroxidases [Welinder, 1992]. This hydrogen bonding network is formed by a His-Asn-Glu triad (Fig. 1.2). Mutation studies suggest that in HRP, the H-bond between the His and Asn is important for the catalytic activity by controlling the precise location of the distal His [Tanaka et al., 1997] and by promoting the deprotonated state of the histidine Nϵ2 site to ensure the acid−base character of the distal His for accepting a proton from peroxide [Poulos and Finzel, 1984; Welinder et al., 1995]. The second part of the hydrogen bonding network is an H-bond between the side chain of Asn and the backbone carbonyl oxygen of the highly conserved Glu residue. This residue also interacts with a distal calcium ion through a hydrogen bond with a water molecule, and structure-function studies indicate that the Glu residue is important for both the catalytic activity and stability of the enzyme [Nagano et al., 1996; Tanaka et al., 1998].

1.4.3.2 Residues on the Proximal Side of the Heme. The amino acids at the proximal side of the heme (Fig. 1.2) contribute to stabilizing the $Fe^{IV}=O$ intermediates of compound I and II, thereby controlling the redox potential and the

rate of O−O bond cleavage reaction. The proximal Asp and His are H-bonded, which results in a greater anionic character to the His, concomitant lowering of the redox potential of the heme iron, and stabilization of the oxoferryl iron in compound I and II. Evidence for the importance of the proximal His for catalytic activity results from studies on the proximal His-to-Ala mutation in HRP [Newmyer et al., 1996]. Reaction of this H170A mutant with H_2O_2 does not give spectroscopically detectable compound I or compound II intermediates but results in gradual degradation of the heme group. However, addition of excess imidazole indicates that imidazole binds in the cavity created by the H170A mutation, coordinates to the heme iron atom, and restores a large part of the catalytic activity by rescuing the rate of compound I formation. Thus, a primary function of the proximal histidine is to tether the iron atom to disfavor sixth-ligand binding, particularly coordination of the iron to the distal histidine. In addition, strong hydrogen bonding of the proximal ligand may be critical for facilitating O−O bond cleavage in the formation of compound I [Newmyer et al., 1996].

1.5 Manganese Peroxidase

In the early 1980s, two extracellular enzymes—lignin peroxidase (LiP) [Glenn et al., 1983; Tien and Kirk, 1983] and manganese peroxidase (MnP) [Kuwahara et al., 1984]—were discovered in *P. chrysosporium*. These enzymes are major components of the extracellular lignin and aromatic pollutant degradation system of this organism [Kirk and Farrell, 1987; Gold et al., 1989; Hammel, 1989]. MnP has been identified as an extracellular enzyme in all of the lignin-degrading fungi which have been examined to date [Périé and Gold, 1991; Orth et al., 1993; Hatakka, 1994; Homolka et al., 1994; Pelaez et al., 1995; Li et al., 1999].

1.5.1 General Properties of Manganese Peroxidase

Manganese peroxidase activity has been assayed in the extracellular medium of a wide variety of white-rot fungal species [Hatakka, 1994]. All of these MnPs have M_rs in the range of 45 to 55 kDa and are glycoproteins. Where examined, they

contain one heme prosthetic group per protein molecule. Furthermore, in the presence of H_2O_2 and an organic acid chelator, these MnPs oxidize Mn^{II} to Mn^{III}.

In *P. chrysosporium*, MnP occurs as a series of isozymes encoded by a family of genes [Gold and Alic, 1993]. The sequences of cDNA [Pease et al., 1989; Pribnow et al., 1989; Mayfield et al., 1994a; Orth et al., 1994] and genomic clones, encoding three alleles of MnP isozymes from this species—*mnp1*, *mnp2* and *mnp3*, [Godfrey et al., 1990; Mayfield et al., 1994a; Alic et al., 1997]—have been determined. The three *mnp* alleles show a genomic sequence identity within the coding regions ranging from 66 to 70% and a deduced amino acid sequence identity ranging from 82 to 84%. The three *P. chrysosporium mnp* genes encode precursor enzymes that consist of mature proteins of 357−358 amino acids, preceded by a leader sequence of 21−25 amino acids [Pribnow et al., 1989; Mayfield et al., 1994a; Alic et al., 1997]. The MnP enzymes are glycosylated and have pIs ranging from 4.2 to 4.9 and molecular masses ranging from 45 to 47 kDa [Glenn and Gold, 1985; Paszczynski et al., 1986; Leisola et al., 1987; Pribnow et al., 1989; Pease and Tien, 1992]. The MnP leader sequences consist of N-terminal, C-terminal, and hydrophobic domains which are characteristic for signal peptides [von Heijne, 1985]. However, the leader sequences do not contain a propeptide, as found in LiP precursor proteins.

1.5.2 Reactions Catalyzed by Manganese Peroxidase

In the presence of dicarboxylic acid chelators, such as malonate and oxalate, or α-hydroxyacids, such as lactate and tartrate, the oxidation of Mn^{II} to Mn^{III} by MnP can be monitored at 270−290 nm [Glenn et al., 1986; Wariishi et al., 1992]. Mn^{III}-malonate formation is used routinely as a quantitative MnP assay [Wariishi et al., 1992]. For the dicarboxylic acid chelators, malonate and oxalate, the stoichiometry between the Mn^{III}−chelator complex formed and H_2O_2 consumed is 2:1 [Wariishi et al., 1992]. Mn^{III}−chelator complexes are efficient oxidants [Wariishi et al., 1988, 1992] and oxidize a wide variety of phenols, amines, and dyes [Glenn and Gold, 1985; Glenn et al., 1986; Paszczynski et al., 1986]. MnP assays based on 2,6-dimethoxyphenol, vanillyl acetone, ABTS, and phenol red oxidation also have been

reported [Glenn and Gold, 1985; Paszczynski et al., 1986; Wariishi et al., 1992]. The Mn^{III}–chelator complex probably is acting as a mediator in the reaction. Mn^{III}–chelator complexes are stable enough to diffuse through a semipermeable membrane to oxidize polymeric substrates at a distance [Glenn et al., 1986]. This supports cytochemical studies showing that MnP is too bulky to diffuse into the wood matrix [Daniel et al., 1990; Blanchette et al., 1997], suggesting that the enzyme does not bind directly to lignin in wood but rather oxidizes the substrate via a diffusable Mn^{III}–chelator complex.

1.5.3 Biophysical Studies of Manganese Peroxidase

1.5.3.1 Spectroscopic Studies. Electronic absorption maxima for native, oxidized, and various ligated forms of MnP have been reported (Table 1.2) [Glenn and Gold, 1985; Gold et al., 1989] and are similar to those of both horseradish peroxidase (HRP) and LiP [Blumberg et al., 1968; Tamura et al., 1972; Dunford and Stillman, 1976; Glenn and Gold, 1985; Renganathan and Gold, 1986; Wariishi et al., 1988]. Spectra indicate that the heme iron is high-spin, ferric, and pentacoordinate, with a histidine acting as the fifth ligand. Detailed EPR, resonance Raman, and NMR studies of various forms of MnP confirm that the native enzyme exists as a high-spin, ferric, heme protein and that the heme environment of MnP is similar to those of HRP and LiP [Mino et al., 1988; Banci et al., 1992, 1993].

1.5.3.2 Catalytic Cycle and Kinetic Mechanism. The catalytic cycle of MnP is shown in Fig. 1.4. The two-electron oxidation of ferric MnP by H_2O_2 yields the oxoferryl, porphyrin π-cation radical intermediate, compound I [Wariishi et al., 1988]. Reduction of compound I by one electron, using 1 equiv of ferrocyanide or Mn^{II}, yields the oxoferryl intermediate compound II [Wariishi et al., 1988]. Compound II is then reduced back to the ferric enzyme by a single-electron step in the presence of the substrate. The addition of excess H_2O_2 to the native enzyme yields compound III [Wariishi et al., 1988], which is inactive. While a variety of phenols or aromatic amines are able to slowly reduce compound I to compound II, only Mn^{II} efficiently reduces compound I to compound II, and compound II to native enzyme (Fig. 1.4) [Wariishi et al., 1988, 1989]. This indicates that Mn^{II} serves as an

Table 1.2

Spectroscopic Characteristics of MnP[a], LiP[a], and HRP

	Electronic absorption maxima (nm)[b]		
	MnP	LiP	HRP
Ferric	406, 502, 632	407, 500, 632	403, 498, 640
Ferrous	433, 544, 585	435, 556, 580	440, 510, 557, 580
Compound I	407, 558, 605, 650	408, 550, 608, 650	400, 557, 622, 650
Compound II	420, 528, 555	420, 525, 556	420, 527, 554
Compound III	417, 545, 579	419, 543, 578	413, 546, 583

[a] From *P. chrysosporium.*

[b] References are cited in the text.

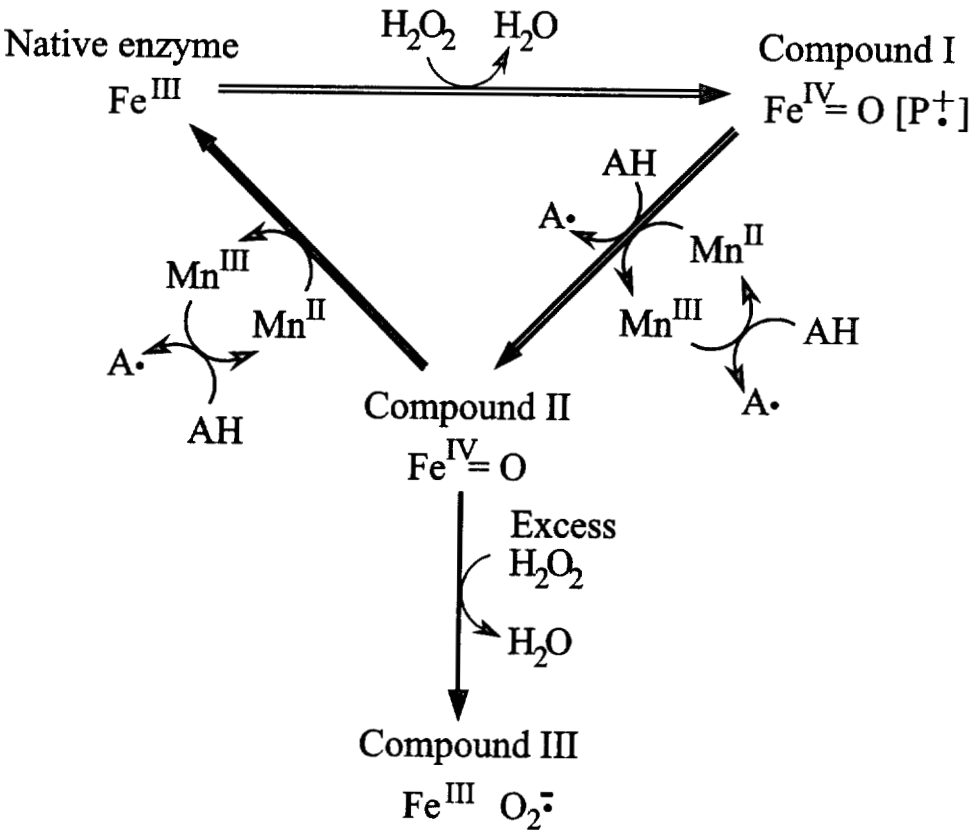

Fig. 1.4 Catalytic cycle of MnP. AH is a phenolic or aromatic amine substrate and $A^{\bullet}$ is the radical produced upon one-electron oxidation. $[P^{+\bullet}]$ is a porphyrin π-cation radical.

obligatory substrate for MnP compound II, enabling the enzyme to complete its catalytic cycle [Wariishi et al., 1988, 1989]. Steady-state and transient-state kinetic analysis of Mn^{II} oxidation indicates a peroxidase-type ping-pong kinetic mechanism [Dunford, 1991; Wariishi et al., 1992].

1.5.3.3 The Role of Chelators. To date, MnP appears to be the only enzyme that uses manganese as a diffusable substrate rather than a permanent enzyme-bound cofactor. Therefore, the enzyme must be able to bind Mn^{II} and release Mn^{III}. The role of chelators in this process has been studied; however, it is still not well understood. As previously mentioned, a dicarboxylic acid or α-hydroxy acid chelator is required for complete turnover of the enzyme by Mn^{II} [Wariishi et al., 1992; Kuan et al., 1993; Kishi et al., 1994]. Although *P. chrysosporium* secretes several organic acids such as oxalate, malonate, citrate and glyoxalate during idiophasic metabolism [Barr et al., 1992; Wariishi et al., 1992; Dutton et al., 1993; Kuan and Tien, 1993], only oxalate is produced at concentrations sufficient to stimulate MnP activity [Kuan and Tien, 1993; Kishi et al., 1994].

The formation and reduction of compound I do not appear to be affected by the presence or type of chelator in reaction mixtures at pH 4.5 [Kuan et al., 1993; Kishi et al., 1994; Sollewijn Gelpke et al., 1999b]. In contrast, the reduction of compound II is greatly affected by chelators [Kuan et al., 1993; Kishi et al., 1994]. Maximum rates for the reduction of compound II are observed when the Mn^{II} in solution is stoichiometrically chelated by oxalate [Kuan et al., 1993; Kishi et al., 1994]. Based on this, the formation of an enzyme-Mn^{II}-oxalate ternary complex during the reaction cycle has been postulated [Kuan et al., 1993]. However, recent NMR [Banci et al., 1998] and crystal structure [Sundaramoorthy et al., 1994] studies show that Mn^{II}, rather than a Mn^{II}-chelator complex, binds to the native ferric enzyme as proposed earlier [Wariishi et al., 1992]. Thus, a chelator possibly facilitates the removal of Mn^{III} from the enzyme [Wariishi et al., 1992].

1.5.4 The Crystal Structure of Manganese Peroxidase

The crystal structure of manganese peroxidase from *P. chrysosporium* has been solved [Sundaramoorthy et al., 1994, 1997]. Previous studies indicated that MnP is a

glycosylated peroxidase containing one iron protoporphyrin IX [Glenn and Gold, 1985; Paszczynski et al., 1986; Pribnow et al., 1989]. Detailed spectroscopic studies show that the heme iron is ferric, high-spin, pentacoordinate, and ligated to a histidine residue, as in other plant and fungal peroxidases [Glenn and Gold, 1985; Mino et al., 1988; Wariishi et al., 1988; Banci et al., 1992]. The crystal structure confirms these observations and further shows that the overall polypeptide fold is similar to that of other plant and fungal peroxidases (Fig. 1.5) [Edwards et al., 1993; Petersen et al., 1993; Kunishima et al., 1994; Sundaramoorthy et al., 1994; Schuller et al., 1996]. The position of the calcium sites is homologous to those in LiP and CiP, although the exact ligands are not conserved [Poulos et al., 1993; Kunishima et al., 1994; Sundaramoorthy et al., 1994]. MnP contains five disulfide linkages, four of which are identical to those in LiP and CiP [Edwards et al., 1993; Petersen et al., 1993; Piontek et al., 1993; Poulos et al., 1993; Kunishima et al., 1994; Sundaramoorthy et al., 1994].

It has been proposed that the most C-terminal disulfide linkage, unique to MnP, not only stabilizes the enzyme's carboxy terminal tail, which is longer than that of LiP, but may also participate in stabilization of the Mn^{II} binding site [Sundaramoorthy et al., 1994]. The MnP crystal structure exhibits N-glycosylation at Asn131 and an O-linked mannose at Ser336 [Sundaramoorthy et al., 1994], which are both putative glycosylation sites predicted by the cDNA sequence [Pribnow et al., 1989]. This is consistent with glycosylation patterns observed in other extracellular fungal peroxidases [Limongi et al., 1995].

1.5.4.1 The Heme Environment and Peroxide Binding Site. Amino acid residues in the distal domain of MnP include His46, Arg 42, Asn80, Glu74, and Phe45 (Fig. 1.2). As in all heme peroxidases, the distal His probably acts as an acid-base catalyst, accepting a proton from peroxide and facilitating cleavage of the O−O bond [Poulos and Finzel, 1984; Howes et al., 1997]. Arg42, the distal arginine, probably stabilizes compound I and may facilitate heterolytic cleavage of the peroxide anion [Poulos and Kraut, 1980]. The distal Arg in many other peroxidases interacts directly, or through a bridging water molecule, with one of the heme propionates, whereas in MnP, this propionate is rotated such that it is a ligand for Mn^{II}

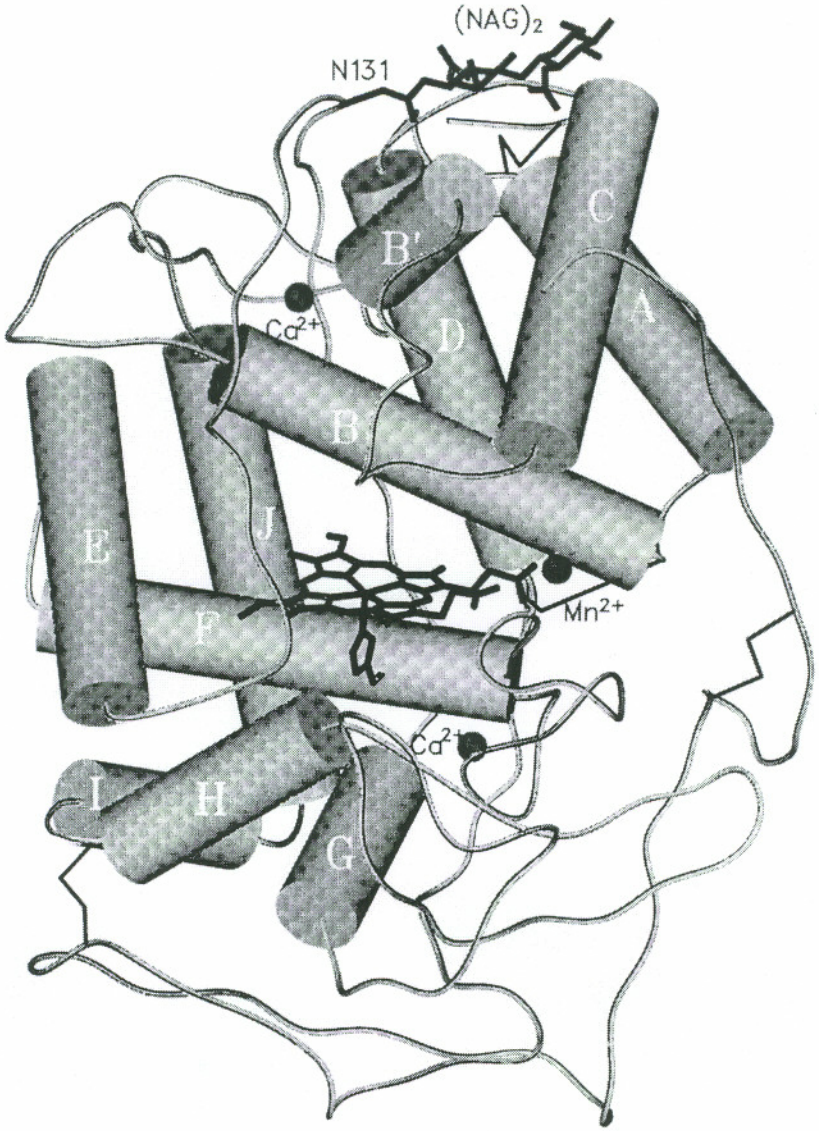

Fig. 1.5 Schematic diagram of the *P. chrysosporium* MnP crystal structure [Sundaramoorthy et al., 1994].

Originally published as Fig. 4 in: Sundaramoorthy, M., Kishi, K., Gold, M. H., and Poulos, T. L. (1994) The crystal structure of manganese peroxidase from *Phanerochaete chrysosporium* at 2.06-Å resolution. *J. Biol. Chem.* **269**, 32759–32767. Used with permission of the *Journal of Biological Chemistry*.

[Sundaramoorthy et al., 1994]. Asn80, Glu74, and His46 form the distal hydrogen bonding network and are believed to participate in modulation of the acid-base character and positioning of the distal His for peroxide cleavage (Fig. 1.2). Finally, extracellular plant and fungal peroxidases contain a Phe residue adjacent to the heme in the position of Phe45 [Welinder, 1991, 1992; Sundaramoorthy et al., 1994], which is believed to stabilize compound I [Smith et al., 1992].

In the proximal domain, His173, Asp242, and Phe190 are important conserved residues (Fig. 1.2). His173, the proximal histidine, is the fifth ligand to the heme iron, thereby tethering the heme to the protein [Sundaramoorthy et al., 1994]. Asp242 forms a hydrogen bond with His173 and thus may render more anionic character to His173, which would increase electro negativity of the heme iron, enabling the formation of the oxyferryl intermediates [Poulos and Finzel, 1984]. Phe190 is situated just proximal to the heme and is conserved in MnP and other heme peroxidases but is replaced by a Trp in CcP and APX [Welinder, 1992] and a Leu in CiP [Petersen et al., 1994]. In CcP, the Trp residue is the location where the second oxidizing equivalent of compound I is stored. This Phe residue has been implicated in the thermal and pH stability of MnP [Kishi et al., 1997; Youngs et al., 2001].

1.5.4.2 The manganese binding site. Prior to the elucidation of the crystal structure of MnP, three manganese binding sites were proposed on the basis of heme modification experiments and homology-based molecular modeling [Harris et al., 1991; Johnson et al., 1994]. The most favorable binding site proposed was the only apparent Mn^{II} binding site in the crystal structure [Sundaramoorthy et al., 1994]. Recent pH titration studies suggest that there may be a second low-affinity Mn^{II} binding site not apparent in the crystal structure [Mauk et al., 1998].

The enzyme-bound manganese at the functional site (Fig. 1.6) appears to be hexacoordinate, with two water ligands and four carboxylate ligands from three acidic amino acids at the surface of the protein, Glu35, Glu39 and Asp179, and heme propionate 6. One water ligand is hydrogen-bonded to heme propionate 7 (Fig. 1.6), and all ligand–metal bond distances range from 2.34 to 2.82 Å [Sundaramoorthy et al., 1994], typical of coordinated Mn^{II}. Electron transfer is presumed to occur via a

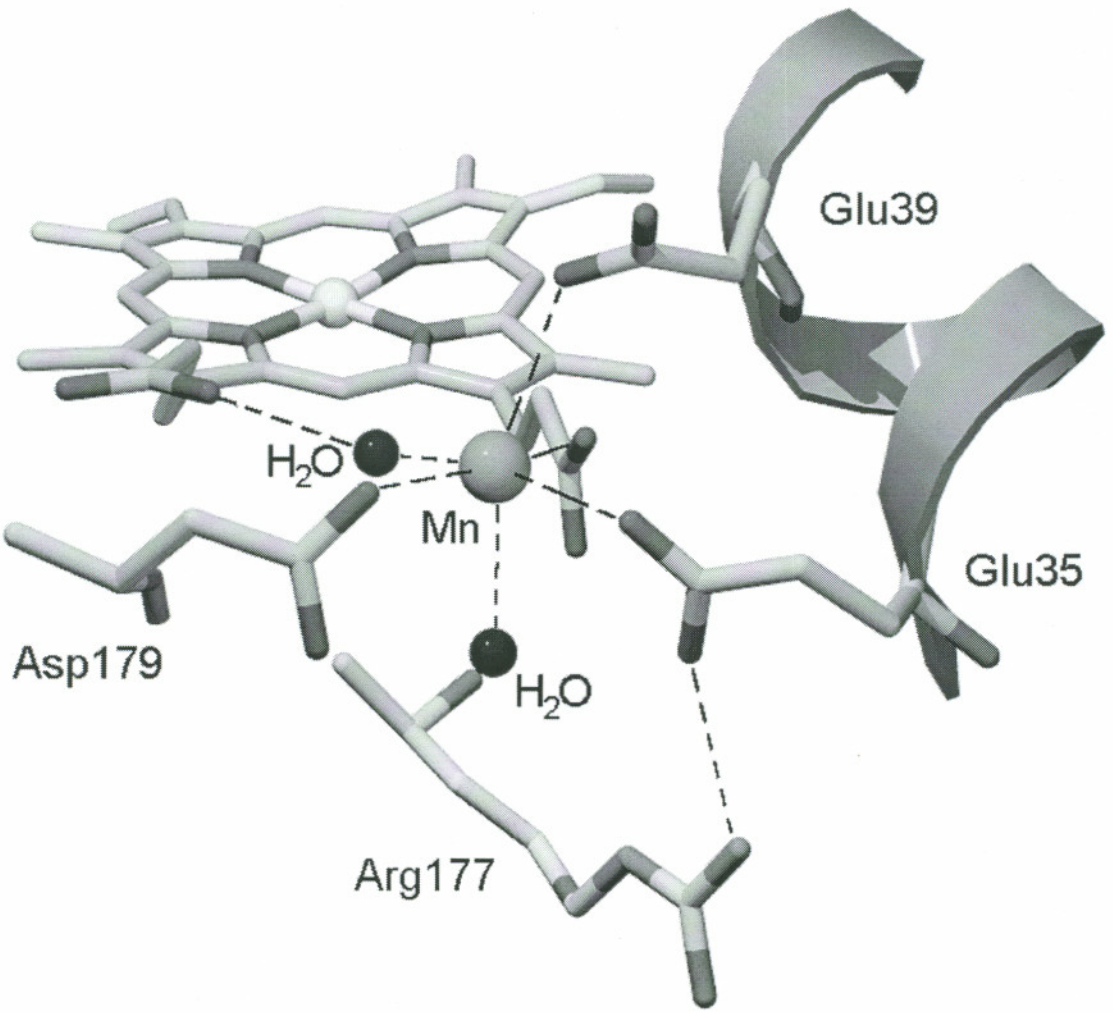

Fig. 1.6 A view of the Mn^{II} binding site of MnP.

direct pathway through the heme propionate 6 ligand. Of the amino acids forming the manganese binding site, only Glu39 is present in LiP and none of the residues are present in CiP/ARP [Petersen et al., 1993; Poulos et al., 1993; Kunishima et al., 1994; Sundaramoorthy et al., 1994]. Arg177 forms a salt bridge with Glu35 (Fig. 1.6) thereby orienting this ligand [Sundaramoorthy et al., 1994]. Arg177 is not conserved in LiP nor, it has been argued, can the LiP structure accommodate Arg177 [Sundaramoorthy et al., 1994]. Most of the amino acid residues which form the manganese binding site have been examined by site-directed mutagenesis.

1.5.5 Structure-Function Studies of Manganese Peroxidase

1.5.5.1 Site-directed mutations of the Mn^{II} binding ligands. In the first site-directed mutagenesis studies on MnP [Kusters-van Someren et al., 1995; Kishi et al., 1996], each of the three amino acid ligands in the proposed Mn binding site was changed to its respective amide to obtain D179N, E35Q, and E39Q. In addition, one double mutant, D179N-E35Q, was constructed. UV-vis and resonance Raman spectra of these mutants show that the coordination and spin states of the heme irons were identical to wtMnP, indicating that the heme environment was apparently not affected by the mutations at the Mn^{II} binding site [Kishi et al., 1996].

Indeed, preservation of the heme environment geometry was confirmed by crystallographic analysis of several mutants [Sundaramoorthy et al., 1997]. Furthermore, mutations at the Mn^{II} binding site do not affect kinetic constants for binding and reactivity towards peroxide, ferrocyanide, and small phenolic compounds such as *p*-cresol [Kusters-van Someren et al., 1995; Kishi et al., 1996]. However, steady-state kinetic analyses of all the mutants showed significant decreases in catalytic efficiency for Mn^{II} oxidation, and transient-state kinetic analyses showed significantly reduced Mn^{II} binding and rates of compound II reduction by Mn^{II} [Kusters-van Someren et al., 1995; Kishi et al., 1996]. Crystal structures of the mutant MnPs indicate much weaker binding of Mn^{II} at the altered sites and changed orientation of the Mn^{II} binding site ligands [Sundaramoorthy et al., 1994, 1997]. All of the mutations resulted in increased exposure of the binding site to solvent,

primarily by rotation of residues Glu35 and Glu39 at the surface of the enzyme to a more open configuration [Sundaramoorthy et al., 1997].

More recently, a different set of Mn^{II} binding site mutations, D179A, E35D and E39D, was constructed and expressed as apoenzyme in *E. coli*, and reconstituted with calcium and heme [Whitwam et al., 1997]. However, no detailed spectroscopic analysis of these mutants has been reported. The binding and reactivity towards ferrocyanide and small phenols were not altered by these mutations of the Mn^{II} binding ligands [Whitwam et al., 1997], confirming previous results [Kusters-van Someren et al., 1995; Kishi et al., 1996]. Steady-state kinetic analyses of D179A and E35D showed results similar to those of the Mn^{II} binding mutants described above [Kishi et al., 1996], and transient-state kinetic analysis revealed that rates of compound I and II reduction by Mn^{II} were significantly reduced for these mutants [Whitwam et al., 1997]. In contrast, the kinetic analysis of E39D suggested that this mutation has little effect on the catalytic properties of the rMnP and that Glu39 is not a ligand to the Mn^{II} [Whitwam et al., 1997]. However, Glu39 is a ligand in the crystal structure [Sundaramoorthy et al., 1994] and is conserved in all *mnp* genes examined to date [Pease et al., 1989; Godfrey et al., 1990; Mayfield et al., 1994a; Orth et al., 1994; Alic et al., 1997]. The E39D mutation does not change the functional carboxylate moiety of the ligand. Studies of mutations such as E39Q [Kishi et al., 1996; Sundaramoorthy et al., 1997] and E39A [Youngs et al., 2001], which eliminate the functional carboxylate, clearly demonstrate that Glu39 is a ligand.

1.6 Lignin Peroxidase

1.6.1 General Properties of Lignin Peroxidase

When grown under nitrogen-limiting conditions, *P. chrysosporium* produces LiP as a family of glycosylated isozymes with molecular masses ranging from 38 to 42 kDa and pIs ranging from 3.2 to 4.7 [Leisola et al., 1987; Farrell et al., 1989; Gold and Alic, 1993]. The isozyme profiles are dependent on the growth conditions and on the type of strains used for LiP production. All of the LiP isozymes examined appear to contain N-linked carbohydrate [Farrell et al., 1989; Glumoff et al., 1990],

which in some cases includes mannose-6-phosphate [Kuan and Tien, 1989; Rothschild et al., 1999], and are likely to contain O-linked carbohydrates as well. All isozymes have the amino acid sequence Asn-X-Thr/Ser which encodes for a potential N-glycosylation site [Gold and Alic, 1993]. The majority of the research on LiP has used isozyme LiP isozyme H8 and isozyme H2.

The lignin peroxidase isozymes of *P. chrysosporium* are encoded by a family of closely related *lip* genes. Multiple cDNA and genomic clones for lignin peroxidase have been sequenced [Gold and Alic, 1993]. The identification of *lip* genes was complicated by the existence of allelic variants; however, the analysis of single basidiospores allowed alleles to be differentiated from closely related *lip* genes [Alic et al., 1987]. Ten lignin peroxidase genes of *P. chrysosporium* have been identified, with nucleotide identities within the coding regions ranging from 71 to 99% and deduced amino acid sequence identities ranging from 68 to 99%. The *P. chrysosporium lip* genes each encode a protein product which includes a 27 or 28 amino acid leader sequence followed by a 343 to 345 amino acid mature protein. Analysis of the LiP leader sequence indicated that the LiP protein is synthesized as a preproenzyme, composed of a 21 amino acid prepeptide followed by a 7 amino acid propeptide [Ritch et al., 1991]. Presumably the prepeptide, or signal peptide, is cleaved after translation of the precursor protein and localization to the endoplasmic reticulum. The propeptide is probably cleaved later in the protein excretion pathway [Gold and Alic, 1993].

Lignin peroxidases have been detected in several white-rot fungi other than *P. chrysosporium*, including *Bjerkandera* sp. strain BOS [ten Have et al., 1998], *Trametes versicolor* [Johansson et al., 1993], and *Phlebia radiata* [Niku-Paavola et al., 1988]. However, LiP could not be detected in other white-rot fungi (Table 1.1) [Hatakka, 1994], and it is assumed that these fungi degrade lignin without the presence of LiP. Several *lip* genes have also been identified and characterized from other white-rot fungi, including *T. versicolor* [Jonsson et al., 1994; Johansson and Nyman, 1996], *Bjerkandera adusta* [Asada et al., 1992] and *P. radiata* [Saloheimo et al., 1989].

1.6.2 Reactions Catalyzed by Lignin Peroxidase

The oxidation of a wide variety of aromatic and halide substrates is catalyzed by LiP, including several lignin model compounds [Glenn et al., 1983; Gold et al., 1984], synthetic lignins [Hammel et al., 1993], lignin model dimers [Miki et al., 1986], phenols [Koduri and Tien, 1995], substituted benzenes [Kersten et al., 1990; Valli et al., 1990; Joshi and Gold, 1996], pollutants [Hammel et al., 1986; Joshi and Gold, 1994], the inorganic ions, bromide and iodide [Renganathan et al., 1987], dyes [Spadaro and Renganathan, 1994], and proteins [Sheng and Gold, 1998, 1999]. LiP catalyzes the H_2O_2-dependent oxidation of non-phenolic lignin substrates by abstraction of one electron to generate aryl cation radicals [Kersten et al., 1985; Miki et al., 1986; Schoemaker and Leisola, 1990], which undergo subsequent non-enzymatic reactions. Oxidation reactions of a variety of lignin model compounds and synthetic lignins by LiP have been studied. Catalytic mechanisms have been elucidated, and the capacity for $C_\alpha - C_\beta$ bond cleavage, ring opening, and other reactions has been demonstrated [Kirk and Farrell, 1987; Eriksson et al., 1990; Gold and Alic, 1993].

The β-O-4 linked dimer, which accounts for more than 50% of the linkages in lignin, is oxidized by LiP to form a cation radical [Kirk et al., 1986b; Miki et al., 1986; Umezawa and Higuchi, 1989]. The cation radical reacts with H_2O or O_2, leading to the formation of monomeric products. Synthetic lignins (DHPs) have been used to demonstrate the ability of LiP to oxidize polymeric lignins. ^{14}C- and ^{13}C-labeled DHPs were used to demonstrate that LiP catalyzes the $C_\alpha - C_\beta$ bond cleavage reaction to yield low molecular weight products [Hammel et al., 1993].

The oxidation of 3,4-dimethoxy benzylalcohol [veratryl alcohol (VA)] by LiP has been well studied. LiP oxidizes VA to veratraldehyde as the dominant product with other minor products such as quinones and lactones. A one-electron oxidation of VA results in the formation of a VA cation radical ($VA^{+\bullet}$) [Schmidt et al., 1989; Joshi and Gold, 1996]. $VA^{+\bullet}$ loses a proton to form the VA benzylic radical, which can be further oxidized by LiP to form veratraldehyde or can react non-enzymatically with O_2 to form veratraldehyde.

1.6.3 Biophysical Studies of Lignin Peroxidase

1.6.3.1 Spectroscopic Studies. The electronic absorption maxima for native LiP and oxidized intermediates as well as various ligated forms of LiP have been reported (Table 1.2) [Gold et al., 1984; Renganathan and Gold, 1986; Wariishi et al., 1990] and are similar to those of MnP and HRP. Together with UV-vis absorption spectroscopy, EPR, NMR, and resonance Raman spectroscopy indicate that the heme iron of the native enzyme is ferric, high-spin, and penta-coordinate with a histidine acting as the fifth ligand [de Ropp et al., 1991; Banci et al., 1993].

1.6.3.2 Catalytic cycle and kinetic mechanism. A scheme of the catalytic cycle of LiP is shown in Fig. 1.7. The productive cycle of LiP includes the two-electron oxidation of the enzyme by H_2O_2, resulting in the formation of compound I (LiPI) [Renganathan and Gold, 1986; Marquez et al., 1988]. Subsequently, a one-electron reduction step of LiPI by VA or another reducing substrate results in the formation of compound II (LiPII). A second one-electron reduction step results in the formation of the native enzyme in the ferric oxidation state to complete the catalytic cycle [Renganathan and Gold, 1986; Marquez et al., 1988; Gold et al., 1989; Harvey et al., 1989; Wariishi et al., 1991a].

Incubation of LiP under non-productive reaction conditions can result in the formation of alternative oxidized intermediates. In the absence of a reducing substrate, LiPI spontaneously decays to LiPII [Renganathan and Gold, 1986] at a rate which is independent of the H_2O_2 concentration [Harvey et al., 1989]. LiPII can be converted to LiP compound III (LiPIII) with considerably less H_2O_2 present than is required for other peroxidases. LiPIII also reacts with H_2O_2 to form LiPIII*, resulting in the inactivation of the enzyme [Wariishi and Gold, 1989, 1990; Mylrajan et al., 1990; Wariishi et al., 1990]. Inactivation of LiP by excess H_2O_2 is prevented by VA. VA can convert LiPIII* back to the ferric enzyme via an apparent single-step process. Alternatively, VA reduces LiPII directly, preventing the formation of LiPIII [Marquez et al., 1988; Wariishi and Gold, 1989, 1990; Wariishi et al., 1990].

The oxidized intermediates of LiP can be identified by their electronic absorption spectra, allowing the transient-state kinetic analysis of reactions involving the specific intermediates. These transient-state kinetic results support the mechanism

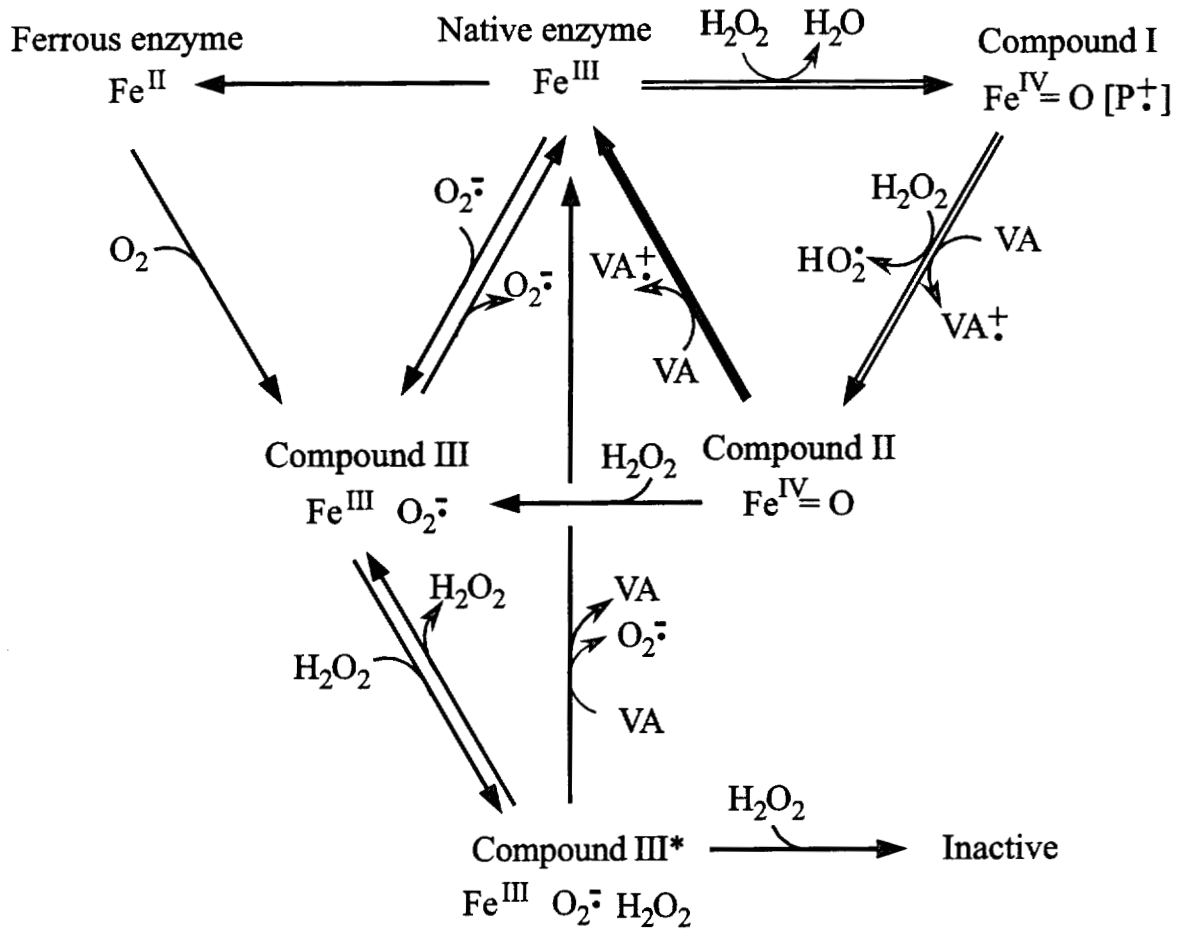

Fig. 1.7 The catalytic cycle of LiP. Interrelationship between the oxidized intermediates of LiP. $VA^{+\bullet}$ is the veratryl alcohol cation radical produced upon one-electron oxidation, $O_2^{-\bullet}$ is superoxide, and $[P^{+\bullet}]$ is a porphyrin π-cation radical.

described above. The formation of LiPI obeys second-order kinetics with a rate constant of around 6.5×10^5 M^{-1} s^{-1} over the pH range of 3.0 to 7.4 [Marquez et al., 1988]. The reduction of LiPI is not dependent on the presence of chelators, as with MnP, but is pH dependent with rates decreasing as pH increases. The reduction of LiPII by VA is a first-order reaction, which involves a rapid binding equilibrium between the substrate and LiPII, followed by electron transfer [Wariishi et al., 1991a]. This reaction is also pH dependent, with a first-order rate constant (k_2) for the reduction of VA of $\sim$35 s^{-1} and a dissociation constant (K_2) for VA of $\sim$200 μM [Wariishi et al., 1991a].

1.6.3.3 The Role of VA in Lignin Peroxidase Catalyzed Reactions. Veratryl alcohol, a secondary metabolite secreted by *P. chrysosporium*, stimulates the rates of LiP-catalyzed oxidations of synthetic lignin [Hammel et al., 1993], proteins [Sheng and Gold, 1998, 1999], and a variety of lignin model compounds and aromatic pollutants [Hammel et al., 1986; Valli et al., 1992; Joshi and Gold, 1994]. Anisyl alcohol and 4-methoxymandelic acid can only be oxidized by LiP in the presence of VA [Valli et al., 1990; Chung and Aust, 1995; Tien and Ma, 1997]. Several mechanisms have been proposed to explain the role of VA in oxidation reactions by LiP.

VA was proposed to act as a mediator, where the oxidized $VA^{+\bullet}$ can diffuse away from the enzyme and, in turn, can oxidize other substrates [Harvey et al., 1986]. Chemical studies on similar compounds indicate that a cation radical of this type is very unstable, due to a fast deprotonation resulting in the formation of the benzylic radical. However, it has been reported that oxidized VA ($VA^{+\bullet}$) is relatively stable in solution with a half-life of $\sim$59 ms, as measured by UV-vis spectroscopy [Candeias and Harvey, 1995; Harvey and Candeias, 1995], and may act as a diffusable mediator, oxidizing terminal substrates away from the enzyme surface.

Other studies suggest that $VA^{+\bullet}$ is not stable in solution (half-life $\sim$ 0.6 ms) but is significantly more stable (half-life $\sim$ 0.5 s) after being oxidized by LiP, where the $VA^{+\bullet}$ may be stabilized by the acidic environment of an enzyme active site [Khindaria et al., 1996]. Kinetic studies of the oxidation of the large polymers ferricytochrome *c* and RNase suggest that VA is oxidized by LiP to $VA^{+\bullet}$, which in

turn oxidizes the secondary substrate while still in its binding site [Wariishi et al., 1994; Sheng and Gold, 1998, 1999]. Studies of methoxybenzene oxidation by LiP also suggest that the $VA^{+\bullet}$ is too unstable to allow significant diffusion [Joshi and Gold, 1996].

Another proposed role for VA is to protect LiP from inactivation by excess H_2O_2, by preventing the formation of LiPIII* or by converting LiPIII* back to native enzyme [Wariishi and Gold, 1990; Wariishi et al., 1990].

1.6.4 The Crystal Structure of Lignin Peroxidase

The crystal structure of LiP from *P. chrysosporium* has been solved. The structures of the two isozymes LiPH8 [Piontek et al., 1993; Poulos et al., 1993] and LiPH2 [Choinowski et al., 1999] show identical overall structural features, which are homologous to other plant and fungal peroxidases including MnP and CiP. The crystal structures show that LiP has a globular shape and is composed of ten major and one minor helices, composing two approximately equal-sized domains, the distal and proximal domains. Each domain contains a structural calcium ion with positions that are conserved among LiP, MnP and CiP, although the ligands are not conserved. The enzyme contains one iron protoporphyrin IX wedged inbetween the proximal and distal domains. LiP contains four disulfide bridges, which are almost identical to those of CiP and to four of the five disulfide bridges in MnP [Petersen et al., 1994; Sundaramoorthy et al., 1994].

1.6.4.1 The heme environment. The heme iron of LiP is pentacoordinate with the proximal His residue as the fifth ligand to the iron, which is displaced from the porphyrin plane by $\sim$0.2 Å. In addition to the His−Fe bond, the heme is anchored in place by hydrophobic protein−heme interactions and by H-bonds of the heme propionates with the enzyme. The heme cavity or peroxide binding pocket of LiP is very similar to that of MnP and CcP. Extending from the distal helix B are three key residues—Arg43, Phe46 and His47—which form the H-bonding network with Asn84 and Glu78. At the proximal side, the distal His176 coordinates with the heme iron and H-bonds with Asp235. The positions of these residues are almost

identical in other heme peroxidases, where these residues play key roles in the reaction with peroxide during compound I formation, as discussed in Section 1.4.3.

An important difference in the structure of LiP as compared with those of other heme peroxidases is that the heme access channel is relatively small and may be inaccessible. Surrounding the access channel are His82, Ile85, E146, Phe148, D183, V184, I185, and Q222. In ARP and HRP, these access channels have been identified by crystal structure analysis as the binding site for the aromatic substrate molecule BHA [Itakura et al., 1997; Henriksen et al., 1998a]. Previous modeling studies have suggested a possible VA binding site in the LiP heme access channel [Poulos et al., 1993; Schoemaker et al., 1994]. VA was proposed to bind 6−7 Å from the heme, with the benzylic OH of VA, forming an H-bond with His82 and additional contacts at Ile85, Val184, Gln222, Phe148, and His82.

1.6.4.2 Environment of Trp171 and Trp171 Hydroxylation. An interesting new feature in the structure of LiP was described [Blodig et al., 1998]. A significant electron density at a single bond distance from the Cβ of Trp171 was observed and interpreted as a hydroxy group. A detailed crystal structure analysis of wtLiP and peptide analysis of tryptic digests of wtLiP and recombinant LiP from *E. coli* showed that the Cβ of amino acid Trp171 of wtLiP is hydroxylated as a result of the oxidation of LiP by H_2O_2 [Blodig et al., 1998]. These studies suggest that the hydroxylation at the Cβ of Trp171 is an autocatalytic reaction which occurs readily under conditions of natural turnover, i.e., in the ligninolytic cultures of *P. chrysosporium*. Additional studies, using spin-trapping combined with peptide analysis, suggest that a transient radical on Trp171 exists during the catalytic cycle of LiP [Blodig et al., 1999]. However, no spectroscopic evidence for a protein radical on Trp171 has been reported, suggesting the possibility that the binding of VA or other substrate initiates the transfer of electrons from VA via Trp171 to the heme edge, resulting in oxidized VA in a concerted mechanism.

The electron transfer pathway and mechanism of the electron transfer from Trp171 to the porphyrin ring or to the proximal His remain unresolved. A direct pathway from Trp171 via the proximal His ligand to the heme through the protein backbone covers a distance of 21.5 Å. An alternative pathway is 12.7 Å long, runs

partly through the protein backbone, and includes two hydrogen bonds. Mutation studies on the amino acids between Trp171 and His176—Met172, Leu173, Ser174 and Ala175—may indicate a possible pathway through the side chain of one of these residues to the heme. However, Met172 and Ser174 are only partially conserved in known LiP sequences.

The amino acid environment around Trp171, the proposed site of VA oxidation, contains several acidic residues (Fig. 1.8) [Poulos et al., 1993] which may be involved in stabilizing the VA cation radical after its formation [Khindaria et al., 1996]. In addition to Trp171, the amino acids Asp165, Glu250, Lys260 and Phe267 are completely conserved among known LiP enzyme sequences, and amino acid Glu168 is conserved only in part. In LiPH8, it appears that Glu250, Asp265 and Lys260 are involved in a H-bonding network to the nitrogen of the Trp171 indole ring, possibly orienting Trp171 in a fixed position. On the other side of Trp171, the acidic residues Glu168 and Glu165 may create an acidic environment, which is proposed to be important for stabilization of the $VA^{+\bullet}$ [Khindaria et al., 1996]. Finally, the aromatic residue, Phe267, may be involved in the binding and oxidation of VA by a stacking interaction of the electron-rich π-systems of Trp171, VA, and Phe267.

1.6.5 Structure-Function Studies of Lignin Peroxidase

The *E. coli* expression system has been used to produce mutant LiP enzymes [Ambert-Balay et al., 1998; Doyle et al., 1998]. Mutations of residues Trp171 and Glu146 were made to identify the site of substrate oxidation and to investigate the roles of these residues in substrate oxidation. A charge neutralization mutation in the classical heme edge substrate access channel of LiP, in which Glu146 was substituted by Gly, showed no substantial effect with respect to VA oxidation. However, this mutant enzyme exhibited a marked increase in pK_a (2.4 pH units) for the oxidation of a negatively charged difluoroazo dye. More surprisingly, the Trp171 mutants W171F and W171S were found to have lost all activity with VA as substrate and compounds I and II were unable to react with VA, whereas compound I formation remained unaffected. Both mutants, however, retained substantial activity with two dye

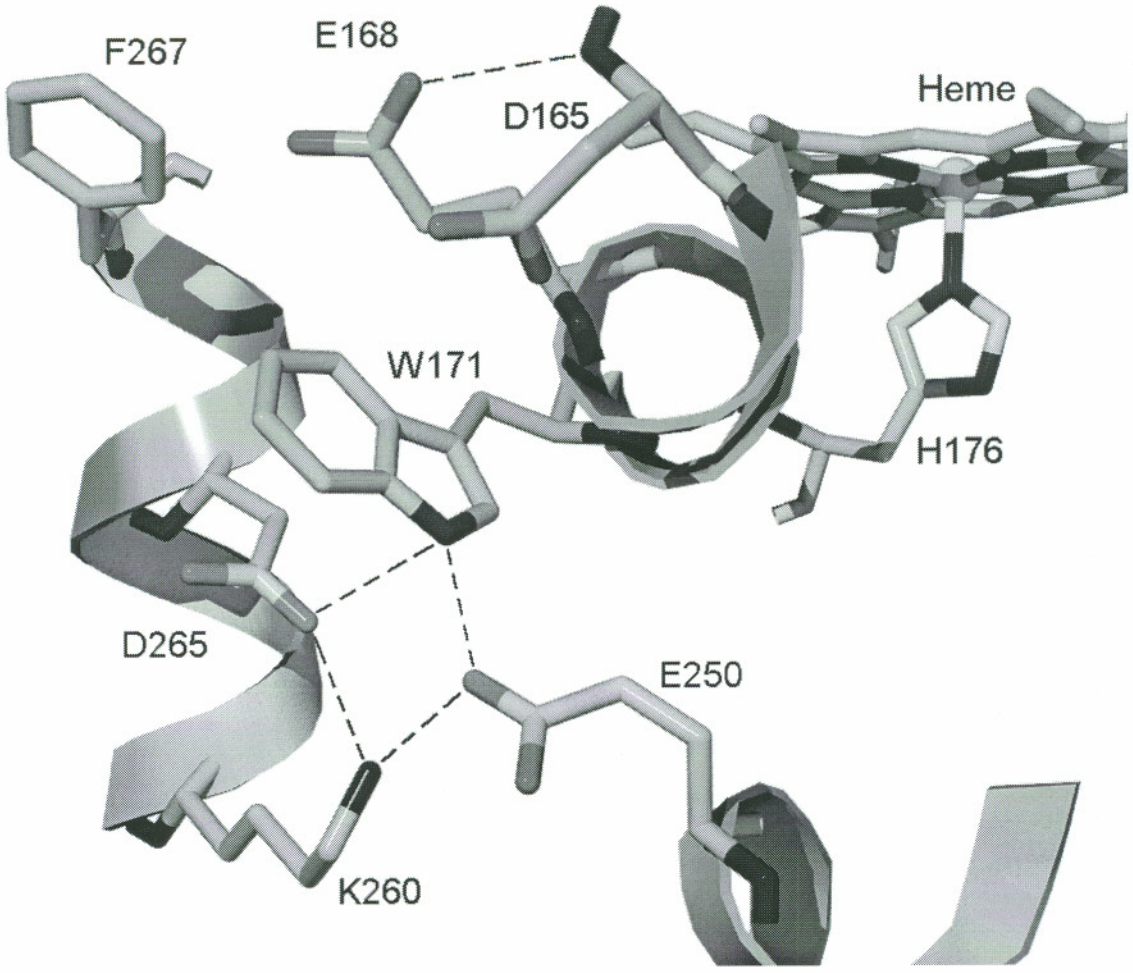

Fig. 1.8 The Trp171 environment of LiP.

substrates [Doyle et al., 1998]. This suggests the existence of two distinct substrate interaction sites in LiP: a heme access channel site typical of those encountered in other peroxidases and a second novel site centered around Trp171, which is required for the oxidation of VA. In addition, it was suggested that when LiP is in the two electron oxidized state, spontaneous electron transfer from Trp171 to the heme edge occurs, resulting in a $Fe^{IV}=O$, $Trp^{+\bullet}$ oxidation state [Doyle et al., 1998]. However, no spectroscopic evidence for this $Trp^{+\bullet}$ has been reported.

CHAPTER 2
ARGININE 177 IS INVOLVED IN Mn(II) BINDING BY MANGANESE PEROXIDASE*

2.1 Introduction

White-rot basidiomycete fungi are capable of degrading the plant cell wall polymer, lignin [Buswell and Odier, 1987; Kirk and Farrell, 1987; Gold et al., 1989], and a variety of aromatic pollutants [Bumpus and Aust, 1987b; Hammel, 1989; Joshi and Gold, 1993; Reddy et al., 1998]. When cultured under lignolytic conditions, the best-studied lignin-degrading fungus, *Phanerochaete chrysosporium*, secretes two families of extracellular peroxidases, lignin peroxidase (LiP) and manganese peroxidase (MnP), which, along with an H_2O_2-generating system, constitute the major enzymatic components of its extracellular lignin-degrading system [Kuwahara et al., 1984; Buswell and Odier, 1987; Kirk and Farrell, 1987; Gold and Alic, 1993; Hammel et al., 1993]. Both LiP and MnP are able to depolymerize lignin *in vitro* [Wariishi et al., 1991b; Hammel et al., 1993; Bao et al., 1994], and MnP activity has been found in essentially all lignin-degrading fungi that have been examined [Périé and Gold, 1991; Orth et al., 1993; Hatakka, 1994; Gold et al., 2000].

MnP from *P. chrysosporium* has been purified to homogeneity and characterized [Glenn and Gold, 1985; Glenn et al., 1986; Gold et al., 1989, 2000; Wariishi et al., 1992]. In addition, genomic and cDNA sequences of *P. chrysosporium* MnP isozymes *mnp1*, *mnp2*, and *mnp3* have been reported [Pease et

---

* Originally published in this or similar form in *Biochemistry* and used here with permission of the American Chemical Society.

Sollewijn Gelpke, M. D., Moënne-Loccoz, P., and Gold, M. H. (1999) Arginine 177 is involved in Mn(II) binding by manganese peroxidase. *Biochemistry* **38**, 11482–11489.

al., 1989; Pribnow et al., 1989; Godfrey et al., 1990; Mayfield et al., 1994a; Orth et al., 1994; Alic et al., 1997]. X-ray crystallographic studies and DNA sequence comparisons indicate that the heme environment of MnP is similar to that of other plant and fungal peroxidases [Pribnow et al., 1989; Edwards et al., 1993; Petersen et al., 1993; Kunishima et al., 1994; Sundaramoorthy et al., 1994; Schuller et al., 1996]. Spectroscopic studies have revealed that the heme iron of the native enzyme is in the ferric, high-spin, pentacoordinate state and is ligated to the proximal histidine [Mino et al., 1988; Banci et al., 1992; Sundaramoorthy et al., 1994]. Kinetic and spectroscopic characterization of the oxidized intermediates, MnP compounds I and II (MnPI and MnPII), indicate that the catalytic cycle of MnP is similar to that of horseradish peroxidase and LiP. However, MnP is unique in its ability to oxidize Mn^{II} to Mn^{III} [Dunford and Stillman, 1976; Glenn et al., 1986; Renganathan and Gold, 1986; Wariishi et al., 1988, 1989a, 1992; Gold et al., 1989). The reactions involved in the MnP catalytic cycle are:

$$MnP + H_2O_2 \rightarrow MnPI + H_2O$$
$$MnPI + Mn^{II} \rightarrow MnPII + Mn^{III}$$
$$MnPII + Mn^{II} \rightarrow MnP + Mn^{III} + H_2O$$

The enzyme-generated Mn^{III} is stabilized by organic acid chelators such as oxalate, which is secreted by the fungus [Wariishi et al., 1992; Kuan et al., 1993; Kishi et al., 1994]. The Mn^{III}–organic acid complex, in turn, oxidizes phenolic substrates such as lignin substructures [Tuor et al., 1992] and aromatic pollutants [Valli and Gold, 1991; Valli et al., 1992; Joshi and Gold, 1993].

Previously, we developed a homologous expression system for MnP isozyme 1 [Mayfield et al., 1994b] in which the *P. chrysosporium* glyceraldehyde-3-phosphate dehydrogenase (*gpd*) gene promoter is used to drive expression of the *mnp1* gene during primary metabolic growth when endogenous MnP is not expressed. This expression system has been used to produce and characterize mutants of Mn binding site ligands and of the heme cavity residue Phe190 [Kusters-van Someren et al., 1995; Kishi et al., 1996, 1997].

The MnP crystal structure [Sundaramoorthy et al., 1994] contains a unique Mn binding site involved in the oxidation of Mn^{II}. In this site, the single Mn atom is hexacoordinate, with carboxylate ligands from the heme propionate 6 and from amino acids Glu35, Glu39, and Asp179. The final two ligands are waters. When Glu35, Glu39, and Asp179 are mutated to their respective amides, a significant effect on the kinetics of Mn^{II} oxidation is observed, confirming that these residues are Mn binding ligands and that the proposed Mn binding site is the productive site [Kusters-van Someren et al., 1995; Kishi et al., 1996; Whitwam et al., 1997]. In addition to these amino acid ligands, Arg177 also appears to be a component of the Mn binding site [Sundaramoorthy et al., 1994]. The crystal structure shows that Arg177 forms a salt bridge with Glu35, orienting this ligand for efficient Mn binding [Sundaramoorthy et al., 1994]. In this study, we investigate the role of Arg177 in Mn^{II} oxidation using spectroscopic and kinetic analyses of two Arg177 mutants.

2.2 Materials and Methods

2.2.1 Organisms

P. chrysosporium wild-type strain OGC101, auxotrophic strain OGC107-1 (Ade1), and prototrophic transformants were maintained as described previously [Alic et al., 1990]. *Escherichia coli* DH5α was used for subcloning plasmids.

2.2.2 Construction of Transformation Plasmids

The R177A and R177K site-directed mutations were introduced into the plasmid pGM1 [Kusters-van Someren et al., 1995], which contains 1.1 kb of the *gpd* promoter fused to the *P. chrysosporium mnp1* gene at the translation start site. The PCR-based Quikchange (Stratagene) protocol was used for site-directed mutagenesis. A forward and reverse primer for each mutation was designed to change the CGC codon (Arg) to a GCC (Ala) or an AAG (Lys) codon. After the mutagenesis reactions, two plasmids, pGM11 and pGM12, containing the R177A and R177K mutations, respectively, were isolated, and the mutations were confirmed by sequencing. Subsequently, the *Xba*I–*Eco*RI fragments of pGM11 and pGM12,

containing the *gpd* promoter and the mutated *mnp1* genes, were subcloned into pOGI18 [Godfrey et al., 1994], a *P. chrysosporium* transformation plasmid, containing the *Schizophyllum commune ade5* gene as a selectable marker. This generated the *P. chrysosporium* transformation plasmids pAGM11 and pAGM12 for the R177A and R177K mutations, respectively. The *mnp1* coding sequences of pAGM11 and pAGM12, including the mutations, were verified by sequencing.

2.2.3 Transformation of *P. chrysosporium*

Protoplasts of the Ade$^-$ strain OGC107-1 were transformed as described previously [Alic et al., 1990], using 1 μg of linearized pAGM11 or pAGM12 as the transforming DNA. Prototrophic transformants were transferred to minimal medium slants to confirm adenine prototrophy and assayed for MnP activity using the *o*-anisidine plate assay described previously [Mayfield et al., 1994b]. Transformants exhibiting the highest activity on plates were purified by fruiting as described [Alic et al., 1987, 1990], and the progeny were rescreened for MnP activity by the plate assay. The purified transformants with highest MnP activity, AGM11 and AGM12, were selected for analysis.

2.2.4 Production and Purification of the MnP Mutant Proteins

Cultures of the selected transformants were maintained on slants and grown in liquid culture from conidial inocula [Mayfield et al., 1994b]. The MnP mutant proteins were purified from the extracellular medium of high-carbon and high-nitrogen (HCHN) liquid shake cultures, grown for 3 days at 28°C [Mayfield et al., 1994b]. For each mutant protein, 14 1-liter HCHN shake cultures in 2-liter flasks were filtered, and the extracellular fluid was pooled and concentrated by ultrafiltration. Subsequently, variant proteins were purified by Phenyl-Sepharose hydrophobic interaction, Blue Agarose affinity, and Mono Q anionic exchange column chromatography as described previously [Kishi et al., 1996]. Wild-type MnP was produced and isolated as described previously [Glenn and Gold, 1985; Wariishi et al., 1989a].

2.2.5 SDS-PAGE Analysis

Sodium dodecyl sulfate–polyacrylamide gel electrophoresis (SDS–PAGE) was performed using a 12% Tris-glycine gel system [Laemmli, 1970] and a Miniprotean II apparatus (Bio-Rad), and gels were stained with Coomassie blue.

2.2.6 Enzyme Assays and Spectroscopic Procedures

Electronic absorption spectra of the various oxidation states of the MnP enzymes and steady-state kinetic assays were recorded and conducted, respectively, at room temperature using a Shimadzu UV-260 spectrophotometer. The extent of Mn^{II} oxidation by MnP was measured by following the formation of the Mn^{III}–malonate complex at 270 nm (ϵ_{270} = 11.6 mM^{-1} cm^{-1}) [Wariishi et al., 1992]. The extent of oxidation of ferrocyanide was measured at 420 nm (ϵ_{420} = 1 mM^{-1} cm^{-1}) as described previously [Cheddar et al., 1989].

MnPI was prepared by mixing 1 equiv of H_2O_2 with the native enzyme in 20 mM potassium phosphate buffer (pH 6.0). MnPII was prepared by the successive addition of 1 equiv of ferrocyanide and 1 equiv H_2O_2 to the native enzyme in 20 mM potassium malonate buffer (pH 4.5). Enzyme concentrations were determined at 407 nm (ϵ_{407} = 129 mM^{-1} cm^{-1}) [Glenn and Gold, 1985].

2.2.7 Kinetic Analysis

Apparent K_m and k_{cat} values for Mn^{II} and H_2O_2 were calculated from double-reciprocal plots of the initial rate of Mn^{III}–malonate formation versus varying Mn^{II} or H_2O_2 concentrations. A double-reciprocal plot of the initial rate of ferricyanide formation versus substrate concentration was used to calculate the apparent K_m and k_{cat} values for ferrocyanide. Reaction mixtures (1 ml) contained H_2O_2 (0.1 mM), 0.5 μg of MnP for Mn^{II} oxidation or 5 μg of MnP for ferrocyanide oxidation, and varying concentrations of $MnSO_4$ (0.02–10 mM) or ferrocyanide (1–15 mM) in 50 mM potassium malonate (pH 4.5) (ionic strength μ = 0.1 M, adjusted with K_2SO_4). To determine apparent K_m values for H_2O_2, reactions were conducted in 5 mM $MnSO_4$.

Transient-state kinetic measurements were taken at 25°C using an Applied Photophysics stopped-flow reaction analyzer (SX.18MV) with sequential mixing and a

diode array detector for rapid scanning spectroscopy. The extent of MnPI formation was measured at 397 nm, the isosbestic point between compounds I and II. Native enzyme (2 μM) in 50 mM potassium malonate (pH 4.5) (ionic strength μ = 0.1 M, adjusted with K_2SO_4) was mixed with a 10–50-fold excess of H_2O_2 in the same buffer. For the reduction of MnPI, this oxidized state was prepared by premixing 4 μM enzyme in H_2O with 1 equiv H_2O_2. The reaction mixture was incubated for 4 s, and MnPI formation was confirmed by rapid scanning. Subsequently, Mn^{II} in 100 mM potassium malonate (pH 4.5), ferrocyanide, or 2,6-dimethoxyphenol (DMP) in 40 mM potassium malonate (pH 4.5), or bromide in 40 mM potassium succinate (pH 3.0) was added in a $\geq$10-fold molar excess. The extent of reduction of MnPI by Mn^{II} was measured at 417 nm, the isosbestic point between MnPII and native MnP. The two-step reduction of MnPI by ferrocyanide or DMP was assessed at 420 nm, the absorption maximum of MnPII. This two-phase reduction of MnPI started with the rapid reduction of MnPI followed by the slow reduction of MnPII in a single combined experiment. The direct two-electron reduction of MnPI to the native enzyme by bromide was followed at 407 nm [Sheng and Gold, 1997]. The reduction of MnPII by Mn^{II} was assessed at 407 nm, the Soret maximum of native enzyme. MnPII was prepared by premixing 4 μM enzyme and 1 equiv of ferrocyanide in 50 mM potassium malonate (pH 4.5) with 1 equiv H_2O_2 in the same buffer. This mixture was incubated for 5 s, and the formation of MnPII was confirmed by rapid scanning spectroscopy. Subsequently, MnPII was mixed with 0.5–10 mM Mn^{II} in the same buffer. All kinetic traces exhibited single-exponential character from which pseudo-first-order rate constants were calculated. Typically, five or six substrate concentrations were used in triplicate measurements.

2.2.8 Resonance Raman Spectroscopy

Resonance Raman (RR) spectra were obtained on a custom spectrograph consisting of a McPherson (Acton, MA) model 2061/207 monochromator operated at a focal length of 0.67 m and a Princeton Instruments (Trenton, NJ) LN1100 CCD detector with a model ST-130 controller. Laser excitation was from Coherent (Santa Clara, CA) Innova 302 krypton (413.1 nm) and Innova 90-6 argon (514.5 nm) lasers.

The laser lines were filtered through Applied Photophysics (Leatherhead, U.K.) prism monochromators to remove plasma emissions. The incident laser powers at the sample were ~20 (413.1 nm) and ~50 mW (514.5 nm). Spectra were collected in a 90°-scattering geometry from solution samples contained in glass capillary tubes at room temperature. Rayleigh scattering was attenuated by the use of Kaiser Optical (Ann Arbor, MI) super-notch filters. The spectral resolution was set to ~3.0 cm^{-1}. Indene and CCl_4 served as frequency and polarization standards, respectively. Optical absorption spectra of the Raman samples were obtained on a Perkin-Elmer Lambda 9 spectrophotometer to monitor sample integrity before and after laser illumination. Samples contained 100 μM MnP in 20 mM phosphate buffer (pH 6.0). Data were calibrated and analyzed with GRAMS/386 spectroscopic software (Galactic Industries Corp., Salem, NH).

2.2.9 Chemicals

Phenyl-Sepharose CL-4B, Cibacron Blue 3GA Agarose, potassium ferrocyanide, and H_2O_2 (30% solution) were obtained from Sigma. DMP was obtained from Aldrich and purified by silica gel column chromatography (the solvent being hexane/ethyl acetate) before use. All other chemicals were reagent grade. Solutions used for kinetic assays were prepared with HPLC-grade water obtained from Aldrich.

2.3 Results

2.3.1 Expression and Purification of the Mutant Enzymes

The *mnp1* coding sequences, including the mutations, of the *P. chrysosporium* transformation plasmids pAGM11 and pAGM12 were verified by DNA sequencing. Transformation of the Ade^- strain (OGC107-1) with linearized pAGM11 or pAGM12 resulted in the isolation of multiple transformants which exhibited MnP activity on the plate assay. For each mutant, five of these transformants were selected and purified by fruiting [Alic et al., 1987, 1990, 1991], and the colonies from single basidiospores were rescreened for MnP activity. From the purified isolates with MnP activity, one

isolate of each mutation was selected to obtain the strains AGM11 (R177A) and AGM12 (R177K). These transformant strains expressed extracellular recombinant MnP enzyme when grown in HCHN shake cultures at 28°C for 3 days, whereas endogenous MnP is not expressed under these conditions [Mayfield et al., 1994b]. The mutant MnPs were purified to homogeneity as determined by SDS-PAGE. The molecular masses of the mutant MnPs (46 kDa) were identical to those of recombinant wild-type MnP (rMnP) and wild-type MnP (wtMnP) [data not shown]. The yields of expressed mutant enzymes were comparable to those of rMnP [Mayfield et al., 1994b]. Typically, mutant enzymes were purified to R_z values of >5.

2.3.2 Spectral Properties of the MnP Mutant Enzymes

The optical absorption spectra of the native and oxidized intermediates, compounds I and II, for each of the MnP mutant enzymes were essentially identical to those of the wild-type enzyme (Table 2.1), suggesting the substitution of Ala or Lys for Arg177 does not significantly alter the heme environment of the protein.

2.3.3 Resonance Raman Spectroscopy

The high-frequency ($\sim$1300–1700 cm^{-1}) RR spectral regions that are characteristic of heme coordination and spin state are shown in panels A and B of Fig. 2.1 for Soret band (413.1 nm) and Q-band (514.5 nm) excitation, respectively. The relative intensities of the ν^3 and ν^{10} mode at 1482/1492 and 1612/1628 cm^{-1}, respectively, are consistent with a mixture of 6cHS and 5cHS heme species in wtMnP. The RR spectrum of wtMnP is identical to that described previously (Kishi et al., 1996). The RR spectra of the R177A and R177K mutant enzymes are essentially identical to that of the wtMnP enzyme. Only minor changes in intensities, but no frequency shifts, can be detected in the heme vibrational spectra. This suggests that the R177A and R177K mutations do not result in any significant perturbation of the heme moiety. The changes in the relative intensities of the ν^3 and ν^{10} bands for the mutants compared those of wtMnP suggest that a slightly greater portion of the hemes in the mutant protein may be in the 5cHS state.

Table 2.1

Absorbance Maxima of Native and Oxidized Intermediates of Wild-type and Mutant MnPs[a]

Enzyme	Native (nm)	Compound I (nm)	Compound II (nm)
wtMnP	407, 503, 637	403, 558, 649	420, 528, 555
R177A	407, 502, 638	400, 557, 648	420, 527, 555
R177K	407, 500, 639	400, 558, 648	420, 528, 556

[a] MnP compounds I and II were prepared as described in the text.

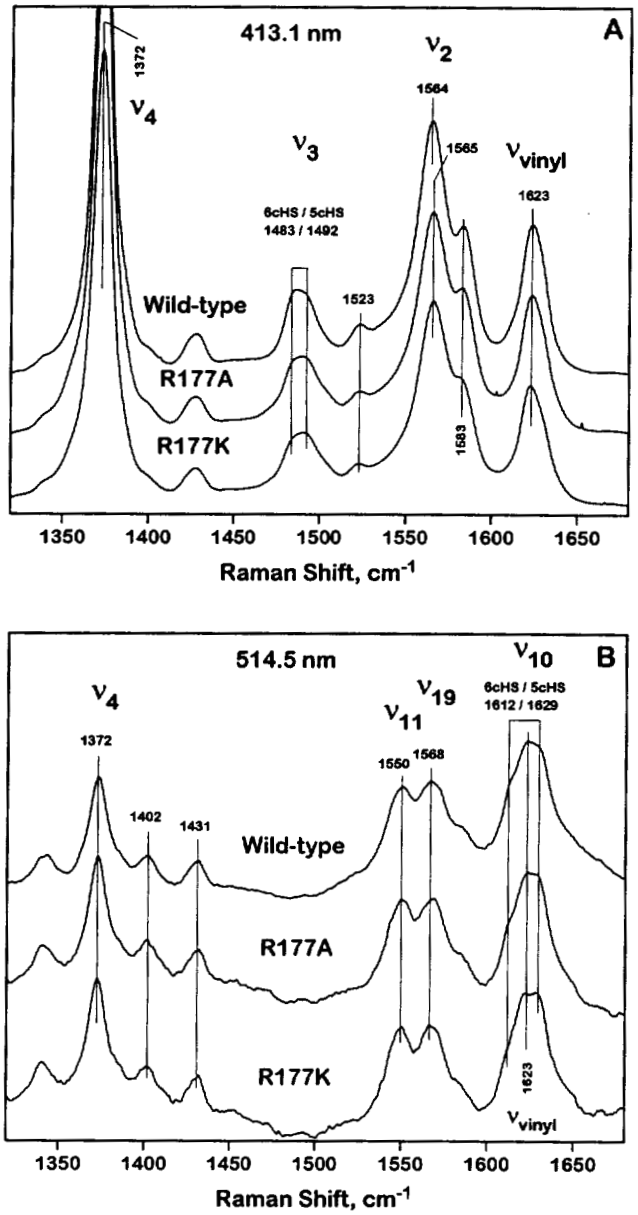

Fig. 2.1 Resonance Raman spectra of the wild-type and mutant enzymes R177A and R177K ($\sim$100 μM) in 20 mM sodium phosphate (pH 6.0). Resonance Raman spectra of MnP enzymes were obtained with (**A**) Soret excitation (413.1 nm, 20 mW, 90° scattering geometry, and ambient temperature) and (**B**) Q-band excitation (514.5 nm, 50 mW, 90° scattering geometry, and ambient temperature). Frequencies and assignments for selected heme bands are shown. Polarization data also were collected to support the assignments.

2.3.4 Steady-State Kinetics

Under steady-state conditions, linear double-reciprocal plots were obtained over a range of Mn^{II}, ferrocyanide, and H_2O_2 concentrations in 50 mM potassium malonate (pH 4.5) (ionic strength μ = 0.1 M, adjusted with K_2SO_4) for the mutant and wtMnP enyzmes. The apparent K_m values for Mn^{II}, ferrocyanide, and H_2O_2 and the apparent k_{cat} values for the Mn^{II} and ferrocyanide oxidation reactions are listed in Tables 2.2 and 2.3, together with the k_{cat}/K_m ratios. The apparent K_m and k_{cat} values of the Mn binding site mutant E35Q [Kishi et al., 1996] are included for comparison. The apparent K_m values for H_2O_2 and ferrocyanide, $\sim$50 μM and $\sim$20 mM, respectively, are similar for the wtMnP and the Arg177 mutant enzymes. Likewise, the k_{cat} values for Mn^{II} and ferrocyanide oxidation, 200–300 and $\sim$40 s^{-1}, respectively, are similar for wtMnP and the Arg177 mutant enzymes. In contrast, the apparent K_m values for Mn^{II} for the R177A and R177K variants are $\sim$20-fold higher than for wtMnP.

2.3.5 Formation of MnP Compound I

Rates of MnPI formation were determined in 50 mM potassium malonate (pH 4.5). We previously demonstrated that the rate of MnPI formation was not affected by the type or concentration of the organic acid chelator [Kishi et al., 1994]. The formation of MnPI was measured at 397 nm, and kinetic traces exhibited exponential character from which pseudo-first-order rate constants (k_{1obs}) were calculated. The k_{1obs} constants were linearly proportional to H_2O_2 concentrations at 10–50-fold excess [data not shown]. The second-order rate constants (k_{1app}) for MnPI formation were similar for wtMnP and the R177A and R177K mutant proteins (Table 2.4).

2.3.6 Reduction of MnP Compound I by Mn^{II}

The reduction of MnPI by Mn^{II} was assessed at the optimal pH of 4.5 at a wavelength of 417 nm, the isosbestic point between compound II and native MnP. The observed rate constants for wtMnP with excess Mn^{II} concentrations are too high to measure for Mn^{II} concentrations 30-fold greater than the enzyme concentration.

Table 2.2

Steady-State Kinetic Parameters for Wild-Type and Mutant MnPs[a]

Enzyme	Mn^{II}			H_2O_2		
	K_m (μM)	k_{cat} (s^{-1})	k_{cat}/K_m (M^{-1} s^{-1})	K_m (μM)	k_{cat} (s^{-1})	k_{cat}/K_m (M^{-1} s^{-1})
wtMnP	90	256	2.84×10^6	55	253	4.60×10^6
R177A	1.64×10^3	187	0.11×10^6	39	190	4.87×10^6
R177K	2.32×10^3	264	0.11×10^6	44	273	6.20×10^6
E35Q[b]	4.4×10^3	0.77	1.75×10^2			

[a] Reactions were carried out in 50 mM potassium malonate (pH 4.5). Apparent K_m and k_{cat} values for Mn^{II} were determined using 0.2 mM H_2O_2. Apparent K_m and k_{cat} values for H_2O_2 were determined using 5 mM Mn^{II}.
[b] From Kishi et al. [1996].

Table 2.3

Steady-State Kinetic Parameters for Wild-Type and Mutant MnPs for Ferrocyanide Oxidation[a]

Enzyme	K_m (mM)	k_{cat} (s^{-1})	k_{cat}/K_m (M^{-1} s^{-1})
WtMnP	21	38	1.8×10^3
R177A	26	42	1.6×10^3
R177K	16	37	2.2×10^3

[a] Reactions were carried out in 20 mM potassium malonate (pH 4.5). Apparent K_m and k_{cat} values for ferrocyanide were determined using 0.2 mM H_2O_2.

Therefore, the second-order rate constant for wtMnP was estimated to be $\sim 3 \times 10^7$ M^{-1} s^{-1} using low concentrations of Mn^{II}, conditions not obeying strict pseudo-first-order kinetics. In contrast, the k_{2obs} values for mutant MnPI reduction with 10–50-fold excess of Mn^{II} are measurable and linearly proportional to the Mn^{II} concentrations with a zero intercept, an indication of irreversible, second-order kinetics [data not shown]. Second-order rate constants (k_{2app}) for MnPI reduction are shown in Table 2.4. The k_{2app} values for the Arg177 mutant enzymes are $\sim$10-fold lower than the estimated k_{2app} for wtMnP.

2.3.7 Reduction of MnP Compound I by Bromide

The reduction of wtMnPI by bromide was recently described as a single, two-electron reduction from MnPI to native enzyme [Sheng and Gold, 1997]. The reduction of the R177K and R177A compounds I with various concentrations of Br^- was assessed at 407 nm and exhibited single-exponential character. As for wtMnP, the k_{2obs} were linearly proportional to the Br^- concentrations with a zero intercept, an indication of irreversible, second-order kinetics. The $k_{2'app}$ for wtMnP and both mutant MnPs were similar (Table 2.4).

2.3.8 Reduction of MnP Compounds I and II by Ferrocyanide and 2,6-Dimethoxyphenol

The reduction of MnPI and MnPII by ferrocyanide or DMP was assessed in a two-phase reaction at 420 nm. This is possible because MnPI reduction by these substrates is at least 100-fold faster than MnPII reduction. Exponential traces of MnPI reduction were used to obtain k_{2obs} values, which were linearly dependent on the substrate concentration for both ferrocyanide and DMP (Fig. 2.2). Apparent second-order rate constants, k_{2app}, are listed in Table 2.5. In contrast to the rates for the reduction of MnPI by Mn^{II}, the k_{2app} values for MnPI reduction by ferrocyanide or DMP were similar for the wild-type and mutant enzymes. The k_{3obs} values for MnPII reduction were also linearly proportional to various ferrocyanide and DMP concentrations used in reactions with both mutant and wtMnP enzymes [data not

Table 2.4

Transient-State Kinetic Parameters for MnPI Formation and Reduction

Enzyme	MnPI formation	MnPI reduction	
	H_2O_2[a] k_{1app} (M^{-1} s^{-1})	Mn^{II} [a] k_{2app} (M^{-1} s^{-1})	Bromide[b] $k_{2'app}$ (M^{-1} s^{-1})
wtMnP	$(6.35 \pm 0.06) \times 10^6$	$\sim 3 \times 10^7$	$(1.15 \pm 0.01) \times 10^3$
R177A	$(5.91 \pm 0.07) \times 10^6$	$(3.41 \pm 0.07) \times 10^6$	$(1.31 \pm 0.01) \times 10^3$
R177K	$(6.13 \pm 0.04) \times 10^6$	$(3.62 \pm 0.03) \times 10^6$	$(1.13 \pm 0.01) \times 10^3$

[a] Reactions were carried out in 50 mM potassium malonate (pH 4.5) (ionic strength 0.1 M).
[b] Reactions were carried out in 20 mM potassium succinate (pH 3.0).

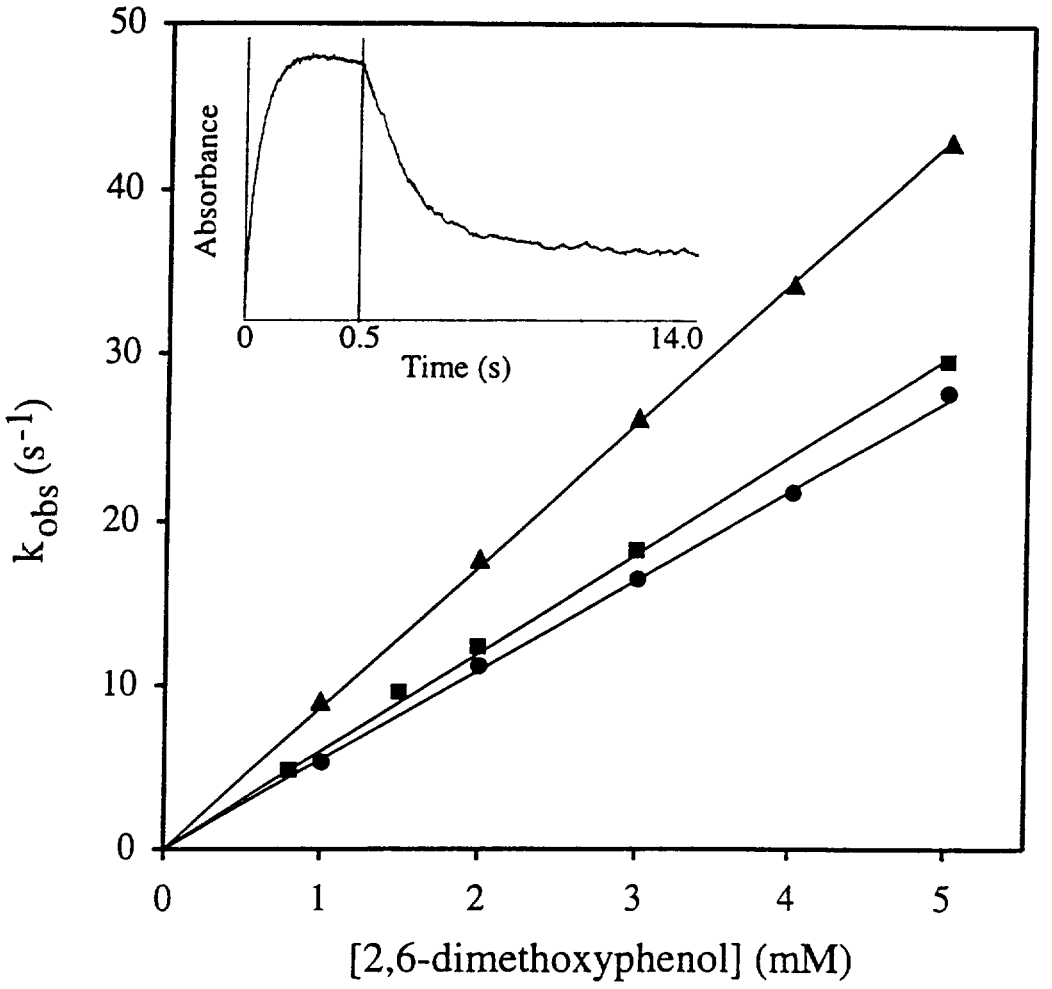

Fig. 2.2 Kinetics of MnPI reduction of wtMnP (•) and the R177A (■) and R177K (▲) mutants by DMP in 20 mM potassium malonate (pH 4.5). **Inset**: A typical trace at 420 nm of the reduction of 1 μM wild-type MnPI and subsequently of MnPII by DMP.

Table 2.5

Kinetic Parameters for the Reduction of MnPI and MnPII by Ferrocyanide and DMP[a]

Enzyme	Ferrocyanide		2,6-Dimethoxyphenol	
	MnPI reduction k_{2app} (M^{-1} s^{-1})	MnPII reduction k_{3app} (M^{-1} s^{-1})	MnPI reduction k_{2app} (M^{-1} s^{-1})	MnPII reduction k_{3app} (M^{-1} s^{-1})
wtMnP	$(1.33 \pm 0.03) \times 10^6$	$(1.80 \pm 0.09) \times 10^3$	$(5.12 \pm 0.07) \times 10^3$	60 ± 6
R177A	$(1.11 \pm 0.01) \times 10^6$	$(1.45 \pm 0.02) \times 10^3$	$(5.61 \pm 0.12) \times 10^3$	60 ± 1.3
R177K	$(2.43 \pm 0.03) \times 10^6$	$(6.63 \pm 0.08) \times 10^3$	$(8.82 \pm 0.10) \times 10^3$	366 ± 39

[a] Reactions were carried out in 20 mM potassium malonate (pH 4.5) (ionic strength of 0.1 M).

shown]. For ferrocyanide and DMP, the calculated k_{3app} values were similar for wtMnP and R177A MnPs (Table 2.5). However, for R177K, the apparent rate constants are ~2-fold higher for compound I and II reduction by ferrocyanide and ~6-fold higher for compound II reduction by DMP than those for the wild-type and R177A MnPs.

2.3.9 Reduction of MnP Compound II by Mn^{II}

The MnPII reduction by Mn^{II} is the rate-limiting step in the MnP catalytic cycle [Wariishi et al., 1988, 1989a; Kuan et al., 1993; Kishi et al., 1994]. The reduction of wild-type and mutant MnP compounds II to native enzyme was followed at 406 nm under pseudo-first-order kinetics, using an excess of Mn^{II}. The plots of the k_{3obs} versus Mn^{II} concentrations leveled off at higher Mn^{II} concentrations (Fig. 2.3). This can be explained by a binding interaction between reactants, according to eqs 1–3:

$$\text{MnPII} + \text{Mn}^{\text{II}} \overset{K_D}{\rightleftharpoons} \text{MnPII} - \text{Mn}^{\text{II}} \overset{k_3}{\rightarrow} \text{MnP} + \text{Mn}^{\text{III}} \quad (1)$$

$$k_{3obs} = k_3/(1 + K_D/[\text{Mn}^{\text{II}}]) \quad (2)$$

$$K_D = [\text{MnPI}][\text{Mn}^{\text{II}}]/[\text{MnPII} - \text{Mn}^{\text{II}}] \quad (3)$$

where k_3 is a first-order rate constant (s^{-1}) and K_D is a dissociation constant (M). The calculated values for the first-order rate constant and the dissociation constant are listed in Table 2.6. Values for the Mn binding site mutant, E35Q, are also listed for comparison. The rate constants k_3 are similar for the wild-type and Arg177 mutant MnPs. In contrast, the dissociation constants, K_D, for the mutant enzymes increased ~20–25-fold. As previously reported [Kishi et al., 1996], both the rate constant and binding constant are affected by the E35Q mutant (Table 2.6). The calculated apparent second-order rate constants, k_3/K_D, for the Arg177 mutant enzymes exhibit a ~30-fold decrease in the rate of reaction.

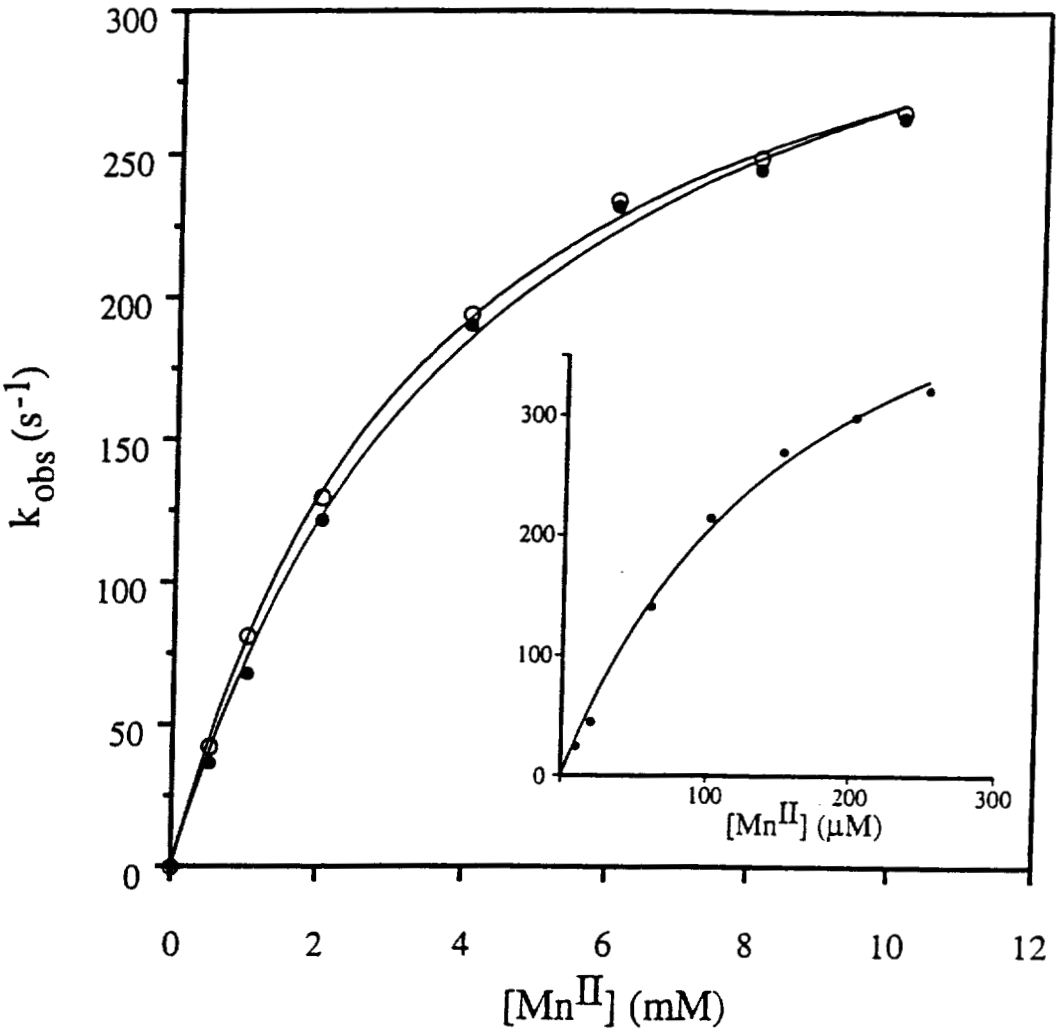

Fig. 2.3 Kinetics of compound II reduction of R177A (○) and R177K (•) by Mn^{II} in 20 mM potassium malonate (pH 4.5). **Inset:** The kinetics of compound II reduction of wild-type MnP in 20 mM potassium malonate (pH 4.5).

Table 2.6

Kinetic Parameters for the Reduction of MnPII by Mn^{II}[a]

Enzyme	k_3 (s^{-1})	K_D (μM)	k_{3app} (M^{-1} s^{-1})
wtMnP	$(5.5 \pm 0.4) \times 10^2$	$(1.7 \pm 0.2) \times 10^2$	3.30×10^6
R177A	$(3.6 \pm 0.06) \times 10^2$	$(3.5 \pm 0.17) \times 10^3$	0.10×10^6
R177K	$(3.8 \pm 0.12) \times 10^2$	$(4.2 \pm 0.3) \times 10^3$	0.09×10^6
E35Q[b]	0.69 ± 0.03	$(8.0 \pm 0.6) \times 10^3$	86.3

[a] Reactions were carried out in 20 mM potassium malonate (pH 4.5) (ionic strength 0.1M).
[b]From Kishi et al. [1996].

2.4 Discussion

Although the catalytic cycle of MnP is similar to that of other fungal and plant peroxidases, this enzyme is unique in that it oxidizes Mn^{II} to Mn^{III} [Dunford and Stillman, 1976; Glenn et al., 1986; Renganathan and Gold, 1986; Wariishi et al., 1988, 1989a, 1992; Gold et al., 1989]. The latter, complexed with an organic acid chelator, diffuses from the enzyme to oxidize the terminal phenolic substrate. The MnP crystal structure [Sundaramoorthy et al., 1994, 1997] indicates there is a cation binding site at the protein surface, consisting of the carboxylates of Asp179, Glu35, Glu39, and heme propionate 6. Mutagenesis studies with the Mn binding ligands, Asp179, Glu35, and Glu39, revealed the role of these ligands in Mn oxidation [Kusters-van Someren et al., 1995; Kishi et al., 1996]. All the Mn binding site mutants, which eliminated the carboxylic acid functional group, exhibit a significant decrease in the level of Mn binding and in the Mn^{II} oxidation rate. These studies indicate that MnP has a single Mn binding and oxidation site [Kusters-van Someren et al., 1995; Kishi et al., 1996; Sundaramoorthy et al., 1997; Whitwam et al., 1997].

In addition to the Mn ligands, Arg177 has been implicated in Mn binding. The crystal structure shows that Arg177 forms a salt bridge with Glu35, thereby orienting Glu35 for efficient Mn binding (Fig. 2.4) [Sundaramoorthy et al., 1994]. Furthermore, deduced amino acid sequence comparisons between several MnP and LiP enzymes from different fungi show that Arg177 is conserved within the MnPs but is replaced by an Ala in the LiPs [Gold et al., 2000].

The *P. chrysosporium* homologous gene expression system [Mayfield et al., 1994b] was used to express mutant genes under the control of the *gpd* gene promoter. Active, heme-containing mutant enzymes were secreted into the extracellular medium and were purified to homogeneity by a combination of chromatographic methods. The R177A and R177K enzymes were essentially identical to wtMnP with respect to chromatographic properties and molecular mass, suggesting that these mutations do not lead to significant conformational alterations of the variant proteins. The optical absorption spectral features of the ferric states and of the oxidized states (MnPI and

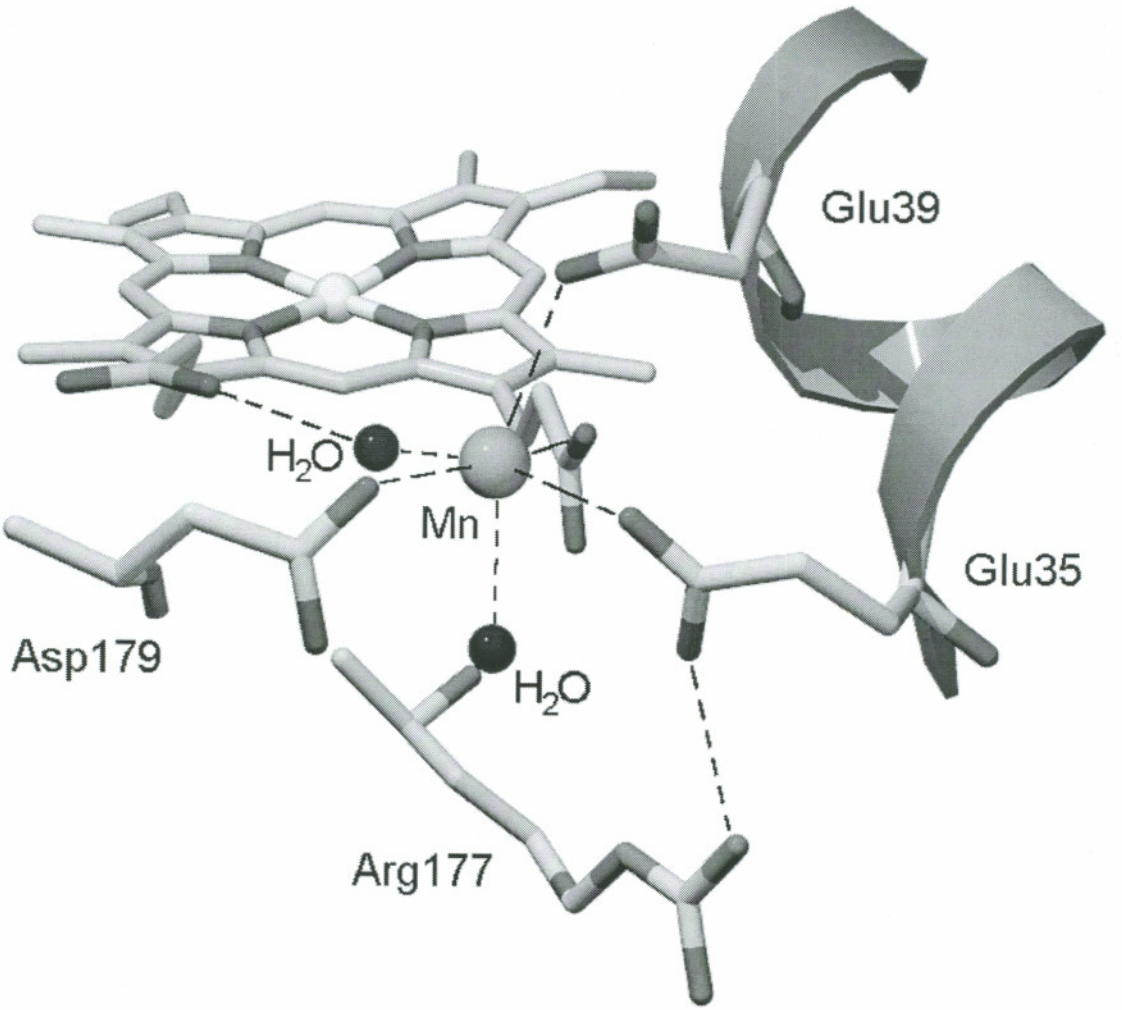

Fig. 2.4 Manganese binding site of manganese peroxidase [Sundaramoorthy et al., 1994].

MnPII) for the R177 variants were essentially identical to those of wtMnP, suggesting that the heme environment of MnP also is not altered significantly by these mutations.

Resonance Raman spectroscopy is well suited for the determination of coordination and spin states of hemes [Spiro, 1988]. In particular, the ν^3 and ν^{10} vibration modes are generally easily identified and, hence, serve as useful indicators. The ν^3 and ν^{10} bands (Fig. 2.1) indicate the coexistence of six-coordinate high-spin and five-coordinate high-spin (6cHS and 5cHS) heme species at room temperature. The mixture of species is consistent with the presence of a six-coordinate heme with water bound in equilibrium with a five-coordinate heme iron lacking a water ligand. In this study and in our previous study of Mn binding site mutants [Kishi et al., 1996], the ν^3 mode exhibits a slightly higher 5cHS versus 6cHS ratio for the mutant enzymes than wtMnP. Otherwise, our RR results indicate that the R177K and R177A mutations appear to have little or no effect on the structure and coordination state equilibrium of the heme, suggesting that the mutant proteins are produced without undergoing significant changes in either the overall structure or the heme environment.

In contrast to a negligible effect on spectroscopic properties, mutations at Arg177 significantly alter the kinetic properties of MnP. The apparent K_m values for oxidation of Mn^{II} by the mutant MnPs increase $\sim$20-fold compared to those of wtMnP, while the turnover numbers (k_{cat}) for the mutant enzymes remain similar to those of wtMnP. These data differ significantly from the kinetic results for the Mn binding site mutants [Kishi et al., 1996], where a 50-fold increase in K_m was accompanied by a 300-fold decrease in k_{cat} for the single mutants. This suggests that, unlike the Mn binding ligands, Arg177 is involved in binding of Mn^{II} but apparently not in electron transfer.

Transient-state kinetic analysis of the individual steps in the MnP catalytic cycle shows that these mutations have a significant effect on the reduction of the oxidized intermediates, MnPI and MnPII, by Mn^{II}. The apparent second-order rate constants (k_{2app}) for MnPI reduction in the mutant enzymes are decreased by $\sim$10-fold compared to those of wtMnP. This second-order constant combines the equilibrium dissociation constant and rate constant; however, we suggest that only the change in

binding of Mn^{II} to MnPI contributes to the decrease in k_{2app} with these mutant enzymes, based on steady-state kinetic analysis. The reduction of MnPII, the rate-limiting step in the catalytic cycle, exhibits saturation kinetics for both the wild-type and mutant MnPs. While the equilibrium dissociation constants, K_D, for the Arg177 mutants are ~22-fold higher than that for wtMnP, the first-order rate constants, k_3, are similar for the wild-type and mutant MnPs. This strongly suggests that the mutations mainly affect the binding of Mn^{II} to the enzyme but have little effect on the rate of electron transfer from the Mn^{II} to the oxidized heme intermediates.

The apparent rate constants for reduction of MnPI and MnPII by substrates apparently not oxidized at the Mn binding site, such as ferrocyanide, 2,6-dimethoxyphenol, and bromide, are similar for the wild-type and mutant MnPs. The K_m and k_{cat} values for the oxidation of ferrocyanide by MnP also are not affected by these mutations, indicating that neither ferrocyanide, phenol [Kishi et al., 1996], nor bromide [Sheng and Gold, 1997] oxidation is affected significantly by mutations at the Mn binding site. This suggests that these substrates neither bind nor are oxidized at this site. Furthermore, the mutations at Arg177 affect neither the K_m for H_2O_2 nor the rate of MnPI formation by H_2O_2, suggesting that neither binding nor reduction of H_2O_2 are significantly altered.

Our results indicate that Mn^{II} oxidation by MnP can be separated into at least two steps: the binding of Mn^{II} to the Mn binding site, followed by the electron transfer from Mn^{II} to the oxidized heme. Steady-state and transient-state kinetic experiments indicate that both Arg177 mutations affect the binding of Mn^{II} to the enzyme. The apparent K_m values increase ~20-fold, and the dissociation constants, K_D, for MnPII reduction increase ~22-fold for both the R177K and the R177A mutants. In particular, the transient-state kinetic measurements of MnPII reduction show that, while the mutants have a reduced ability to bind Mn^{II}, the first-order rate constants for the reduction of MnPII by Mn^{II} are similar for the wild-type and mutant MnPs, indicating that, once the Mn is bound, electron transfer proceeds efficiently regardless of the mutation at Arg177. Binding of Mn^{II} to the protein results in the hexacoordinate ligation of this metal with the probable lowering of the redox potential for Mn^{II} oxidation. Since the Mn^{II} binding ligands remain unchanged in the Arg177

mutants, the ligation geometry of Mn^{II} in the binding site in the presence of high Mn concentrations probably is unaffected. In fact, lack of change in the electron-transfer rates for the Arg177 variants suggests a lack of change in the redox potential between the mutant and wild-type enzymes. In contrast, mutation of a Mn ligand such as Asp179, Glu35, or Glu39 has been shown to affect the ligation geometry of the Mn^{II} binding site [Sundaramoorthy et al., 1997] and the electron-transfer rate. Indeed, electron transfer from Mn^{II} to the heme in the E35Q, E39Q, and D179N ligand mutants is much slower than for the wild type [Kishi et al., 1996], suggesting that the redox potential of the bound Mn in the latter variants is higher than that of Mn bound to wtMnP.

Crystallographic studies of the Mn ligand mutants suggest that Glu35 and Glu39 assume alternate conformations upon Mn^{II} binding, whereby the side chains of Glu35 and Glu39 swing out toward the protein surface, forming an open configuration in the absence of Mn^{II}, but adapt a closed configuration when Mn^{II} is bound [Sundaramoorthy et al., 1997]. The interaction between Arg177 and Glu35 may control this conformational change at the Mn binding site. Crystallographic studies with the D179N mutant [Sundaramoorthy et al., 1997] show that the R177–E35 bond is $\sim$2.81 Å long in the closed (Mn-occupied) structure, while in the open (Mn-unoccupied) structure, the distance increases to $\sim$4.39 Å. Breaking this salt bridge by mutation in R177A and R177K or in E35Q probably affects the ability of the enzyme to adopt the closed conformation upon Mn binding, resulting in an increase in the apparent Mn binding constant. Indeed, the results of this study show that disruption of the salt bridge between Arg177 and Glu35 by mutation of Arg177 results in a decrease in Mn^{II} affinity, indicating that this salt bridge is essential for Mn binding.

Several mutations of the Mn ligand, Glu35, have been reported, including E35Q [Kishi et al., 1996] which changes the carboxylate to an amide and E35D [Whitwam et al., 1997] which shortens the side chain of the ligand without changing the functional carboxylate group. Nevertheless, both mutations significantly affect both the binding of Mn^{II} and the rate of electron transfer from Mn^{II} to the oxidized heme. Since both mutations exhibit a decrease in the rate of electron transfer, the

ligation of Mn^{II} in the binding site is likely to be affected. This suggests, as confirmed in the crystal structure, that Arg177 may anchor the position of the carboxylate of Glu35 in the Mn^{II}-occupied closed configuration of the protein. Shortening the side chain of this residue by one methylene in the E35D mutant probably does not affect the salt bridge to Arg177, but it may restrain the carboxylate of this ligand from making a strong bond with the Mn^{II} atom, resulting in a disruption of the ligation for Mn^{II} and hence in the electron-transfer rate as observed [Whitwam et al., 1997]. Crystal structure analysis of these R177 and E35D mutant enzymes should reveal their ligation geometry. Additional, studies aimed at examining these possibilities are planned.

CHAPTER 3
ROLE OF ARGININE 177 IN THE Mn^{II} BINDING SITE OF MANGANESE PEROXIDASE: STUDIES WITH R177D, R177E, R177N, AND R177Q MUTANTS*

3.1 Introduction

White-rot basidiomycetous fungi are the only organisms capable of degrading the phenylpropanoid plant cell wall polymer, lignin, to CO_2 and H_2O (Buswell and Odier, 1987; Kirk and Farrell, 1987; Gold et al., 1989). These fungi are also able to degrade a variety of aromatic pollutants when cultured under ligninolytic conditions (Bumpus and Aust, 1987a; Hammel, 1989; Joshi and Gold, 1993; Reddy et al., 1998). During idiophasic growth, the best-studied lignin-degrading fungus, *Phanerochaete chrysosporium*, secretes two familes of extracellular peroxidases, lignin peroxidase (LiP) and manganese peroxidase (MnP), which constitute the major enzymatic components of its extracellular lignin-degrading system, along with an H_2O_2-generating system (Buswell and Odier, 1987; Kirk and Farrell, 1987; Gold and Alic, 1993; Hammel et al., 1993). Both LiP and MnP are able to depolymerize lignin *in vitro* (Wariishi et al., 1991b; Hammel et al., 1993; Bao et al., 1994), and the mechanisms of lignin model compound degradation by these enzymes have been studied (Hammel et al., 1985; Miki et al., 1986; Tuor et al., 1992; Higuchi, 1993; Lundell et al., 1993; Joshi and Gold, 1996).

---

* Originally published in this or similar form in the *European Journal of Biochemistry* and used here with permission of Blackwell Science Ltd.

Sollewijn Gelpke, M. D., Youngs, H. L., and Gold, M. H. (2000) Role of arginine 177 in the Mn^{II} binding site of manganese peroxidase. Studies with R177D, R177E, R177N, and R177Q mutants. *Eur. J. Biochem.* **267,** 7038–7045.

MnP from *P. chrysosporium* has been extensively characterized (Glenn and Gold, 1985; Glenn et al., 1986; Gold et al., 1989; Gold et al., 2000). The heme iron of the native enzyme is ferric, high-spin, and pentacoordinate with a proximal histidine ligand (Mino et al., 1988; Banci et al., 1992; Sundaramoorthy et al., 1994). Kinetic and spectroscopic characterization of the oxidized intermediates, MnP compounds I and II (MnPI and MnPII), indicate that the catalytic cycle of MnP is similar to that of horseradish peroxidase and LiP (Dunford and Stillman, 1976; Renganathan and Gold, 1986; Wariishi et al., 1988). However, MnP is unique in its ability to oxidize Mn^{II} to Mn^{III} (Glenn et al., 1986; Wariishi et al., 1988, 1992). The reactions involved in the MnP catalytic cycle are:

$$MnP + H_2O_2 \rightarrow MnPI + H_2O$$

$$MnPI + Mn^{II} \rightarrow MnPII + Mn^{III}$$

$$MnPII + Mn^{II} \rightarrow MnP + Mn^{III} + H_2O$$

The enzyme-generated Mn^{III} is stabilized by chelators such as malonate and oxalate, the latter of which is secreted by the fungus (Wariishi et al., 1992; Kuan et al., 1993; Kishi et al., 1994). The Mn^{III}–organic acid complex, in turn, oxidizes phenolic substrates such as lignin substructures and aromatic pollutants (Tuor et al., 1992; Joshi and Gold, 1993; Reddy et al., 1998), as well as radical mediators (Wariishi et al., 1989b; Bao et al., 1994).

Genomic and cDNA sequences of several MnP-encoding genes, including *P. chrysosporium* MnP isozymes *mnp1*, *mnp2*, and *mnp3*, have been reported (Pease et al., 1989; Pribnow et al., 1989; Gold and Alic, 1993; Alic et al., 1997; Gold et al., 2000). X-ray crystallographic studies and DNA sequence comparisons indicate that important catalytic residues in the heme pocket, including the proximal His173 and Asp242 and the distal His46, Arg42, Asn80, and Glu74, are conserved, indicating that the heme environment of MnP is similar to that of other plant and fungal peroxidases (Pribnow et al., 1989; Welinder, 1992; Edwards et al., 1993; Petersen et al., 1993; Sundaramoorthy et al., 1994; Schuller et al., 1996).

Crystallographic (Sundaramoorthy et al., 1994) and site-directed mutagenesis studies (Kusters-van Someren et al., 1995; Kishi et al., 1996; Whitwam et al., 1997) indicate that MnP contains a unique binding and oxidation site for Mn^{II}. In this site,

the single Mn atom is hexacoordinate, with two water ligands and four carboxylate ligands from heme propionate 6 and amino acids Glu35, Glu39, and Asp179. The crystal structure also suggests that Arg177 forms a salt-bridge with Glu35, thereby orienting this ligand for efficient Mn^{II} binding (Sundaramoorthy et al., 1994). Breaking this Arg177–Glu35 salt-bridge by mutations such as R177A and R177K (Sollewijn Gelpke et al., 1999) or E35Q (Kishi et al., 1996) probably affects the ability of the enzyme to adopt a closed conformation upon Mn^{II} binding (Sundaramoorthy et al., 1997), resulting in an increase in the apparent Mn^{II} binding constant. Indeed, disruption of the salt-bridge between Arg177 and Glu35 by mutation of Arg177 results in a decrease in Mn^{II} affinity. Herein, we elucidate the role of Arg177 using spectroscopic and kinetic analysis of four new Arg177 mutants. Unlike the mutants previously reported, both the electron transfer rate and Mn^{II} binding are affected in these new mutants.

3.2 Materials and Methods

3.2.1 Organisms

P. chrysosporium wild-type strain OGC101, auxotrophic strain OGC107-1 (Ade1), and prototrophic transformants were maintained as described previously (Alic et al., 1990). *Escherichia coli* DH5α was used for subcloning plasmids.

3.2.2 Construction of Transformation Plasmids

The R177D, R177E, R177N, and R177Q site-directed mutations were introduced separately into the plasmid pGM1 (Kusters-van Someren et al., 1995), which contains 1.1 kb of the glyceraldehyde-3-phosphate dehydrogenase promoter (*gpd*) fused to the *P. chrysosporium mnp1* gene at the translation start site. The PCR-based Quikchange (Stratagene) protocol was used for site-directed mutagenesis. Forward and reverse primers were designed for each mutagenesis reaction. Following these reactions, four plasmids, pGM-RD, pGM-RN, pGM-RE, and pGM-RQ, containing the R177D, R177N, R177E, and R177Q mutations, respectively, were isolated. The complete *mnp1* coding sequences, including the mutations, were

verified by sequencing. Subsequently, the *Xba*I-*Eco*RI fragments of the mutant pGM plasmids, containing the *gpd* promoter and the mutated *mnp1* genes, were subcloned into pOGI18 (Godfrey et al., 1994), a *P. chrysosporium* transformation plasmid containing the *Schizophyllum commune ade*5 gene as a selectable marker, generating the *P. chrysosporium* transformation plasmids pAGM-RD, pAGM-RN, pAGM-RE, and pAGM-RQ for the R177D, R177N, R177E, and R177Q mutations, respectively.

3.2.3 Transformation of *P. chrysosporium*

Protoplasts of the Ade$^-$ strain OGC107-1 were transformed as described previously (Alic et al., 1990), using 1 μg of linearized pAGM-RD, pAGM-RN, pAGM-RE, or pAGM-RQ as transforming DNA. Prototrophic transformants were transferred to minimal medium slants to confirm adenine prototrophy and assayed for MnP activity using the *o*-anisidine plate assay described previously (Mayfield et al., 1994). Transformants exhibiting the highest activity on plates were purified by fruiting as described (Alic et al., 1987, 1990), and the progeny were rescreened for MnP activity by the plate assay. For each mutation, the purified transformant with highest MnP activity was selected for further analysis.

3.2.4 Production and Purification of the MnP Mutant Proteins

The selected transformants were grown from conidial inocula at 37°C in high-carbon and high-nitrogen (HCHN) liquid stationary cultures, containing 0.2% tryptone, for 2 days (Mayfield et al., 1994). For each mutant protein, 14 1-liter HCHN shake cultures in 2-liter flasks, inoculated with homogenized mycelium from one liquid stationary culture, were grown for 3 days at 28°C (Mayfield et al., 1994). The extracellular medium of HCHN liquid shake cultures was concentrated by hollow-fiber ultrafiltration (10-kDa cutoff, Amicon). Subsequently, the proteins were purified by phenyl-Sepharose hydrophobic interaction, Blue Agarose affinity, and Mono Q anion-exchange column chromatography as described previously (Kishi et al., 1996). Wild-type MnP (wtMnP) was produced and isolated as described previously (Glenn and Gold, 1985; Wariishi et al., 1989a; Youngs et al., 2000).

3.2.5 SDS-PAGE Analysis

Sodium dodecyl sulfate-polyacrylamide gel electrophoresis (SDS-PAGE) was performed using a 12% Tris-glycine gel system and a Miniprotean II apparatus (Bio-Rad), and gels were stained with Coomassie blue.

3.2.6 Enzyme Assays and Spectroscopic Procedures

Electronic absorption spectra of the various oxidation states of the MnP enzymes and steady-state kinetic assays were recorded at room temperature using a Shimadzu UV-260 spectrophotometer. The extent of Mn^{II} oxidation by MnP was measured by following the formation of the Mn^{III}–malonate complex at 270 nm (ϵ_{270} = 11.6 mM^{-1} cm^{-1}) (Wariishi et al., 1992). MnPI was prepared by mixing 1 equiv of H_2O_2 with the native enzyme in water. MnPII was prepared by the successive addition of 1 equiv of ferrocyanide and 1 equiv of H_2O_2 to the native enzyme in 20 mM potassium malonate buffer (pH 4.5). Enzyme concentrations were determined using ϵ_{406} = 129 mM^{-1} cm^{-1} (Glenn and Gold, 1985). H_2O_2 concentrations were determined using ϵ_{240} = 43.6 M^{-1} cm^{-1} (Kulmacz, 1986).

3.2.7 Kinetic Analysis

Steady-state kinetic constants for Mn^{II} oxidation were calculated from double reciprocal plots of the initial rate of Mn^{III}–malonate formation versus varying Mn^{II} or H_2O_2 concentrations. Reaction mixtures (1 ml) contained 0.1 mM H_2O_2, 0.5 μg of wtMnP or 2 μg of mutant MnP, and varying concentrations of $MnSO_4$ (0.02–10 mM) in 50 mM potassium malonate (pH 4.5) (ionic strength μ = 0.1 M, adjusted with K_2SO_4). To determine apparent K_m values for H_2O_2, reactions were conducted using 10 mM $MnSO_4$, 0.5 μg of wtMnP or 2 μg of mutant MnP, and varying concentrations of H_2O_2 (10–100 μM) in 50 mM potassium malonate (pH 4.5) (μ = 0.1 M).

Transient-state kinetic measurements were conducted at 25 $\pm$ 0.1°C, using an Applied Photophysics stopped-flow reaction analyzer (SX.18 MV) with sequential mixing and a diode array detector for rapid scanning spectroscopy. The extent of MnP compound I formation was measured at 397 nm, the isosbestic point between compounds I and II. Native enzyme (2 μM) in 50 mM potassium malonate (pH 4.5)

(μ = 0.1 M), was mixed with a 10- to 50-fold excess of H_2O_2 in the same buffer. For the reduction of MnPI, this oxidized state was prepared by premixing 4 μM enzyme in H_2O with 1 equiv of H_2O_2. The reaction mixture was incubated for 4 s, and MnPI formation was confirmed by rapid scanning. Subsequently, Mn^{II} in 50 mM potassium malonate (pH 4.5) or ferrocyanide in 20 mM potassium malonate (pH 4.5), or bromide in 20 mM potassium succinate (pH 3.0) was added in a $\geq$10-fold molar excess. Succinate was used as the buffer in the bromide oxidations because these reactions do not require a chelator. Furthermore, pH 3.0 is the optional pH for bromide oxidation [Sheng and Gold, 1997]. The reduction of MnPI by Mn^{II} or ferrocyanide was measured at 417 nm, the isosbestic point between MnPII and native MnP. The direct two-electron reduction of MnPI to the native enzyme by bromide was followed at 407 nm (Sheng and Gold, 1997). The reduction of MnPII by Mn^{II} or ferrocyanide was also measured at 407 nm, the Soret maximum of the native enzyme. MnPII was prepared by premixing 4 μM enzyme and 1 equiv of ferrocyanide in 20 mM potassium malonate (pH 4.5), with 1 equiv of H_2O_2 in the same buffer. This mixture was incubated for 5 s, and the formation of MnPII was confirmed by rapid scanning spectroscopy. Subsequently, MnPII was mixed with 0.025–10 mM Mn^{II} in 50 mM potassium malonate (pH 4.5), or MnPII was mixed with 0.05–1 mM ferrocyanide in 20 mM potassium malonate (pH 4.5). All kinetic traces displayed single exponential character from which pseudo-first-order rate constants were calculated. Typically, five or six substrate concentrations were used in triplicate measurements.

3.2.8 Protein Modeling

Atomic coordinates of the MnP crystal structure (Sundaramoorthy et al., 1994) were obtained from the Protein Data Bank (PDB entry 1MNP). The coordinates of Arg177 were replaced by an initial set of coordinates for each specific amino acid, using the Swiss-PdbViewer v3.51 software (Glaxo Wellcome Experimental Research), to create a set of coordinates for the R177D, E, N, Q, and K mutants. These mutant data sets were then subjected to energy minimization routines using the Sculpt (MDL Information Systems, Inc.) and GROMOS96 (Biomos, University of Groningen)

simulation packages, to optimize the orientations of the introduced side chains. The resulting sets of coordinates were re-examined with the Swiss-PdbViewer software by generating a superimposed view of the wild-type and mutated Mn^{II} binding sites.

3.2.9 Chemicals

Phenyl-Sepharose CL-4B, Cibacron Blue 3GA agarose, potassium ferrocyanide, and H_2O_2 30% (w/w) solution were obtained from Sigma. All other chemicals were reagent grade. Solutions used for kinetic assays were prepared with HPLC-grade water obtained from Aldrich.

3.3 Results

3.3.1 Expression and Purification of the Mutant Enzymes

The *P. chrysosporium* homologous expression system (Mayfield et al., 1994) was used to express the mutant MnP enzymes R177D, R177E, R177N, and R177Q in the extracellular medium of HCHN shake cultures. The expression constructs for each of the mutant enzymes were used to transform the Ade^- strain (OGC107-1) (Alic et al., 1990), resulting in the isolation of multiple transformants. These transformants were examined by the plate assays [Mayfield et al., 1994; Kishi et al., 1996] for MnP activity. Basidiospores of each transformant exhibiting maximal activity were further purified, and one isolate for each mutation was selected to obtain the strains AGM-RD, AGM-RN, AGM-RE, and AGM-RQ. These transformant strains expressed extracellular recombinant MnP enzyme when grown in HCHN shake cultures at 28°C for 3 days, conditions under which endogenous MnP is not expressed (Mayfield et al., 1994).

The mutant MnP enzymes were purified to homogeneity as determined by SDS-PAGE. The molecular masses of the mutant MnPs (46 kDa) were identical to those of recombinant wild-type MnP (rMnP) and wild-type MnP (wtMnP) [data not shown]. The yields of expressed mutant enzymes were similar to those of rMnP (Mayfield et al., 1994). Typically, mutant enzymes were purified to R_z values of >5.

3.3.2 Spectral Properties of the MnP Mutant Enzymes

The optical absorption spectra of the native and oxidized intermediates, compound I and II, for each of the R177E mutant enzymes were essentially identical to those of the wild-type enzyme (Fig. 3.1). The other mutants exhibited identical absorption spectra [data not shown], suggesting that substitution of Asp, Glu, Asn, or Gln for Arg177 does not significantly alter the heme environment of the protein.

3.3.3 Steady-State Kinetics

Under steady-state conditions, initial reaction rates of Mn^{II} oxidation by each mutant enzyme were determined for a range of Mn^{II} and H_2O_2 concentrations in 50 mM potassium malonate (pH 4.5). Double-reciprocal plots were used to determine the apparent K_m and k_{cat} values for Mn^{II} and H_2O_2 (Table 3.1) and the catalytic efficiency (k_{cat}/K_m) ratios. The apparent K_m and k_{cat} values for the binding site mutants R177A, R177K (Sollewijn Gelpke et al., 1999) and E35Q (Kishi et al., 1996) are included for comparison. The k_{cat} values for Mn^{II} oxidation by the R177D, E, N, and Q mutants were ~10-fold lower than those of the wtMnP and the R177A and R177K variants (Sollewijn Gelpke et al., 1999). The apparent K_m values for Mn^{II} for the R177D, E, N, and Q mutants (~3 mM) were similar to those of the R177A and K mutants and were ~30-fold higher than that of wtMnP. None of the Arg177 mutations have an effect on the catalytic efficiency (k_{cat}/K_m) with respect to the reduction of H_2O_2 under steady-state conditions.

3.3.4 Formation of MnP Compound I

The kinetic traces for MnP compound I formation by the mutant and wild-type MnP enzymes exhibited exponential character from which pseudo-first-order rate constants (k_{1obs}) were calculated. The k_{1obs} values were linearly proportional to H_2O_2 concentrations at 10- to 50-fold excess [data not shown]. The apparent second-order rate constants (k_{1app}) for MnPI formation were similar for wtMnP and the R177D, E, N, and Q mutant proteins (Table 3.2), indicating that the mutations do not affect the reduction of H_2O_2, in agreement with the steady-state results.

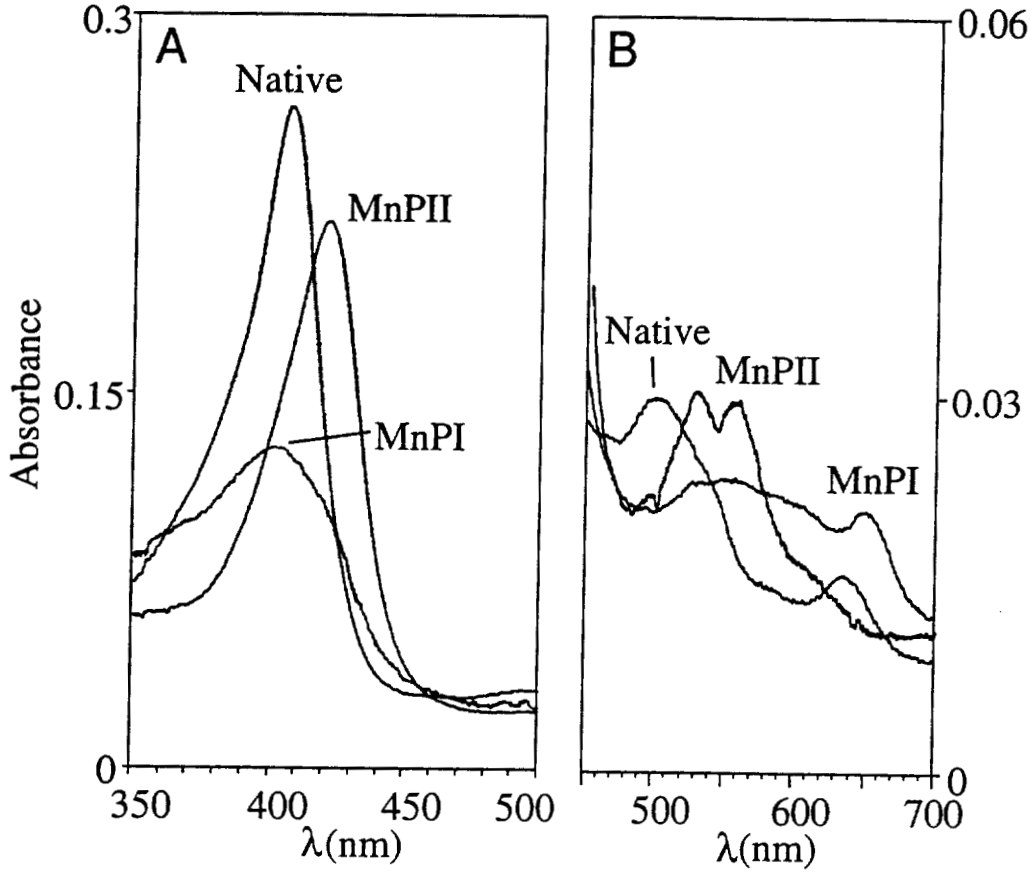

Fig. 3.1 Absorption spectra of the native state and oxidized intermediates, MnPI and MnPII, for 2 μM of the R177E mutant enzyme, showing the Soret peak between 350 and 500 nm (**A**), and the visible region between 450 and 700 nm (**B**). MnPI and MnPII were prepared as described in the text.

Table 3.1

Steady-State Kinetic Parameters for Mn^{II} Oxidation by wtMnP and Mutant Enzymes[a]

Enzyme	Mn^{II}			H_2O_2		
	K_m (mM)	k_{cat} (s^{-1})	k_{cat}/K_m (M^{-1} s^{-1})	K_m (μM)	k_{cat} (s^{-1})	k_{cat}/K_m (M^{-1} s^{-1})
wtMnP[b]	0.09	256.00	2.84×10^6	55.0	253.0	4.60×10^6
R177D	2.15	30.20	1.40×10^4	12.6	28.8	2.28×10^6
R177N	3.61	34.60	9.58×10^3	12.1	35.8	3.00×10^6
R177E	3.90	25.50	6.54×10^3	5.7	17.3	3.04×10^6
R177Q	2.91	25.00	8.59×10^3	7.8	23.2	2.97×10^6
R177A[b]	1.64	184.00	1.12×10^5	39.0	190.0	4.87×10^6
R177K[b]	2.32	262.00	1.13×10^5	44.0	273.0	6.20×10^6
E35Q[c]	4.40	0.77	1.75×10^2			

[a] Reactions were carried out in 50 mM potassium malonate (pH 4.5). Apparent K_m and k_{cat} values for Mn^{II} were determined using 0.2 mM H_2O_2. Apparent K_m and k_{cat} values for H_2O_2 were determined using 10 mM Mn^{II}.
[b] From Sollewijn Gelpke et al. [1999].
[c] From Kishi et al. [1996].

Table 3.2

Apparent Second-Order Rate Constants for MnP Compound I Formation[a]

Enzyme	k_{1app} (M^{-1} s^{-1})
wtMnP[b]	6.49×10^6
R177D	5.09×10^6
R177N	5.59×10^6
R177E	5.80×10^6
R177Q	5.62×10^6
R177A[b]	5.77×10^6
R177K[b]	6.12×10^6

[a] MnPI formation was followed at 397 nm, the isosbestic point between MnPI and MnPII. Reactions were performed in 50 mM potassium malonate (pH 4.5) (ionic strength of 0.1 M), using 1 μM enzyme.
[b] From Sollewijn Gelpke et al. [1999].

3.3.5 Reduction of MnP Compound I

The reduction of MnPI was assessed using Mn^{II}, ferrocyanide and bromide as substrates. The observed rate constants (k_{2obs}) were too high to measure accurately for Mn^{II} concentrations 30-fold higher than the enzyme concentration. Therefore, the second-order rate constant for wtMnP was estimated to be $\sim 3 \times 10^7$ M^{-1} s^{-1} using low concentrations of Mn^{II}, conditions not obeying strict pseudo-first-order kinetics [data not shown]. However, k_{2obs} values for the reduction of the Arg177 mutant enzymes by Mn^{II} were measurable under pseudo-first-order conditions, using a 10- to 100-fold excess of Mn^{II}. The k_{2obs} values were linearly proportional to the Mn^{II} concentrations with zero intercepts, indicating irreversible second-order kinetics (Fig. 3.2). The apparent second-order rate constants (k_{2app}) for the Arg177 mutant enzymes were $\sim$10- to 20-fold lower than the estimated k_{2app} value for wtMnP and were $\sim$2-fold lower than the k_{2app} values for the R177A and R177K mutant MnPs (Table 3.3).

Reduction of MnPI by substrates which do not bind at the Mn^{II} binding site were also examined. Rates for the single two-electron reduction of MnPI to native enzyme were assessed at various concentrations of bromide (Sheng and Gold, 1997) for each Arg177 mutant and for wtMnP at pH 3.0. The individual traces exhibited an exponential character, and the observed rate constants ($k_{2'obs}$) for wtMnP and Arg177 mutant enzymes were linearly proportional to the bromide concentrations with zero intercepts (Fig. 3.3). The apparent second-order rate constants ($k_{2'app}$) were similar for wtMnP and all the Arg177 mutant enzymes (Table 3.3). The rate of MnPI reduction by various ferrocyanide concentrations also was measured. k_{2obs} values were linearly proportional to the ferrocyanide concentration for each mutant enzyme, and the k_{2app} values were similar for the wild-type and mutant enzymes (Table 3.3).

3.3.6 Reduction of MnP Compound II

The reduction of MnPII for the wild-type and mutant MnPs by Mn^{II} was examined under pseudo-first-order conditions. Exponential traces were obtained and used to calculate the observed rate constants (k_{3obs}) for wtMnP and the R177D, E, N, and Q mutant enzymes. The plots of the k_{3obs} values versus Mn^{II} concentrations yield

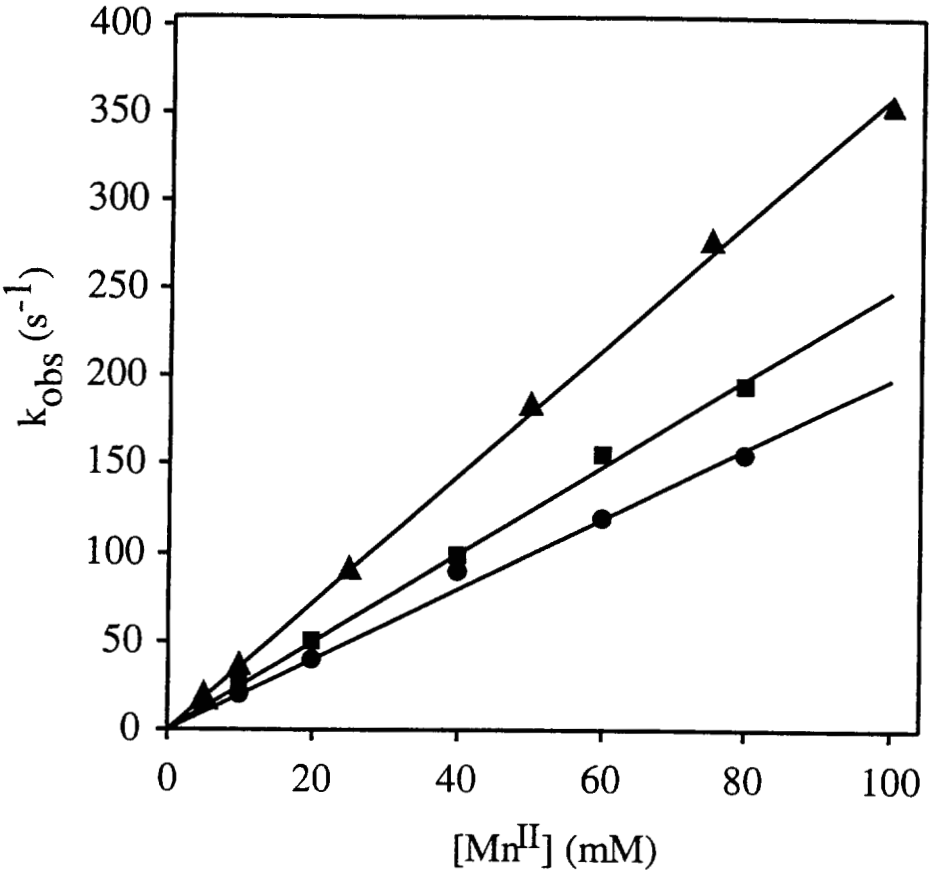

Fig. 3.2 Kinetics for MnPI reduction of R177K (▲), R177E (■) and R177Q (•) by Mn^{II} in 50 mM potassium malonate (pH 4.5), indicating irreversible second-order kinetics for the one-electron reduction of MnPI to MnPII by Mn^{II}.

Table 3.3

Apparent Second-Order Rate Constants for the Reduction of MnPI by Mn^{II}, Bromide, and Ferrocyanide[a]

Enzyme	Mn^{II}	Bromide	Ferrocyanide
	k_{2app} (M^{-1} s^{-1})	$k_{2'app}$ (M^{-1} s^{-1})	k_{2app} (M^{-1} s^{-1})
wtMnP	$\sim 3 \times 10^{7}$ [b]	2.4×10^{3}	1.3×10^{6} [b]
R177A	3.4×10^{6} [b]	2.6×10^{3}	1.1×10^{6} [b]
R177K	3.6×10^{6} [b]	2.3×10^{3}	2.4×10^{6} [b]
R177N	3.0×10^{6}	2.0×10^{3}	1.0×10^{6}
R177D	1.4×10^{6}	2.4×10^{3}	1.1×10^{6}
R177E	2.4×10^{6}	2.9×10^{3}	1.3×10^{6}
R177Q	1.8×10^{6}	2.2×10^{3}	1.1×10^{6}

[a] The reduction of MnPI by Mn^{II} or ferrocyanide was performed in 50 mM or 20 mM potassium malonate (pH 4.5) (ionic strength 0.1 M), respectively. Compound I reduction by bromide was performed in 20 mM potassium malonate (pH 3.0).

[b] From Sollewijn Gelpke et al. [1999].

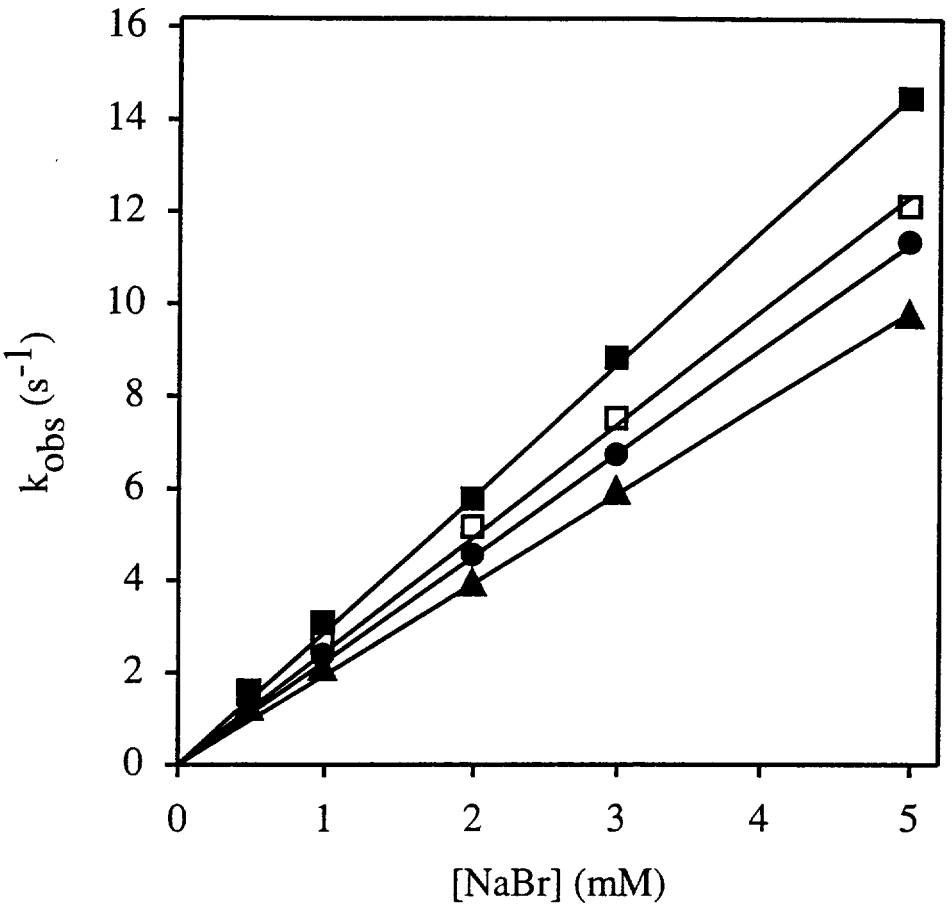

Fig. 3.3 Kinetics for MnPI reduction of wtMnP (□), R177K (▲), R177E (■), and R177Q (•) by bromide (NaBr) in 20 mM sodium succinate (pH 3.0), indicating second-order kinetics for this single two-electron reduction of MnPI to native enzyme.

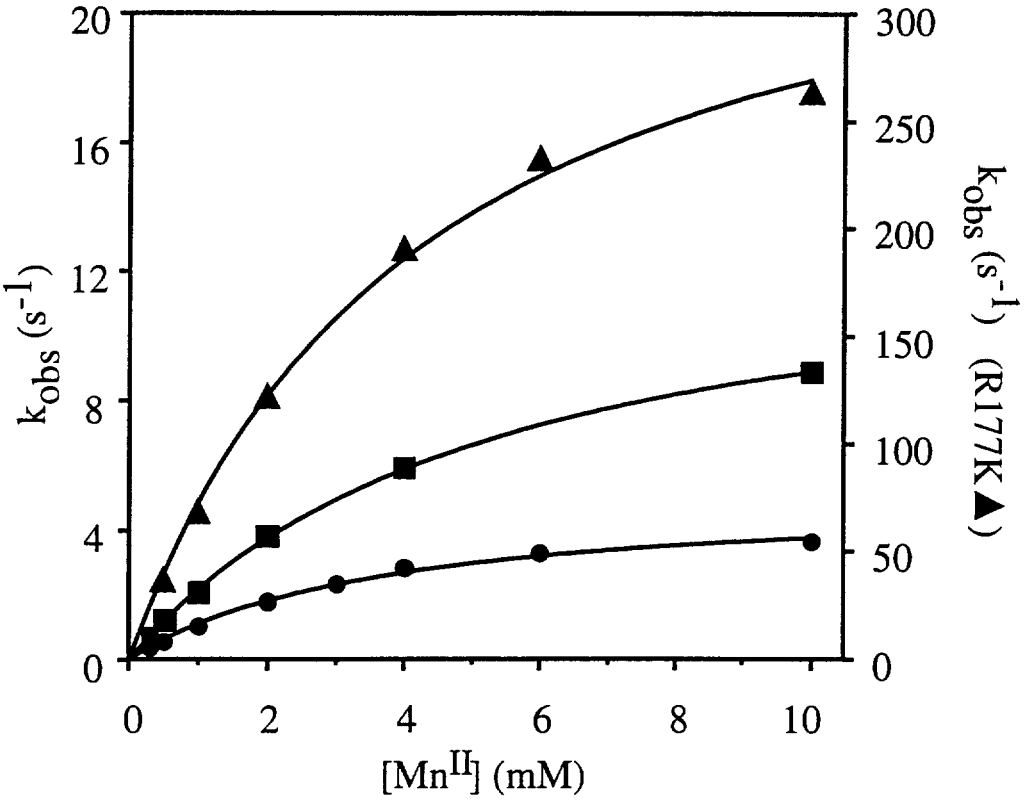

Fig. 3.4 Kinetics for MnPII reduction of R177K (■), R177E (▲), and R177Q (•) by Mn^{II} in 50 mM potassium malonate (pH 4.5), showing saturation kinetics.

rectangular hyperbolae (Fig. 3.4), indicating the accumulation of an enzyme-substrate complex of MnPII and Mn^{II}, with a dissociation constant (K_D). The complex undergoes a subsequent first-order reaction to native MnP and Mn^{III}, with a first-order rate constant (k_3) (Kishi et al., 1994). The values for k_3 and K_D of wild-type and Arg177 mutant enzymes were calculated using a nonlinear least squares fit to the data and are listed in Table 3.4. The k_3 values for the R177D, E, N, and Q mutant enzymes were ~15- to 90-fold lower than those of the wtMnP and R177A and K mutant enzymes. However, the K_D values were similar among the Arg177 mutant enzymes, exhibiting a ~30-fold increase compared to the wtMnP. The calculated apparent second-order rate constants (k_{3app}) for MnPII reduction in the R177D, E, N, and Q mutant enzymes decreased ~10^3-fold compared to wtMnP and ~50-fold compared to the R177A and R177K variants.

The rate of reduction of MnPII by ferrocyanide, which does not bind at the Mn^{II} binding site (Kishi et al., 1996), was assessed in 20 mM potassium malonate (pH4.5). The k_{3obs} values were linearly proportional to the ferrocyanide concentration indicating second-order kinetics. The k_{3app} values for MnPII reduction by ferrocyanide in each of the mutants were similar to that of wtMnP (Table 3.4).

3.4 Discussion

Although the catalytic cycle of MnP is similar to that of other fungal and plant peroxidases, this enzyme is unique in its ability to efficiently oxidize Mn^{II} to Mn^{III} (Glenn et al., 1986; Wariishi et al., 1988, 1992; Gold et al., 1989). The latter, complexed by an organic acid chelator, diffuses from the enzyme to oxidize the terminal substrate, lignin. Crystallographic (Sundaramoorthy et al., 1994, 1997) and mutagenesis studies of MnP (Kusters-van Someren et al., 1995; Kishi et al., 1996; Whitwam et al., 1997) demonstrate a cation binding site at the protein surface, consisting of the carboxylates of Asp179, Glu35, Glu39, and heme propionate 6. Mutations of these ligands, D179N, E35Q, and E39Q, which eliminate the carboxylic acid functional group, significantly decrease Mn^{II} binding and oxidation rates. Thus,

Table 3.4

Kinetic Parameters for MnPII Reduction by Mn^{II} and Ferrocyanide[a]

Enzyme	Mn^{II}		Ferrocyanide	
	k_3 (s^{-1})	K_D (mM)	k_{3app} (M^{-1} s^{-1})	k_{3app} (M^{-1} s^{-1})
wtMnP[b]	550.0	0.17	3.3×10^6	1.8×10^3
R177A[b]	360.0	3.50	1.0×10^5	1.5×10^3
R177K[b]	380.0	4.20	0.9×10^5	6.6×10^3
R177D	10.3	5.70	1.8×10^3	1.3 x 10^3
R177N	42.4	5.80	7.3×10^3	1.4×10^3
R177E	11.9	4.40	2.7×10^3	1.3×10^3
R177Q	5.9	4.80	1.3×10^3	1.1×10^3

[a] MnPII reduction by Mn^{II} or ferrocyanide was performed in 50 mM or 20 mM potassium malonate (pH 4.5) (ionic strength 0.1 M), respectively, using 1 μM enzyme.
[b] From Sollewijn Gelpke et al. [1999].

these ligands form the functional Mn^{II} oxidation site in MnP (Kusters-van Someren et al., 1995; Kishi et al., 1996; Sundaramoorthy et al., 1997).

In addition to the Mn^{II} ligands, Arg177 has been implicated in Mn^{II} binding. Deduced amino acid sequence comparisons of several MnP and LiP enzymes from different white-rot fungi show that Arg177 is conserved within MnPs but is replaced by an Ala in LiP enzymes (Gold et al., 2000). Previous mutagenesis studies, using steady-state and transient-state kinetics, show that the binding of Mn^{II} to the active site is decreased in the R177A and R177K mutant proteins. However, the rates of Mn^{II} oxidation by these mutants in the presence of excess Mn^{II} remain unchanged (Sollewijn Gelpke et al., 1999). The crystal structure of wtMnP suggests that Arg177 forms a salt-bridge with Glu35, thereby orienting Glu35 for efficient Mn^{II} binding (Sundaramoorthy et al., 1994). Crystallographic studies of the Mn^{II} ligand mutants (Sundaramoorthy et al., 1997) suggest that Glu35 and Glu39 assume alternate conformations upon Mn^{II} binding. The side chains of Glu35 and Glu39 apparently swing out toward the protein surface, forming an open configuration in the absence of Mn^{II}, but adapt a closed configuration when Mn^{II} is bound. The disruption of the Arg177–Glu35 salt-bridge by the R177A and R177K mutations resulted in a decreased Mn^{II} affinity, possibly by affecting the ability of the enzyme to adopt the closed conformation upon Mn^{II} binding (Sollewijn Gelpke et al., 1999). However, because the electron transfer rates were unaffected by the R177A and R177K mutations, it is likely that when Mn^{II} is bound, the Mn^{II} coordination and binding site geometries of R177A and R177K are similar to those of wtMnP.

In the present study, we further investigate the role of Arg177 in MnP by characterizing four additional mutant proteins: R177D, R177E, R177N, and R177Q. The purified, homologously expressed R177D, E, N, and Q variants were essentially identical to wtMnP with respect to chromatographic properties and molecular mass, suggesting that these mutations do not result in overall structural alterations in the variant proteins. The spectroscopic features of the ferric and the oxidized states (MnPI and MnPII) for the Arg177 variants also were essentially identical to those of wtMnP, suggesting that the heme environments of the mutant MnPs are not significantly altered (Fig. 3.1).

The kinetic properties for the reduction of H_2O_2 were probably not affected by the mutation of Arg177. Under steady-state conditions, the k_{cat} and k_{cat}/K_m are two fundamental constants which vary independently, while the K_m is the ratio of these two. Here, the k_{cat} values for the oxidation of Mn^{II} decrease, which results in a decrease of K_m values for H_2O_2 in such a way that the Arg177 variant catalytic efficiency (k_{cat}/K_m) values for H_2O_2 exhibit no change compared to wtMnP, indicating that the reactions of H_2O_2 with the mutant enzymes are unaffected by their mutations. Furthermore, k_{1app} values for the MnPI formation were similar for the mutant and wild-type MnPs, indicating that the R177D, E, N, and Q mutations do not affect the binding of H_2O_2 or the oxidation of the enzyme by H_2O_2.

Rates for reduction of the oxidized intermediates of the R177D, E, N, and Q variants by ferrocyanide or bromide, substrates which do not bind to and are not oxidized at the Mn^{II} binding site (Kusters-van Someren et al., 1995; Kishi et al., 1996; Sollewijn Gelpke et al., 1999), were similar to those of wtMnP. The single two-electron reduction of MnPI by bromide exhibited second-order kinetics (Sheng and Gold, 1997) with k_{2app} values that were similar for the wild-type and all the Arg177 mutant MnPs. The reduction of both MnPI and MnPII by ferrocyanide also exhibited second-order kinetics. The apparent second-order rate constants for the Arg177 variants were similar to those of wtMnP. Together, these results indicate that mutations of Arg177 do not affect binding of ferrocyanide or bromide, nor do they affect reduction of enzyme intermediates by these substrates.

In contrast to the negligible effect on spectroscopic properties, and reactivity of the enzyme towards the substrates H_2O_2, ferrocyanide, and bromide, the new mutations at Arg177 significantly alter the kinetic properties of Mn^{II} oxidation by MnP. The steady-state kinetic analysis of Mn^{II} oxidation showed that the apparent K_m values for Mn^{II} of the R177D, E, N, and Q mutants were $\sim$30-fold higher than those of wtMnP and were similar to those of R177A and R177K mutants. The apparent k_{cat} values for the oxidation of Mn^{II} under steady-state conditions decreased by $\sim$10-fold for the R177D, E, N, and Q mutants compared to wtMnP. These decreased k_{cat} values contrast with those of the R177A and R177K variants determined previously

(Sollewijn Gelpke et al., 1999) where the k_{cat} values were similar to the wild-type enzyme. These steady-state results indicate that, in addition to affecting Mn^{II} binding, the R177D, E, N, and Q mutations significantly affect the rate of electron transfer.

Transient-state kinetic analysis of the individual steps in the MnP catalytic cycle indicate that the rates of compound I and compound II reduction by Mn^{II} were significantly decreased in these four Arg177 variants compared to those of wtMnP. The second-order rate constants for compound I reduction of R177D, E, N, and Q by Mn^{II} were $\sim$10- to 20-fold lower than those of wtMnP and were $\sim$2-fold lower than those of R177A and K (Table 3.3). These second-order rate constants combine the first-order rate constant and equilibrium dissociation constants; therefore, it is difficult to calculate independent changes in either binding or electron transfer. However, saturation kinetics were observed for the reduction of MnPII, enabling separate determination of binding constants and electron transfer rates.

The K_D values for Mn^{II} binding to MnPII of the R177D, E, N, and Q mutants were similar to those of the R177A and K mutant enzymes, each exhibiting a $\sim$30-fold increase compared to that of wtMnP. The k_3 values of the Arg177 mutants produced in this study exhibited a $\sim$15- to 90-fold decrease compared to that of wtMnP, while the k_3 values of R177A and K mutants were similar to those of wtMnP. Previous work with MnP mutants suggested that MnPII reduction can be separated into two steps: those affecting binding of Mn^{II} to the Mn^{II} binding site (Sollewijn Gelpke et al., 1999) and those affecting both binding and electron transfer from Mn^{II} to the oxidized heme (Kishi et al., 1996). Our previous study with the R177A and R177K mutants indicated that disruptions of the salt-bridge between Arg177 and Glu35 by selected mutations of the Arg177 residue resulted in a decrease in Mn^{II} affinity without affecting the electron transfer rates, suggesting that this salt-bridge is important for Mn^{II} binding (Sollewijn Gelpke et al., 1999). In the present study, both steady-state and transient-state kinetic results indicate that the R177D, E, N, and Q mutations also reduce Mn^{II} binding. The apparent K_m values and the dissociation constants for the current mutants increased by a factor similar to those for R177A and R177K, suggesting that Mn^{II} binding to the enzyme is similarly disrupted, independent of the mutation introduced.

Binding of Mn^{II} to the wild-type protein results in the hexacoordinate ligation of the metal (Sundaramoorthy et al., 1994) with a probable concomitant lowering of the redox potential for Mn^{II} oxidation. Mutation of the Mn^{II} ligands affects the ligation geometry of the Mn^{II} binding site (Sundaramoorthy et al., 1997) and the electron transfer rate (Kusters-van Someren et al., 1995; Kishi et al., 1996; Whitwam et al., 1997). The present study shows that, in addition to reduced Mn^{II} binding, the R177D, E, N, and Q mutants exhibit reduced electron transfer rates. Furthermore, the decrease in the k_3 values for compound II reduction appears to be affected by the type of mutation that is introduced. The R177D and R177E mutations, both introducing a carboxylate functional group, exhibit a $\sim$50-fold decrease in k_3 value. In contrast, the k_3 value decreases $\sim$90-fold in the R177Q mutant but decreases only $\sim$15-fold for the R177N mutation, where an amide functional group is introduced. The introduced carboxylate functional group could act as an additional ligand, possibly displacing other ligand amino acid side chains or a ligating water. An additional carboxylate group also introduces an extra negative charge at the Mn^{II} binding site which may repel the three acidic amino acid ligands. It also may introduce possible disruption or addition of H-bonding interactions. An amide functional group may also introduce additional H-bonding interactions to the Mn^{II} binding site, possibly disturbing the orientation or flexibility of the amino acid ligands. In addition, the increase in size of the mutant amide side chains, from Asn to Gln, results in an additional decrease in electron transfer rate, possibly because Gln protrudes further into the Mn^{II} binding site. However, a size increase of the mutant acidic side chains apparently has no additional effect on the electron transfer rate. In contrast, the R177K or R177A mutations apparently do not inhibit electron transfer. The methyl side chain of Ala is most likely too small to have an effect on the interaction of the Mn^{II} binding site ligands with bound Mn^{II}. The positively charged butylammonium side chain of Lys is similar in charge and size to that of Arg, indicating that the Lys side chain may adopt an orientation similar to the side chain of the original Arg and as a result does not interfere with the coordination geometry of the bound Mn^{II} with its binding site ligands.

The exact conformation of the mutant R177 residues and the resulting changes in ligation geometry would be revealed by crystal structure analysis. Preliminary molecular modeling of the R177D, E, N, Q, A, and K mutant enzyme structures provides some indication as to the geometries of the mutant Mn^{II} binding sites. Superimposed views of the wild-type Mn^{II} binding site and energy minimized R177E and K (Fig. 3.5) and R177D, N, Q, and A (not shown) mutant Mn^{II} binding sites show that the side chains of the R177D, E, N, and Q mutants protrude into the Mn^{II} binding site, although to different extents. In contrast, the R177K mutant side chain yields an optimized conformation that aligns with the original Arg side chain. These simulations suggest that the mutant side chains of the R177A and R177K variants apparently do not disturb the Mn^{II} binding site geometry of the Mn^{II} saturated proteins, whereas the side chains of the R177D, E, N, and Q mutants probably disrupt the optimal Mn^{II} binding geometry, in agreement with the kinetic results.

In summary, the R177D, E, N, and Q variants used in this study exhibit reduced Mn^{II} binding efficiency and reduced electron transfer rates, suggesting a disruption in the Arg177–Glu35 salt-bridge and suggesting a higher redox potential for the enzyme-bound Mn^{II} in these mutants. In contrast, the lack of change in the electron transfer rates of R177A and R177K mutants suggests that the redox potential is not altered for those mutants when Mn^{II} is bound. These kinetic and molecular modeling results suggest that the side chains of these four mutant residues may disturb the orientation or position of one or more of the Mn^{II} ligands, preventing the formation of the optimal Mn^{II} coordination and ligation geometry.

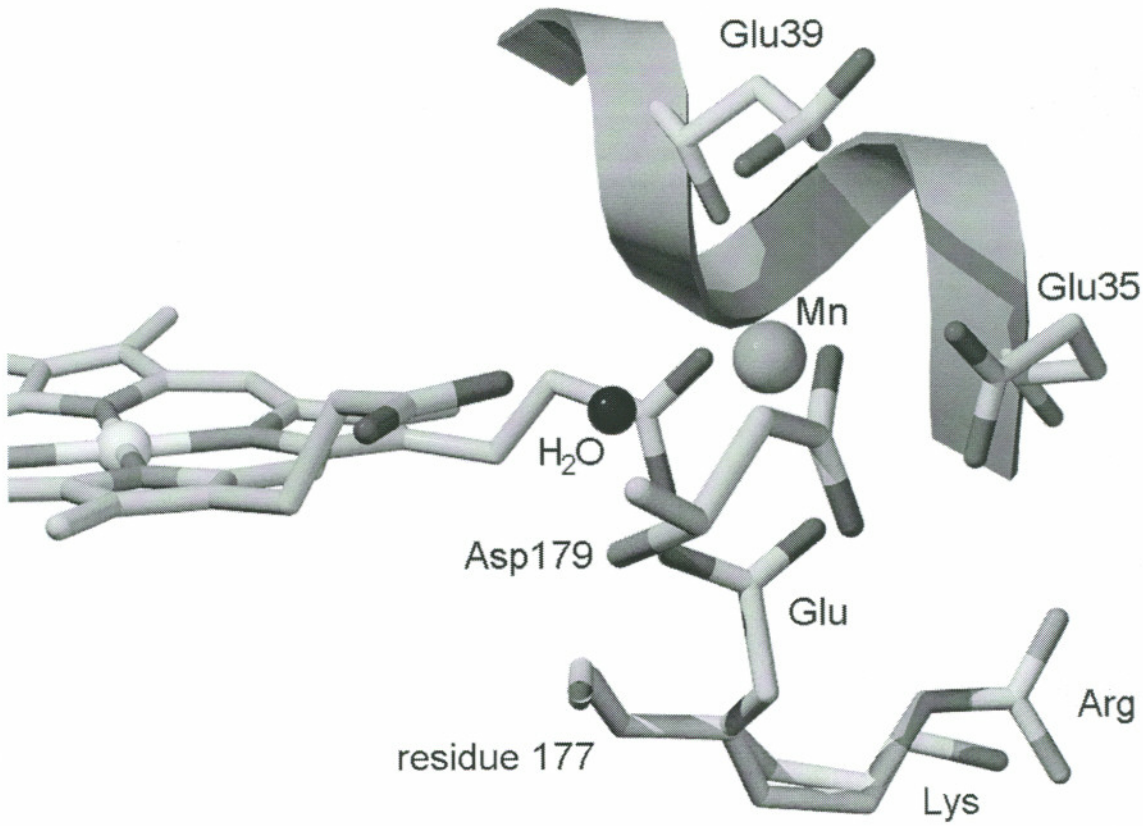

Fig. 3.5 Manganese binding site of MnP (Sundaramoorthy et al., 1994), with the modeled R177E and R177K mutant Mn^{II} binding site superimposed on that of wtMnP.

CHAPTER 4

HOMOLOGOUS EXPRESSION OF RECOMBINANT LIGNIN PEROXIDASE IN *PHANEROCHAETE CHRYSOSPORIUM*[*]

4.1 Introduction

The white-rot basidiomycete *Phanerochaete chrysosporium* has been the focus of numerous studies on the degradation of lignin [Buswell and Odier, 1987; Kirk and Farrell, 1987; Gold et al., 1989] and aromatic pollutants [Bumpus and Aust, 1987b; Hammel, 1992]. Two peroxidases, manganese peroxidase (MnP) and lignin peroxidase (LiP), along with an extracellular H_2O_2-generating system, are thought to be the major extracellular components of the lignin-degrading system [Kirk and Farrell, 1987; Gold and Alic, 1993; Hammel et al., 1993] of this organism. Both MnP and LiP occur as a series of isozymes encoded by a family of genes which are expressed under secondary metabolic growth conditions [Gold and Alic, 1993; Cullen, 1997; Gettemy et al., 1998]. The major isozymes, MnP1 (H3) and LiPH8 have been characterized in detail [Gold and Alic, 1993], and the X-ray structures of MnP1 [Sundaramoorthy et al., 1994] and LiPH8 [Piontek et al., 1993; Poulos et al., 1993] have been reported. In addition, a homologous expression system [Mayfield et al., 1994b] and several heterologous expression systems for MnP have been established [Stewart et al., 1996; Whitwam and Tien, 1996], allowing structure-function studies of mutant MnPs [Kishi et al., 1996, 1997; Whitwam et al., 1997]. In contrast, to date the efficient expression of active recombinant LiPH8 has not been achieved. The

---

[*] Originally published in this or similar form in *Applied and Environmental Microbiology* and used here with permission of the American Society for Microbiology.

Sollewijn Gelpke, M. D., M. Mayfield-Gambill, G. P. L. Cereghino, and M. H. Gold. (1999) Homologous expression of recombinant lignin peroxidase in *Phanerochaete chrysosporium*. *Appl. Environ. Microbiol.* **65**, 1670–1674.

use of *Escherichia coli* as a LiP expression host has resulted in expression; however, refolding of denatured LiP from *E. coli* inclusion bodies resulted in the isolation of active rLiPH8 [Doyle and Smith, 1996] and rLiPH2 [Nie et al., 1998] in relatively low yield. In addition, neither isozyme was glycosylated and, in one case, the recombinant protein contained seven extra N-terminal amino acids [Doyle and Smith, 1996)]

In this paper, we report the first successful homologous expression of rLiPH8 in *P. chrysosporium* and the characterization of the recombinant enzyme.

4.2 Materials and Methods

4.2.1 Organisms

P. chrysosporium wild-type strain OGC-101 [Alic et al., 1987], auxotrophic strain OGC316-7 (Ura11) [Akileswaran et al., 1993], and prototrophic transformants where maintained as described previously [Alic and Gold, 1985]. *E. coli* DH5α/F′ was used for subcloning of plasmids.

4.2.2 Construction of the Ura Transformation Plasmid

A 1.5-kb blunt-ended *Bsp*MI–*Eco*RI fragment of pEF1 [Froeliger et al., 1989; Akileswaran et al., 1993], containing the *Schizophyllum commune ura1* gene, was ligated into the blunt-ended EcoO109 site of pUC18 (GibcoBRL) to obtain pUB. This *P. chrysosporium* transformation plasmid contains the complete pUC18 plasmid and the full *S. commune ura1* coding region, including 200 bp of the promoter region.

4.2.3 Construction of pUGL

The promoter from the *P. chrysosporium gpd* gene [Mayfield et al., 1994b] and the *P. chrysosporium lip2* gene [Ritch and Gold, 1992] were fused at their TATA box sites and subcloned into the multiple cloning site of pUB. The 1.1-kb *gpd* promoter fragment was prepared by PCR using Vent DNA Polymerase (Biolabs, Inc.), pAGM1 [Mayfield et al., 1994b] as the template, a forward primer (5′-

AATTAACCCTCACTAAAGGG) 1.15 kb upstream of the *gpd* translation start site, and a reverse primer (5′-AAGGTTTTCGTCATCGATTGG) starting immediately 5′ of the *gpd* TATA box. The *lip2* fragment was prepared by PCR, using a forward primer (5′-TATAAAAGGGACGATGCG) from and including the *lip2* TATA box and a reverse primer (5′-TCACGCAGAAAGCATCC) within the coding region of *lip2* with pLH8 [Ritch and Gold, 1992] as the template. The *gpd* promoter PCR fragment was cut with *Xba*I at a site 55 bp from the 5′ end. The *lip2* coding region PCR fragment was cut with *Xho*I 25 bp upstream of the 3′ end. Both fragments were phosphorylated and then subcloned into Bluescript II SK-*Xba*I–*Hin*dIII, together with a 1-kb *Xho*I–*Hin*dIII coding region fragment from pLH8 [Ritch and Gold, 1992] in a four-fragment ligation, to create a blunt junction between the *gpd* promoter fragment and the *lip* PCR fragment, to obtain pGL1. Subsequently, the 3.0-kb *Xba*I–*Kpn*I fragment from pGL1 encompassing the *gpd* promoter and the *lip2* gene was subcloned into pUB to obtain the pUGL expression vector (Fig. 4.1). The ligation sites and newly synthesized coding sequence were verified by sequencing.

4.2.4 Transformation of the *P. chrysosporium* Uracil Auxotroph Ura11

Protoplasts of *P. chrysosporium* Ura11 were transformed with *Eco*RI-linearized pUGL or pUB as described previously [Alic et al., 1991; Akileswaran et al., 1993]. Prototrophic transformants were transferred to minimal medium, screened, and purified by isolating single basidiospores [Alic et al., 1987, 1991].

4.2.5 Screening for Expression of Recombinant LiP Isozyme H8 (rLiPH8)

Conidia from slants of pUGL prototrophic transformants were used to inoculate 25 ml of high-carbon high-nitrogen (HCHN) medium [Kirk et al., 1978] containing 2% glucose, 20 mM sodium 2,2-dimethyl succinate, 24 mM ammonium tartrate, and 3 mM veratryl alcohol (VA) at pH 4.5 in stationary flasks. After 3 days at 28°C, the extracellular medium was assayed periodically for LiP activity with the diammonium 2,2′-azinobis(3-ethylbenzothiazoline-6-sulfonate) (ABTS) assay [Glenn and Gold, 1985] using 0.1 mM H_2O_2 and 0.5 mM VA.

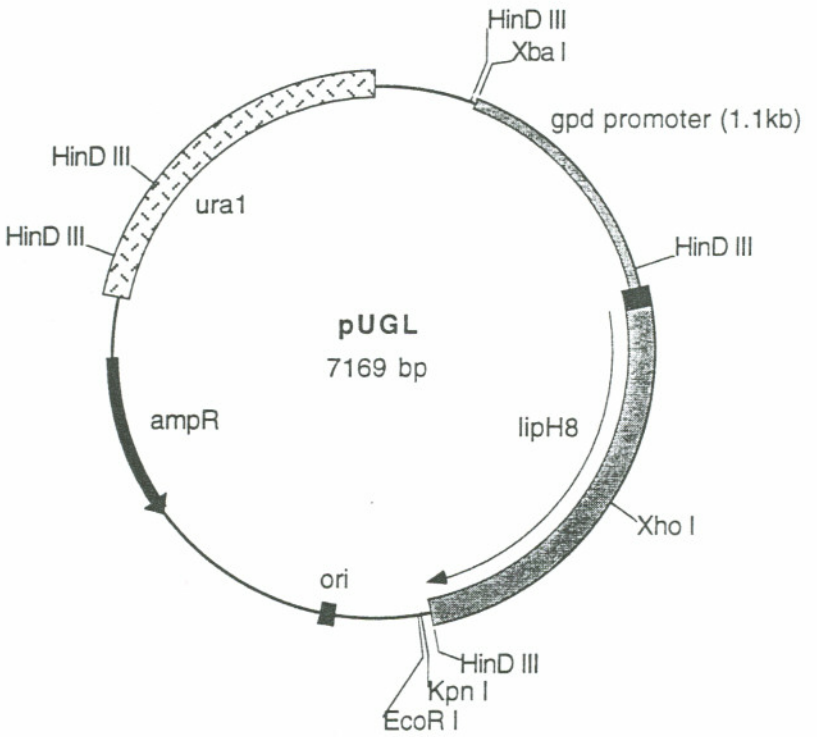

Fig. 4.1 Restriction map of the LiPH8 expression vector pUGL, containing the *ura1* gene and the *gpd* promoter fused to the *lip* gene at their TATA box sites.

4.2.6 Production of rLiPH8

Selected pUGL transformants were grown for 2 days at 37°C from conidial inocula as stationary cultures in 1-liter flasks containing 80 ml of HCHN medium with 0.2% tryptone. The mycelial mats were homogenized and used as inocula for 1-liter HCHN cultures, containing 3 mM VA and 0.1% Tween 80. The 1-liter cultures were incubated at 28°C for 4 days at 150 rpm on a rotary shaker.

4.2.7 Purification of rLiPH8

The filtrate obtained from seven 1-liter cultures was concentrated to ~400 ml at 4°C using a hollow-fiber filter system (10-kD molecular mass cutoff; Amicon). $(NH_4)_2SO_4$ was added to a final concentration of 1.5 M, the mixture was subjected to centrifugation for 1 h at 18,000 × *g*, and the pellet was discarded. All subsequent steps were performed at 4°C.

4.2.8 Phenyl Sepharose Chromatography

The concentrated culture filtrate was applied to a Phenyl Sepharose CL-4B (Pharmacia) column (100 ml) equilibrated with 20 mM sodium acetate (pH 4.5) containing 1.5 M $(NH_4)_2SO_4$. The column was washed with 200 ml of 20 mM sodium acetate (pH 4.5) containing 0.8 M $(NH_4)_2SO_4$, and the protein was eluted with a gradient of 0.8 to 0.2 M $(NH_4)_2SO_4$ in 20 mM sodium acetate (pH 4.5). Fractions with LiP activity were pooled and concentrated to ~2 ml by membrane ultrafiltration.

4.2.9 Size Exclusion Chromatography

The Phenyl Sepharose fraction was applied to a 100-ml Sephadex G-100 column, equilibrated with 20 mM sodium succinate buffer (pH 4.5), and protein was eluted with the same buffer. Fractions with LiP activity were desalted and concentrated.

4.2.10 Anion Exchange FPLC

The pooled, concentrated Sephadex G-100 protein fraction was applied to a Mono Q HR 5/5 column (Pharmacia) equilibrated with 10 mM sodium acetate (pH

6.0) in a fast protein liquid chromatography (FPLC) system. The protein was eluted with a nonlinear gradient (0.01 to 0.5 M sodium acetate, pH 6.0). Fractions containing LiP activity were desalted and concentrated.

4.2.11 SDS-PAGE and IEF

Sodium dodecylsulfate-polyacrylamide gel electrophoresis (SDS-PAGE) was performed using a 12% Tris-glycine gel system [Laemmli, 1970] and a Miniprotean II apparatus (BioRad). The gels were stained with Coomassie blue [Hames and Rickwood, 1981]. The Bio-Rad SDS-PAGE Low Range standard mix was used for comparison. Isoelectric focusing (IEF) electrophoresis was performed using the Pharmacia Phastsystem with IEF Phastgels (pH 3 to 9). The gels were stained with Coomassie blue. The Sigma IEF MIX 3.6–6.6 marker kit was used as a standard.

4.2.12 Spectroscopic and Kinetic Procedures

Enzyme absorption spectra and assays were determined with a Shimadzu UV-260 spectrophotometer at room temperature, using a 1-cm light path cuvette. LiP oxidation of VA to veratraldehyde was performed as described previously [Kirk and Farrell, 1987; Gold et al., 1989] and followed at 310 nm. LiP oxidation of ABTS was carried out in sodium succinate (pH 3.0) in the presence of 0.1 mM H_2O_2 and 0.5 mM VA and followed at 415 nm as described previously [Glenn and Gold, 1985]. For steady-state kinetic measurements, VA oxidation was determined in the presence of various H_2O_2 concentrations at a constant VA concentration (0.5 mM) or with various VA concentrations at a constant H_2O_2 concentration (0.1 mM) in 20 mM sodium-succinate (pH 3.0) with 1 μg of enzyme/ml.

4.2.13 Transient-State Kinetics

Kinetic measurements were conducted at 25°C using an Applied Photophysics stopped-flow reaction analyzer (SX.18MV) with sequential mixing. LiP compound I formation was measured at 397 nm. Native LiP (2 μM) was mixed with a 10- to 50-fold excess of H_2O_2 in 20 mM sodium succinate (pH 3.0). LiP compound I reduction was measured by first mixing 4 μM enzyme and 1 equiv H_2O_2 in H_2O. Then VA in

40 mM sodium succinate (pH 3.0) was added, and compound I reduction was measured at 416 nm. LiP compound II reduction was measured at 397 nm by sequential mixing of 4 μM enzyme, 1 equiv of ferrocyanide, and 1 equiv of H_2O_2 in H_2O and then by adding VA in 40 mM sodium succinate (pH 3.0).

4.3 Results

4.3.1 Expression of rLiP

Transformation of the Ura11 auxotroph with 2 μg of the linearized LiPH8 expression construct pUGL (Fig. 4.1) resulted in the isolation of 35 Ura^+ transformants. Twelve transformants were grown in HCHN stationary cultures and screened for extracellular LiP activity using the ABTS assay in the presence of VA. Total RNA was extracted from 4-day-old cells, and northern blots were carried out on the same sample of transformants. Hybridization with a *lip* H8 cDNA probe revealed that LiP mRNA was present in all transformants, although in varying amounts [data not shown]. Two of the pUGL transformants with the highest rLiP activity in this initial screening were purified by isolating single basidiospores [Alic et al., 1987] and were analyzed further in large liquid shake cultures. A Southern blot of DNA from one of the transformants probed with pUC18 showed that the transforming DNA was chromosomally integrated [data not shown].

The time courses for the appearance of LiP activity in shaken HCHN cultures of basidiospore purified transformants and controls are shown in Fig. 4.2. Extracellular LiP activity was detected only in the cultures of pUGL-transformed strains, and maximal activity was reached after 6 days. The wild-type strain OGC-101 and the Ura11 auxotroph transformed with the transformation vector, pUB, exhibited no LiP activity even after 10 days of incubation. This is the period during which endogenous LiP is expressed in low-nitrogen cultures [Kirk and Farrell, 1987; Gold et al., 1989; Cullen, 1997]. These observations suggest that the activity observed in the transformants was rLiP.

The effect of several culture parameters on the expression of rLiP was examined. The addition of 3 mM VA to the cultures is essential for efficient rLiP

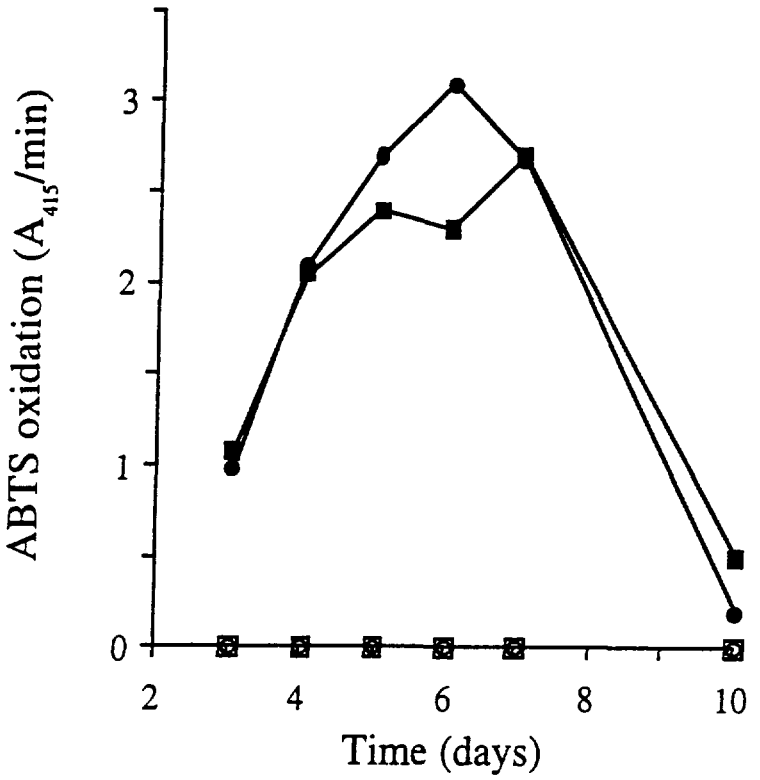

Fig. 4.2 LiP activity in the extracellular medium of primary metabolic cultures of *P. chrysosporium*. UGL10 (●) and UGL11 (■) were pUGL transformants, UB1.7 (○) was a pUB transformant, and OGC-101 (□) was the wild-type strain. Agitated cultures were grown under high-carbon, high-nitrogen conditions, and ABTS oxidation rates were measured as described in the text.

expression. In contrast to the results obtained with rMnP expression [Mayfield et al., 1994b] where an initial pH of 6.5 yielded optimal expression, pH 4.5 was found to be optimal for rLiP expression.

The rLiPH8 was purified from large shake cultures of the transformant UGL10. Successive steps of concentration, hydrophobic-interaction, size exclusion, and anion-exchange chromatography were performed. Mono Q anion exchange chromatography demonstrated that rLiP activity eluted as a single peak corresponding to that of wild type (wtLiPH8) [data not shown].

The R_z value (A_{407}/A_{280}) of the purified rLiPH8 was ~4.2. The specific activity of rLiPH8 for VA was 25.4 U/mg, which is similar to the wild-type (wt) LiPH8 specific activity of 27.6 U/mg. Approximately 2 mg of purified rLiP was obtained from 1 liter of extracellular culture fluid, which corresponds to a yield of ~60%. An SDS-polyacrylamide gel (Fig. 4.3A) of rLiPH8 showed a single band with a molecular mass of 42 kD, which was identical to that of the wtLiPH8. An IEF gel (Fig. 4.3B) also showed a single band of rLiPH8 protein with a pI of 3.3 which was identical to that of wtLiPH8.

4.3.2 Spectral and Kinetic Properties

The absorption spectrum of rLiPH8 (Fig. 4.4) exhibited a Soret maximum at 407 nm and visible bands at 500 and 635 nm. The shapes and intensities of the absorption bands of rLiPH8 were very similar to those of wtLiP, suggesting that the heme environments of wtLiP and rLiP are very similar.

Under steady-state conditions, linear Lineweaver-Burke plots were obtained for 1/v versus $1/H_2O_2$ and 1/v versus 1/VA over a range of H_2O_2 and VA concentrations. The calculated K_m, k_{cat}, k_{cat}/K_m for rLiP and wtLiP were similar (Table 4.1).

Transient-state kinetic measurements were determined for each step in the catalytic cycle. The calculated second-order rate constants ($k_{1\ app}$) for compound I formation under transient-state conditions are shown in Table 4.2. The reduction of compound I for both the wild-type and recombinant enzymes followed similar second-order kinetics. The calculated second-order rate constants ($k_{2\ app}$) are also listed in Table 4.2. For compound II reduction by VA, the plots of the observed rate

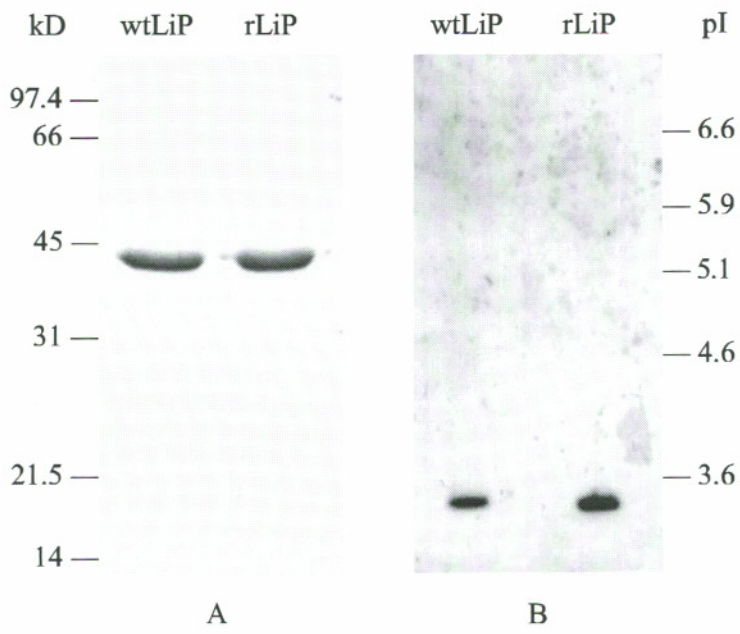

Fig. 4.3 (**A**) SDS-PAGE of rLiPH8 and wtLiPH8. A total of 2 μg of each protein was loaded onto a 12% Tris-glycine-polyacrylamide gel. The gel was stained with Coomassie brilliant blue. The positions of the BRL low-molecular-weight markers are indicated. (**B**) IEF of rLiPH8 and wtLiPH8. A total of 2 μg of each protein was loaded onto a Pharmacia Phastgel with a pH gradient of 3 to 9. The positions of the Sigma IEF MIX 3.6–6.6 markers are indicated.

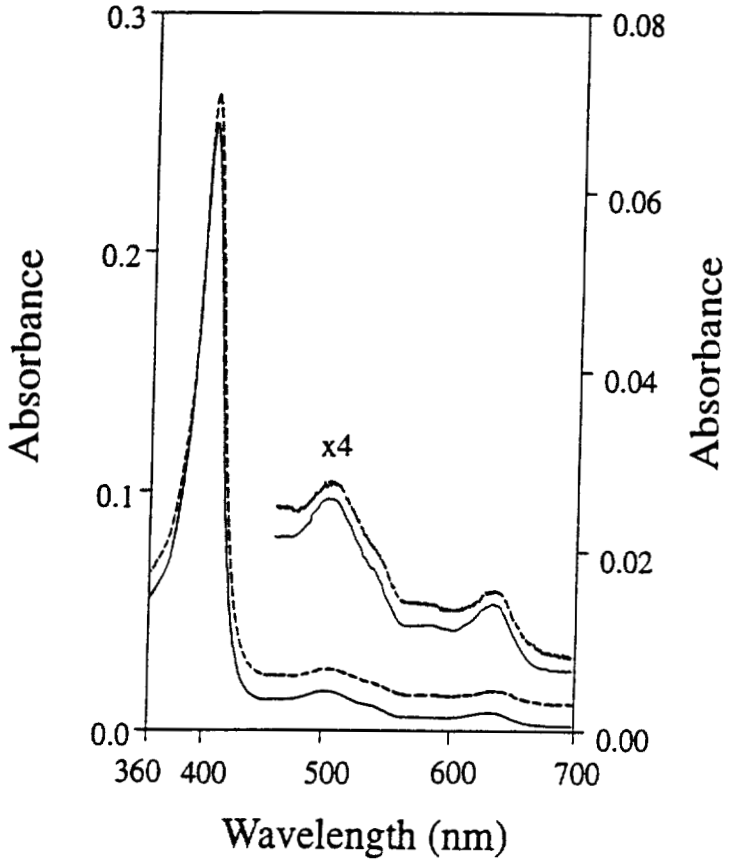

Fig. 4.4 Comparison of the absorption spectra of rLiP (---) and wtLiP (—). The spectra were determined in the presence of 20 mM sodium succinate (pH 3.0) as described in the text.

Table 4.1

Steady-State Kinetic Parameters for rLiPH8 and wtLiPH8[a]

Enzyme	Substrate	K_m (μM)	k_{cat} (s^{-1})	k_{cat}/K_m (M^{-1} s^{-1})
rLiP	H_2O_2	53.1	21.2	4.0×10^5
wtLiP	H_2O_2	47.7	23.0	4.8×10^5
rLiP	VA	89.4	23.2	2.6×10^5
wtLiP	VA	92.8	22.9	2.5×10^5

[a] Reactions were carried out in 20 mM sodium succinate (pH 3.0). Apparent K_m and k_{cat} values for VA were determined by using 0.1 mM H_2O_2. Apparent K_m and k_{cat} values for H_2O_2 were determined by using 0.5 mM VA.

Table 4.2

Transient-State Kinetic Parameters for rLiPH8 and wtLiPH8[a]

Enzyme	Compound I formation	Compound I reduction by VA	Compound II reduction by VA		
	$k_{1\ app}$ ($M^{-1}\ s^{-1}$)	$k_{2\ app}$ ($M^{-1}\ s^{-1}$)	$k_{3\ app}$ (s^{-1})	K_3 (μM)	$k_{3\ app}$ ($M^{-1}\ s^{-1}$)
rLiP	4.7×10^5	1.03×10^5	31	242	1.3×10^5
wtLiP	4.5×10^5	0.97×10^5	40	224	1.8×10^5

[a] Reactions were carried out in 20 mM sodium succinate (pH 3.0) with 1 μM enzyme as described in the text. Compound I formation was monitored at 397 nm. Compound I reduction and compound II reduction in the presence of VA were monitored at 416 and at 397 nm, respectively.

constants k_{obs} versus [VA] were hyperbolic, indicating saturation kinetics. The first-order rate constant $k_{3\ app}$ and the apparent dissociation constant K_3 were calculated from the least-squares fit of k_{obs} versus [VA] and are shown in Table 4.2. The initial slope of the hyperbolic curve could be used to estimate a second-order rate constant $k_{3\ app}$ for compound II reduction.

4.4 Discussion

LiP is a major extracellular component of the lignin-degrading system of *P. chrysosporium* as well as a variety of other white-rot fungi [Kirk and Farrell, 1987; Gold and Alic, 1993; Hatakka, 1994; Cullen, 1997]. The enzyme is capable of oxidizing lignin and nonphenolic aromatics with redox potentials beyond the reach of other peroxidases [Kirk and Farrell, 1987; Schoemaker, 1990; Hammel, 1992; Joshi and Gold, 1996]. Extensive spectroscopic and kinetic studies have been carried out on LiP [Kirk and Farrell, 1987; Wariishi and Gold, 1990; Gold and Alic, 1993; Koduri and Tien, 1995; Khindaria et al., 1996; Sheng and Gold, 1998]. However, a variety of questions concerning the mechanism of this enzyme are still under discussion. For example, the amino acids involved in the substrate binding site have not been determined [Poulos et al., 1993; Smith and Veitch, 1998]. Secondly, the role of VA in the catalytic cycle and its presumed role as a mediator in LiP reactions [Candeias and Harvey, 1995; Koduri and Tien, 1995; Joshi and Gold, 1996; Khindaria et al., 1996; Sheng and Gold, 1998] warrant further research. Studies on site-directed mutant forms of LiP will shed light on these questions.

Previously, we developed a homologous expression system for MnP in *P. chrysosporium* [Mayfield et al., 1994b]. Here, a similar strategy using a Ura$^-$ strain [Akileswaran et al., 1993] and the Ura biosynthetic gene [Froeliger et al., 1989] as a selectable marker has enabled the expression of rLiP under primary metabolic conditions during which endogenous *lip* genes are not expressed [Gold and Alic, 1993].

Ectopic integration of the transformation construct required screening of Ura^+ transformants for optimal *lip* expression. Differences in mRNA levels and enzyme activity were used as criteria to select a transformant which expressed LiP efficiently. Neither strain OGC-101 (wild-type) nor the transformant UB1.7 (control plasmid) expressed detectable LiP under primary metabolic conditions, strongly suggesting that the expressed protein was rLiP.

The addition of 3 mM VA to the growth medium was required for the recovery of rLiP. Since *lip* expression is under the control of the *gpd* promoter in these experiments, it is unlikely that VA is involved in regulation of *lip* expression, supporting previous conclusions [Cancel et al., 1993]. It is more likely that VA is involved in the stabilization or protection of the enzyme from H_2O_2 inactivation [Tonon and Odier, 1988; Wariishi and Gold, 1990].

Our current yield of ~3 mg of rLiPH8/liter in the crude extracellular medium was sufficient for structural and kinetic studies. While we obtain ~10 mg of LiP activity/liter in wild-type cultures, this activity represents all of the isozymes of LiP; therefore, the LiPH8 yields in the two systems are comparable.

Purification of rLiP was achieved by sequential hydrophobic interaction, gel filtration, and anion-exchange chromatographies. SDS-PAGE analysis indicates that rLiP and wtLiP are nearly identical in molecular mass at about 42 kD. IEF shows that the rLiPH8 is a homogeneous isolate and that it has the same isoelectric point as wtLiPH8 (Fig. 4.3A and B). This suggests that the LiP protein expressed is encoded by the introduced gene rather than by an endogenous gene. This also suggests that both proteins undergo very similar posttranslational processing, including cleavage of signal and propeptide sequences [Ritch et al., 1991], folding, and glycosylation. The successful homologous expression of both MnP [Mayfield et al., 1994b] and LiP suggests further that factors that positively regulate the expression of these proteins during secondary metabolism act at the transcriptional level and are mediated by the promoter regions of these genes, since all other factors such as translation, processing, and secretion appear to function during primary metabolic growth.

The wild-type and recombinant enzymes also have identical UV-visible spectral features (Fig. 4.4), indicating that the insertion, environment, and orientation

of the heme are similar. Homologously expressed rLiP exhibits K_m, k_{cat}, and k_{cat}/K_m values for VA and H_2O_2 that are very similar to those of the wild-type enzyme (Table 4.2), suggesting that the substrate binding and catalytic efficiency of rLiP and wtLiP are similar. Furthermore, transient-state kinetic analysis indicates that the rates of the three steps in the LiP catalytic cycle for the two proteins are very similar (Tables 4.1 and 4.2).

Taken together, these results indicate that the rLiP and wtLiP are very similar, and they suggest that this expression system will enable the generation of site-directed mutant proteins which will be folded and processed in a manner identical to that of wtLiP but will be altered only at the designated site. Structure-function studies on such LiPH8 mutant proteins using this expression system are in progress.

CHAPTER 5

Mn^{II} IS NOT A PRODUCTIVE SUBSTRATE FOR WILD-TYPE OR RECOMBINANT LIGNIN PEROXIDASE ISOZYME H2*

5.1 Introduction

When cultured under ligninolytic conditions, the lignin-degrading fungus *Phanerochaete chrysosporium* secretes two families of extracellular peroxidases: lignin peroxidase (LiP) and manganese peroxidase (MnP). These enzymes, along with a H_2O_2-generating system, comprise the major enzymatic components of this organism's extracellular lignin-degrading system [Kirk and Farrell, 1987; Gold and Alic, 1993]. Both MnP and LiP occur as a series of isozymes encoded by a family of genes which are expressed under secondary metabolic growth conditions [Gold and Alic, 1993; Cullen, 1997; Gettemy et al., 1998]. The genomic and cDNA sequences of several MnP and LiP isozymes have been reported [Gold and Alic, 1993; Cullen, 1997; Gold et al., 2000]. The major isozymes MnP1 (H3) and LiPH8 have been characterized [Gold and Alic, 1993; Gold et al., 2000], and the crystal structures of MnP1 [Sundaramoorthy et al., 1994] and LiPH8 [Piontek et al., 1993; Poulos et al., 1993] have been reported. These studies, and deduced amino acid sequence comparisons, show that the overall structures of these enzymes are very similar. Important catalytic residues in the heme pocket, including the proximal His and Asp and the distal His, Arg, Asn, and Glu, are conserved. In addition, homologous expression systems for MnP1 [Mayfield et al., 1994] and LiPH8 [Sollewijn Gelpke et al., 1999a]

---

* Originally published in this or similar form in *Archives of Biochemistry and Biophysics* and used here with permission of Academic Press.

Sollewijn Gelpke, M. D., Sheng, D., and Gold, M. H. (2000) Mn^{II} is not a productive substrate for wild-type or recombinant lignin peroxidase isozyme H2. *Arch. Biochem. Biophys.* **381,** 16-24.

and bacterial expression systems for both MnP and LiP have been established [Doyle and Smith, 1996; Whitwam et al., 1997; Nie et al., 1998].

LiP catalyzes the H_2O_2-dependent oxidation of nonphenolic lignin model compounds via the formation of a substrate aryl cation radical and subsequent nonenzymatic reactions [Kirk and Farrell, 1987; Schoemaker, 1990]. Characterization of the oxidized intermediates, LiPI, LiPII, and LiPIII, indicates that the oxidation states and catalytic cycle of LiP are similar to those of HRP and MnP [Dunford and Stillman, 1976; Renganathan and Gold, 1986]. Veratryl alcohol [3,4-dimethoxybenzyl alcohol (VA)], a secondary metabolite of *P. chrysosporium* and a LiP substrate, appears to play an important role in LiP-catalyzed reactions. VA is a preferred substrate which rapidly reduces LiPI and LiPII [Wariishi et al., 1991; Koduri and Tien, 1994], resulting in enzyme turnover and preventing the formation of the inactive intermediate, LiPIII [Wariishi and Gold, 1990]. Recent structure–function studies of LiPH8 indicate that the enzyme oxidation site for VA may be located at Trp171, an amino acid residue which is conserved in LiP enzymes [Doyle et al., 1998].

Kinetic and spectroscopic characterizations of the oxidized intermediates of MnP, MnP compounds I and II (MnPI and MnPII), suggest that the catalytic cycle of MnP is similar to that of HRP and LiP. However, MnP is unique in its ability to oxidize Mn^{II} to Mn^{III} [Glenn et al., 1986; Wariishi et al., 1992]. The enzyme-generated Mn^{III} is stabilized by organic chelators such as oxalate and malonate [Wariishi et al., 1992; Kuan et al., 1993; Kishi et al., 1994], and the Mn^{III}–organic acid complex, in turn, oxidizes phenolic substrates such as lignin substructures and aromatic pollutants [Tuor et al., 1992; Reddy et al., 1998]. Structure–function studies of MnP have identified a unique Mn^{II} binding site, composed of amino acid residues Glu35, Glu39, Asp179, and Arg177, which is essential for the oxidation of Mn^{II} by MnP [Kusters-van Someren et al., 1995; Kishi et al., 1996; Sundaramoorthy et al., 1997; Whitwam et al., 1997; Sollewijn Gelpke et al., 1999b]. Analysis of deduced amino acid sequences of several MnP and LiP enzymes from different white-rot fungi shows that the amino acids composing the Mn^{II} binding site are conserved in all sequenced MnPs [Gold et al., 2000]. In contrast, in the various LiP enzymes

studied, only one acidic amino acid ligand (equivalent to Glu39 in MnP1) is conserved.

In previous work, it was claimed that LiP isozyme H2 (LiPH2) was able to oxidize Mn^{II} at a rate sufficient to promote catalytic turnover of the enzyme [Khindaria et al., 1995]. A later report from the same laboratory [Sutherland et al., 1996] indicated that compound I of other LiP isozymes (H1, H6, H7, H8, and H10) could be reduced by Mn^{II} at higher rates than by VA, but compound II of these isozymes could not be reduced by Mn^{II}. Herein, we investigate the ability of purified wild-type LiPH2 (wtLiPH2), purified wild-type LiPH8 (wtLiPH8), and homologously expressed recombinant LiPH2 (rLiPH2), all uncontaminated with MnP, to turn over under steady-state conditions with Mn^{II} as the sole reducing substrate. We also use transient-state kinetics to investigate the abilities of Mn^{II} and VA to reduce the enzyme intermediates, LiPI and LiPII, of isozymes H2 and H8.

5.2 Experimental Procedures

5.2.1 Organisms

P. chrysosporium wild-type strain OGC101, auxotrophic strain OGC316-7 (Ura11) [Akileswaran et al., 1993], and prototrophic transformants where maintained as described previously [Alic et al., 1987]. *Escherichia coli* DH5α was used for subcloning plasmids.

5.2.2 Isolation of the *lipH2* Gene

The full-length genomic copy of the *lipH2* gene from *P. chrysosporium* BKM-1767, GLG4 [Stewart et al., 1992] (kindly provided by D. Cullen, U.S. Forest Products Laboratory, Madison, WI), was used to probe our *P. chrysosporium* OGC101 λ-EMBL-3 genomic library as described previously [Godfrey et al., 1990]. From hybridizing clones, a single ~3.7-kb *Bst*I fragment was subcloned in pBluescript SK^- to obtain plasmid pLH2. This *Bst*I fragment was sequenced and

compared to the *lipH2* cDNA sequence CLG4 [de Boer et al., 1988] to identify the promoter, exons, and introns and to confirm its identity.

5.2.3 Construction of the LiPH2 Expression Vector

P. chrysosporium gpd gene promoter (1.1-kb) [Mayfield et al., 1994] was fused immediately 5′ of the *lipH2* coding region. In the promoter of the *lipH2* gene, a *Kpn*I site was created 4 bp upstream of the *lipH2* translation initiation codon. The 1.1-kb *Spe*I–*Kpn*I *gpd* promoter fragment and the 3.0-kb *Kpn*I–*Eco*RI *lipH2* fragment, containing the *lipH2* coding region and terminator region, were subcloned into the *P. chrysosporium* transformation vector pUB [Sollewijn Gelpke et al., 1999a] to obtain the *lipH2* expression vector pUGLH2 (Fig. 5.1). The ligation sites and newly synthesized coding sequence were verified by sequencing.

5.2.4 Transformation of the *P. chrysosporium* Uracil Auxotroph Ura11 with pUGLH2

Protoplasts of *P. chrysosporium* Ura11 were transformed with *Eco*RI-linearized pUGLH2 as described previously [Akileswaran et al., 1993], and prototrophic transformants were transferred to minimal medium. Conidia from slants of pUGLH2 prototrophic transformants were used to inoculate stationary cultures as described previously [Mayfield et al., 1994; Sollewijn Gelpke et al., 1999a]. After 3 days at 28°C, the extracellular medium was assayed for LiP activity with the diammonium 2,2′-azinobis(3-ethylbenzothiazoline-6-sulfonate) (ABTS) assay [Glenn and Gold, 1985], using 40 μM ABTS, 0.1 mM H_2O_2, and 0.5 mM VA. Positive transformants were purified by isolating single basidiospores as described previously [Alic et al., 1987].

5.2.5 Expression and Purification of Recombinant LiPH2

Conidia from the selected pUGLH2 transformant were used to inoculate stationary cultures in 1-liter flasks, containing 80 ml of high-carbon high-nitrogen (HCHN) medium with 0.2% tryptone, and were grown for 2 days at 37°C. The

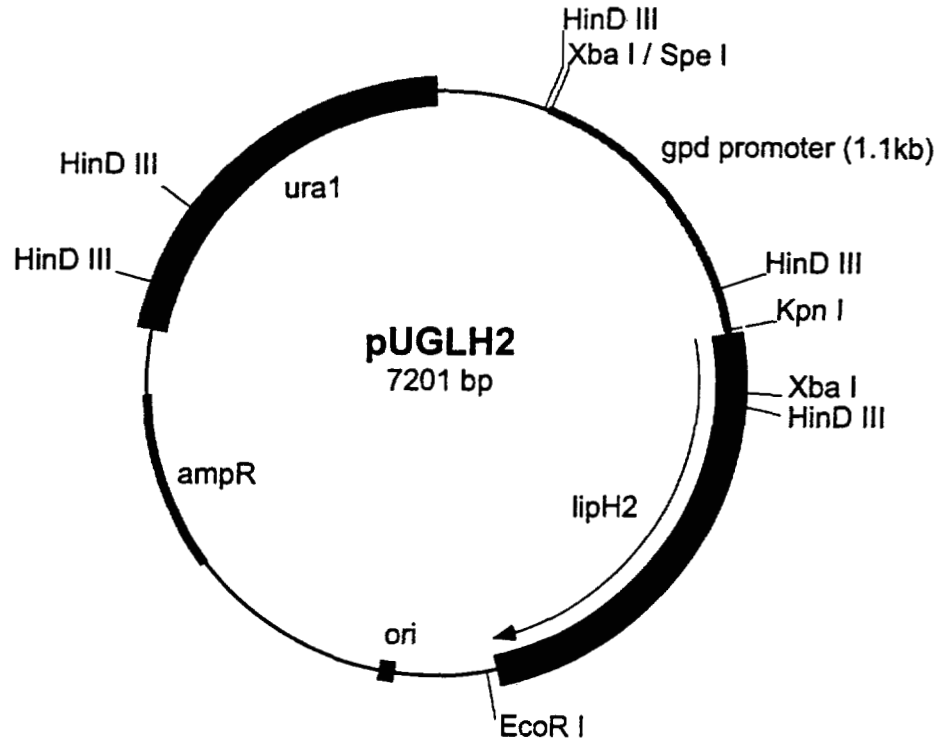

Fig. 5.1 Restriction map of the LiPH2 expression vector pUGLH2 containing the *Schizophyllum commune ura1* gene as a selectable marker. The *P. chrysosporium gpd* promoter was cloned immediately 5′ upstream of the *lipH2* coding region.

mycelial mats were then homogenized and used to inoculate 2-liter flasks, containing 1 liter of HCHN medium with 3 mM VA and 0.02% Tween-80. Cultures were incubated at 28°C for 4 days at 150 rpm on a rotary shaker. The filtrate from seven 1-liter cultures, containing the rLiPH2 enzyme, was concentrated by using a hollow-fiber filter system with a 10-kDa cutoff (Amicon) and treated by consecutive steps of phenyl-Sepharose, Sephadex G-100 size exclusion, and Mono-Q (Pharmacia) anion-exchange chromatographies as described previously for the purification of rLiPH8 [Sollewijn Gelpke et al., 1999a].

5.2.6 Isolation and Purification of Wild-Type LiPH2 and Wild-Type LiPH8

P. chrysosporium OGC101 was grown in agitated, high-carbon low-nitrogen (HCLN), acetate-buffered cultures as described previously [Wariishi and Gold, 1990]. For comparison, LiPH2 was isolated from HCLN cultures with minimal salts [Kirk et al., 1978], containing 30 μM $MnSO_4$, and from HCLN cultures with modified minimal salts, containing no $MnSO_4$. The wtLiP isozymes H2 and H8 were isolated from the filtrate of 7-day-old cultures using chromatography on DEAE-Sepharose, Sephadex G-100 [Gold et al., 1984], and MonoQ FPLC (Pharmacia) [Sollewijn Gelpke et al., 1999a].

5.2.7 SDS-PAGE and Isoelectric Focusing

SDS-PAGE was performed using a 10% Tris-glycine gel system and a Miniprotean II apparatus (Bio-Rad). The Bio-Rad SDS-PAGE low-range standard mix was used for comparison. Isoelectric focusing (IEF) electrophoresis was performed using the Pharmacia Phastsystem with IEF Phastgels (pH 3–9). The Sigma IEF MIX 3.6–6.6 marker kit was used for comparison. Both gels were stained with Coomassie blue.

5.2.8 Spectroscopic Procedures

Electronic absorption spectra and assays were determined with a Shimadzu UV-260 spectrophotometer at room temperature, using a 1-cm light path cuvette. LiP oxidation of VA was determined by following veratryl aldehyde formation at 310 nm

(ϵ_{310} = 9.3 mM^{-1} cm^{-1}). Mn^{II} oxidation was measured by following the formation of the Mn^{III}–malonate complex at 270 nm (ϵ_{270} = 11.6 mM^{-1} cm^{-1}) [Wariishi et al., 1992]. Additional details are provided in the table legends.

5.2.9 Transient-State Kinetics

Kinetic measurements were conducted at 25 ± 0.1°C, using an Applied Photophysics stopped-flow reaction analyzer (SX.18MV) with sequential mixing. LiP compound I was prepared by premixing 4 μM ferric enzyme with 1 equiv of H_2O_2 in water. Subsequently, compound I reduction was measured at 417 nm, the isosbestic point between LiPII and the ferric enzyme, by adding VA in 20 mM (final concentration) sodium succinate (pH 3.0 or 4.5) or by adding $MnSO_4$ in 50 mM (final concentration) potassium malonate (pH 4.5) or 20 mM (final concentration) potassium succinate (pH 4.5) in at least 10-fold molar excess. The ionic strength of all solutions was adjusted to 0.1 M with K_2SO_4. LiPII was prepared by sequential mixing of 4 μM enzyme and 1 equiv of ferrocyanide in water, followed by 1 equiv of H_2O_2 in water. Subsequently, the reduction of LiPII was measured at 407 nm by adding VA in 20 mM (final concentration) sodium succinate (pH 3.0 or 4.5) or $MnSO_4$ in 50 mM (final concentration) potassium malonate (pH 4.5), each in at least 10-fold molar excess of enzyme. All kinetic traces exhibited single exponential character from which pseudo-first-order rate constants were calculated. Typically five or six substrate concentrations were used in triplicate measurements.

5.3 Results

5.3.1 Expression of Recombinant LiPH2

The *P. chrysosporium* OGC101 *lipH2* gene was identified on a ~3.7-kb *Bst*I genomic DNA fragment by hybridizing the *P. chrysosporium* BKM-1767 *lipH2* gene to our genomic library (λ-EMBL-3), followed by sequencing of the complete fragment. The sequence alignment of the *Bst*I genomic DNA fragment with the BKM-1767 *lipH2* cDNA CLG4 [de Boer et al., 1988] revealed that the *Bst*I fragment contained the complete *P. chrysosporium* OGC101 *lipH2* gene, including a 660-bp

promoter region and a 1.4-kb 3′ region. The *P. chrysosporium* OGC101 *lipH2* gene consists of 9 exons and 8 introns, and the coding region shows a total of 26 nucleotide mismatches with the CLG4 cDNA sequence. However, a comparison of the deduced amino acid sequence of the *lipH2* gene and the CLG4 cDNA showed identity for all but two amino acids. The CLG4 residue Arg106 is a Pro in *lipH2*, and the C-terminal residue Asn344 is a Lys in *lipH2*. Both amino acids have no known function in catalysis when compared to the LiPH8 deduced amino acid sequence and crystal structure [data not shown]. The OGC101 *lipH2* gene was used to construct the *P. chrysosporium lipH2* expression vector pUGLH2 (Fig. 5.1). Transformation of the Ura11 auxotroph with pUGLH2 resulted in the isolation of 26 Ura^+ transformants, which were grown in HCHN stationary cultures and screened for extracellular LiP activity using the ABTS assay [Glenn and Gold, 1985; Sollewijn Gelpke et al., 1999a]. Two transformants with the highest LiP activity in this initial screening were purified by isolating single basidiospores [Alic et al., 1987], which were screened again, resulting in the isolation of the transformant strain UGLH2-T20:6.

5.3.2 Enzyme Purification

Attempts were made to purify the wtLiPH2 enzyme from HCLN cultures of *P. chrysosporium* OGC101 grown in the presence or absence of 30 μM $MnSO_4$. FPLC profiles of concentrated extracellular medium from cultures with $MnSO_4$ showed that LiPH2 and MnP elute from the MonoQ column under very similar conditions [data not shown]. Additional chromatoghraphy by DEAE-Sepharose and by Sephadex G-100 columns failed to completely separate LiPH2 from MnP. Extracellular medium from cultures grown in the absence of $MnSO_4$ showed four major peaks in the FPLC profile (Fig. 5.2). Samples from each of these peaks, corresponding to LiP isozymes H1, H2, H6, and H8, respectively, were able to oxidize VA but were unable to oxidize Mn^{II} under steady-state conditions. SDS-PAGE (Fig. 5.3A) and IEF (Fig. 5.3B) electrophoresis showed that wild-type LiPH2, purified from cultures without $MnSO_4$, has a M_r of ~38 kDa and a *p*I of ~4.4 as reported earlier [Farrell et al.,

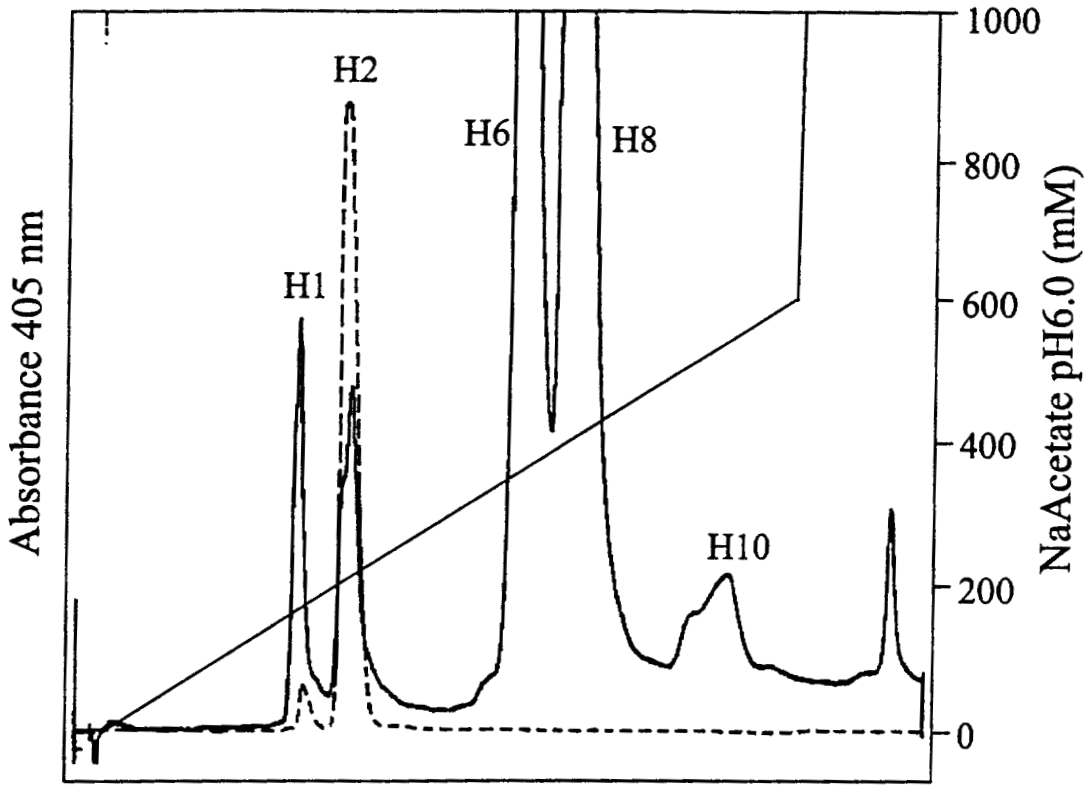

Fig. 5.2 Mono-Q ion exchange FPLC profiles of the concentrated extracellular medium of *P. chrysosporium* OGC101 (—) and of the pUGLH2 transformant strain (---). The column was eluted with a 10 mM^{-1} M sodium acetate gradient at pH 6.0. The wild-type strain was grown on low nitrogen (1.2 mM NH_4-tartrate) medium in the absence of $MnSO_4$ for 7 days at 28°C. The transformant strain was grown on high nitrogen (24 mM NH_4-tartrate) medium for 4 days at 28°C.

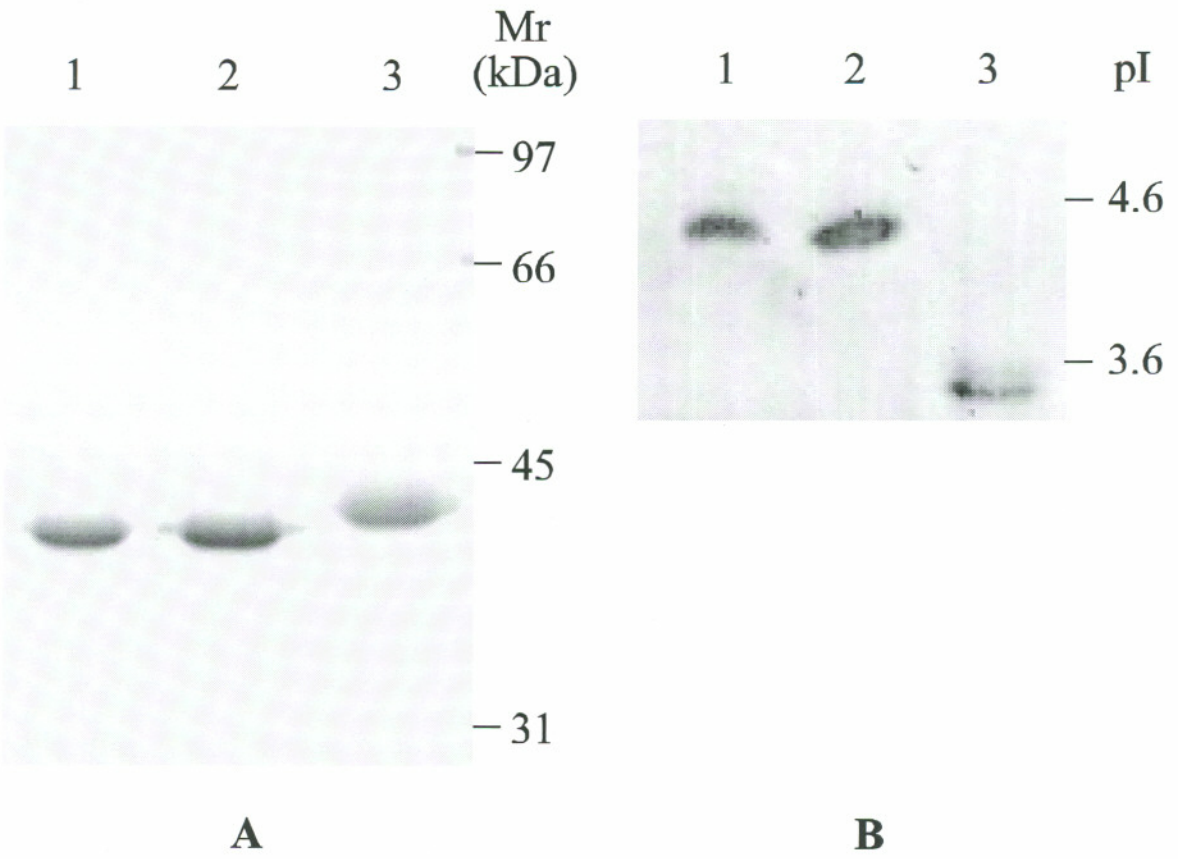

Fig. 5.3 (**A**) SDS-PAGE of wtLiPH2 (lane 1), rLiPH2 (lane 2), and wtLiPH8 (lane 3). 1 μg of each protein was loaded on a 10% Tris-glycine-polyacrylamide gel. The positions of the BRL low-molecular-mass markers are indicated. (**B**) IEF of wtLiPH2 (lane 1), rLiPH2 (lane 2), and wtLiPH8 (lane 3). 4 μg of each protein was loaded onto a Pharmacia Phastgel with a pH gradient of 3–9. The positions of several Sigma IEF 3.6–6.6 markers are indicated.

1989]. SDS-PAGE showed that no MnP1 (M_r ~ 46 kDa) was apparent in wild-type cultures grown in the absence of Mn^{II} (Fig. 5.3A).

Agitated HCHN cultures of the basidiospore-purified rLiPH2 expression strain UGLH2-T20:6 were grown for 4 days when LiP activity was detected in the extracellular medium. Wild-type *P. chrysosporium* OGC101 exhibits no LiP activity in HCHN cultures for at least 10 days [Sollewijn Gelpke et al., 1999a], suggesting that all the LiP activity observed in the transformant cultures is rLiPH2. Likewise, no MnP activity was detected in the cultures over this time period. The rLiPH2 enzyme was purified to homogeneity by successive steps of hydrophobic interaction, size-exclusion, and anion-exchange chromotography. MonoQ anion-exchange chromatography showed that rLiPH2 absorption at 405 nm eluted as a major peak, corresponding to the wtLiPH2 peak (Fig. 5.2) [Farrell et al., 1989]. A minor peak with absorption at 405 nm, corresponding to wtLiPH1, eluted near the recombinant LiPH2 peak.

SDS-PAGE (Fig. 5.3A) of the purified rLiPH2 exhibited a single band with a molecular mass of ~38 kDa, which was identical to that of wtLiPH2. IEF electrophoresis (Fig. 5.3B) demonstrated that the recombinant and wtLiPH2 migrated as single bands with identical *p*Is of ~4.4. The absorption spectrum of rLiPH2 exhibited a Soret maximum at 407 nm and visible bands at 502 nm and 635 nm, essentially identical to the bands of wtLiPH2 [data not shown], suggesting that the heme environments of rLiPH2 and wtLiPH2 are very similar.

5.3.3 Steady-State Kinetics

Under steady-state conditions, linear double-reciprocal plots were obtained over a range of H_2O_2 and VA concentrations for rLiPH2, wtLiPH2, and wtLiPH8. The apparent K_m, k_{cat}, and k_{cat}/K_m values are listed in Table 5.1. Mn^{II} oxidation by LiP was examined by following Mn^{III}–malonate formation at 270 nm [Wariishi et al., 1992]. In contrast to previous reports [Khindaria et al., 1995; Nie et al., 1998], Mn^{II} oxidation was not detectable with purified preparations of rLiPH2, wtLiPH2, or wtLiPH8 (Table 5.2). Absorption spectral analysis of reaction mixtures containing 1 μM enzyme, 5 mM $MnSO_4$, 0.1 mM H_2O_2, and 50 mM potassium malonate (pH

Table 5.1

Steady-State Kinetic Parameters for VA Oxidation by LiP[a]

Enzyme	K_m (μM)		k_{cat} (s^{-1})	k_{cat}/K_m (M^{-1} s^{-1})
	VA[b]	H_2O_2[c]		VA
wtLiPH2	131	30	11	8.4×10^4
rLiPH2	164	29	12	7.1×10^4
wtLiPH8[d]	93	48	23	2.5×10^5

[a] Reactions were carried out in 20 mM potassium succinate (pH 3.0).
[b] K_m for VA was determined using 0.1 mM H_2O_2.
[c] K_m for H_2O_2 was determined using 0.5 mM VA.
[d] From Sollewijn Gelpke et al. [1999a].

Table 5.2

Steady-State Kinetic Parameters for Mn^{II} Oxidation by LiP

Enzyme	K_m (μM)		k_{cat} (s^{-1})	k_{cat}/K_m (M^{-1} s^{-1})
	Mn^{II}	H_2O_2		Mn^{II}
wtLiPH2[a]	n.o.	n.o.	0	n.o.
rLiPH2[a]	n.o.	n.o.	0	n.o.
wtLiPH8[a]	n.o.	n.o.	0	n.o.
wtLiPH2[b]	19	42	202	1.0×10^7
rLiPH2[c]	n.r.	n.r.	14	n.r.
wtMnP[d]	90	55	256	2.8×10^6

[a] Reactions contained 50 mM potassium malonate (pH 4.5), 2 μg of enzyme, 5 mM Mn^{II}, and 0.1 mM H_2O_2.
[b] From Khindaria et al. [1995].
[c] From Nie et al. [1998].
[d] From Sollewijn Gelpke et al. [1999b].
n.o. = no oxidation observed; n.r. = not reported.

4.5) [data not shown], revealed that compound III* [Wariishi and Gold, 1990], an inactive enzyme intermediate, was formed by all three enzymes, apparently via the conversion of LiPII to LiPIII and then to LiPIII* in the presence of excess H_2O_2 [Wariishi and Gold, 1990].

5.3.4 Transient-State Kinetics

The reduction of LiPI by VA was determined at pH 4.5 and at the optimal pH of 3.0 by following the absorbance at 417 nm, the isosbestic point between LiPII and the ferric enzyme. The observed rate constants ($k_{2,obs}$) for LiPI reduction by a 10- to 50-fold excess of VA were linearly proportional to the VA concentration and had a zero intercept indicating irreversible second-order kinetics [data not shown]. The calculated second-order rate constants ($k_{2,app}$) for LiPI reduction by VA are shown in Table 5.3. The $k_{2,app}$ values for LiPI reduction by VA at pH 3.0 are very similar for the LiPH2 and LiPH8 isozymes. At pH 4.5, the reduction rates are ~3-fold slower than those at pH 3.0.

The reduction of LiPI by Mn^{II} was followed at 417 nm at the optimal pH for Mn^{II} oxidation by MnP1 (pH 4.5) [Glenn and Gold, 1985]. In malonate buffer, the $k_{2,obs}$ values with Mn^{II} concentrations of 1 to 15 mM were very low. The plots of the $k_{2,obs}$ values versus Mn^{II} concentrations were linearly proportional with increasing Mn^{II} concentrations for rLiPH2, wtLiPH2, and wtLiPH8 (Fig. 5.4). However, the plots did not have a zero intercept, most likely because the spontaneous rate (k_{obs}) of LiPI reduction was significant compared to the k_{obs} in the presence of Mn^{II}. The $k_{2,app}$ values for the reduction of LiPH2 and LiPH8 compound I by Mn^{II} at pH 4.5 were $\sim 2 \times 10^5$-fold lower than the $k_{2,app}$ for MnPI reduction by Mn^{II} and were $\sim 2 \times 10^3$-fold lower than the $k_{2,app}$ for LiPI reduction by VA under these conditions. In contrast, the rates of LiPI reduction in the presence of Mn^{II} in succinate (pH 4.5) were not higher than those of the spontaneous reduction.

LiPH2 compound II reduction by VA was followed at 407 nm, the Soret maximum of ferric LiPH2 at pH 3.0 and 4.5. The plot of the pseudo-first-order rate constants ($k_{3,obs}$) versus the VA concentration yields a rectangular hyperbola,

Table 5.3

Kinetic Parameters for the Reduction of Compound I by VA or Mn^{II}

Enzyme	Compound I reduction by VA[a] $k_{2,app}$ (M^{-1} s^{-1})		Compound I reduction by Mn^{II} [b] $k_{2,app}$ (M^{-1} s^{-1})
	pH 3.0	pH 4.5	pH 4.5
wtLiPH2[c]	0.89×10^6	2.8×10^5	1.7×10^2
rLiPH2[c]	0.76×10^6	n.d.	1.8×10^2
wtLiPH8[c]	0.97×10^6	4.1×10^5	1.1×10^2
wtLiPH8[d]	2.23×10^6	5.4×10^5	n.r.
wtLiPH2[e]	n.r.	n.r.	$>10^7$
wtLiPH8[f]	n.r.	n.r.	$>10^7$
wtMnP[g]	n.r.	n.r.	$\sim 3 \times 10^7$

[a] Reactions were carried out in 20 mM potassium succinate (pH 3.0 or 4.5).
[b] Reactions were carried out in 50 mM potassium malonate (pH 4.5).
[c] This work.
[d] From Wariishi et al. [1991].
[e] From Khindaria et al. [1995].
[f] From Sutherland et al. [1996].
[g] From Sollewijn Gelpke et al. [1999b].
n.d. = not determined; n.r. = not reported.

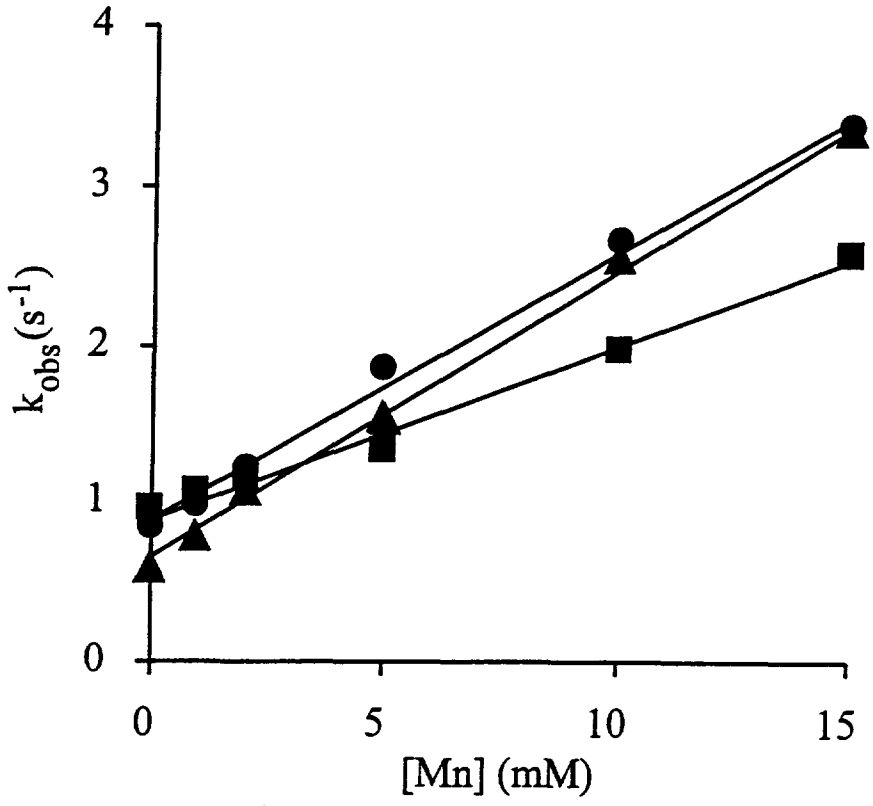

Fig. 5.4 Transient-state kinetics of LiP compound I reduction by Mn^{II} in 50 mM potassium malonate (pH 4.5). The kinetics of rLiPH2 (▲), wtLiPH2 (•), and wtLiPH8 (■) are very similar and exhibit rates that are $\sim 2 \times 10^5$-fold lower than those observed for reduction of MnPI by Mn^{II} and $\sim 2 \times 10^3$-fold lower than those observed for the reduction of LiPI by VA.

suggesting the formation of an enzyme-substrate complex as shown previously for LiPH8 [Wariishi et al., 1991]. The first-order rate constants (k_3) and the dissociation constants (K_D) are listed in Table 5.4. The rates of LiPII reduction by VA were essentially identical for wtLiPH2 and rLiPH2. The reduction of LiPII by Mn^{II} in 50 mM potassium malonate (pH 4.5) also was followed at 407 nm. The plots of the observed rate constants (k_{3obs}) versus Mn^{II} concentrations, ranging from 1 to 15 mM indicated that Mn^{II} could not reduce compound II of rLiPH2, wtLiPH2, or wtLiPH8.

5.4 Discussion

LiP and MnP are major components of the lignin-degrading system of *P. chrysosporium* as well as of a variety of other white-rot fungi [Kirk and Farrell, 1987; Gold and Alic, 1993; Hatakka, 1994; Cullen, 1997]. Although the catalytic cycle of MnP is similar to that of LiP (Scheme 1) and other peroxidases, this enzyme is unique in that it oxidizes Mn^{II} to Mn^{III}. The latter, complexed with an organic acid chelator, diffuses from the enzyme to oxidize aromatic substrates [Tuor et al., 1992; Wariishi et al., 1992; Bao et al., 1994].

SCHEME 1

$$\text{LiP} + H_2O_2 \xrightarrow{k_1} \text{LiP compound I} + H_2O$$

$$\text{LiP compound I} + S \xrightarrow{k_2} \text{LiP compound II} + S_{ox}$$

$$\text{LiP compound II} + S \xrightarrow{k_3} \text{MnP} + S_{ox} + H_2O$$

The development of recombinant expression systems for MnP has enabled mutagenesis studies of this enzyme and its active site [Kishi et al., 1996; Whitwam et al., 1997; Gold et al., 2000]. Although the crystal structures of MnP and LiP exhibit structural similarities, MnP contains a cation binding site at the protein surface, consisting of the carboxylates of Asp179, Glu35, Glu39, and heme propionate 6.

Table 5.4

Kinetic Parameters for the Reduction of LiP Compound II by VA or Mn^{II}

Enzyme	Compound II reduction by VA[a]				Compound II reduction by Mn^{II} [b]
	pH 3.0			pH 4.5	pH 4.5
	k_3 (s^{-1})	K_D (μM)	$k_{3,app}$ ($M^{-1}\ s^{-1}$)	$k_{3,app}$ ($M^{-1}\ s^{-1}$)	$k_{3,app}$ ($M^{-1}\ s^{-1}$)
wtLiPH2[c]	22.6	57.2	3.9×10^5	6.0×10^4	n.o.
rLiPH2[c]	23.1	59.2	3.9×10^5	5.8×10^4	n.o.
wtLiPH8[d]	40.0	224.0	1.8×10^5	5.3×10^4	n.o.[c]
wtLiPH2[e]	n.r	n.r.	n.r.	1×10^4[f]	1.4×10^7
wtLiPH8[f]	n.r	n.r.	n.r.	2×10^4	70
wtMnP[g]	n.r	n.r.	n.r.	n.r.	3.3×10^6

[a] Reactions were carried out in 20 mM succinate (pH 3.0 or 4.5).
[b] Reactions were carried out in 50 mM potassium malonate (pH 4.5) (μ = 0.1 M, K_2SO_4).
[c] This work.
[d] From Wariishi et al. [1991].
[e] From Khindaria et al. [1995].
[f] From Sutherland et al. [1996].
[g] From Sollewijn Gelpke et al. [1999b].
n.r. = not reported, n.o. = no reduction observed

Mutagenesis studies of the Mn^{II} binding ligands Asp179, Glu35, and Glu39 show that conversion of each carboxylic acid functional group to an amide results in significant decreases in Mn^{II} binding and in Mn^{II} oxidation rates [Kusters-van Someren et al., 1995; Kishi et al., 1996; Sundaramoorthy et al., 1997]. Sequence comparisons and X-ray crystallographic studies show that the specific Mn^{II} binding and oxidation site is conserved in all MnP enzymes but not in LiP enzymes [Gold et al., 2000].

A view of the Mn^{II} binding site from the crystal structure of MnP [Sundaramoorthy et al., 1994], superimposed on the crystal structure of LiPH8 [Poulos et al., 1993] (Fig. 5.5), shows the differences between the MnP binding site structure and the corresponding LiPH8 structure. Site-directed mutagenesis studies of MnP showed that the mutational changes of D179N, E35Q [Kusters-van Someren et al., 1995; Kishi et al., 1996], and R177A [Sollewijn Gelpke et al., 1999b] reduced the catalytic efficiency $\sim 10^4$-fold, $\sim 10^4$-fold, and $\sim$20-fold, respectively. These mutations correspond to the three changes in the wtLiPH8 structure and the wtLiPH2 sequence, strongly suggesting that an effective Mn binding site does not exist in LiP. Indeed, this triple mutant in MnP would be incapable of oxidizing Mn^{II}. In addition, it was demonstrated that the ability to slowly oxidize Mn^{II} was introduced into CcP after reconstruction of a Mn^{II} binding site [Yeung et al., 1997; Wilcox et al., 1998]. Therefore, it is unlikely that Mn^{II} can be oxidized efficiently by LiPH2, which does not contain this site. Recent mutagenesis studies of LiP revealed that Trp171 is conserved within LiP sequences, but a Ser or Ala occurs at this position in MnP sequences [Gold et al., 2000; Timofeevski et al., 2000], and that this Trp171 is essential for VA oxidation [Doyle et al., 1998], further suggesting that the primary reducing substrate binding sites of these two enzyme families are different.

Both LiP and MnP occur as a series of isozymes encoded by a family of genes which are expressed under secondary metabolic growth conditions [Gold and Alic, 1993; Cullen, 1997; Gettemy et al., 1998]. The isozymes are at least partially separated by anion-exchange chromatography on a MonoQ column [Farrell et al., 1989], although respective expression levels are dependent on growth conditions. For example, the presence of Mn^{II} allows the expression of MnP isozymes [Brown et al., 1990; Gettemy et al., 1998]. While the purification of the separate isozymes MnP1

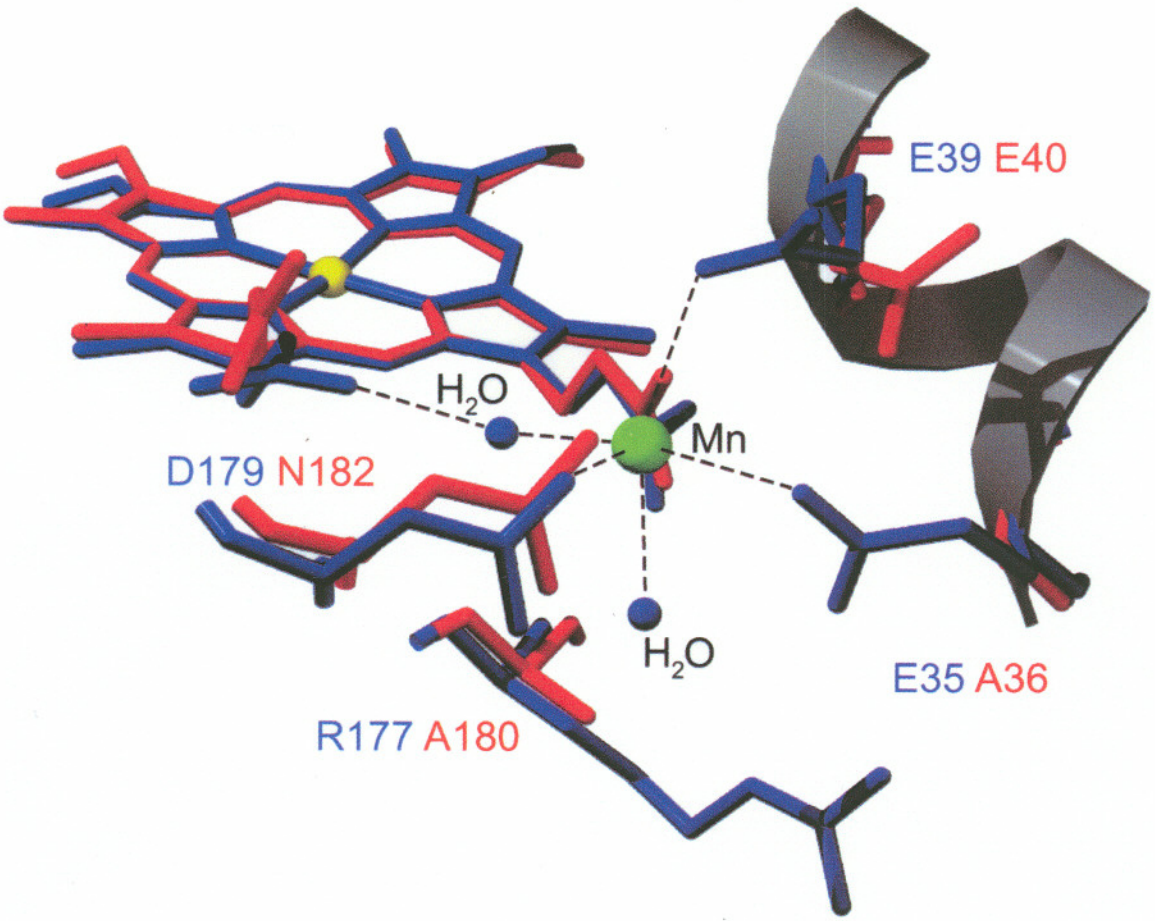

Fig. 5.5 The Mn^{II} binding site from the crystal structure of MnP [Sundaramoorthy et al., 1994] superimposed on the same region of the crystal structure of LiPH8 [Poulos et al., 1993]. The number and identity of MnP amino acid ligands are shown in blue, and the number and identity of LiPH8 residues are shown in red. Sequence comparison shows that these residues in LiPH8 are conserved in LiPH2. The heme, Mn atom, and two water ligands are also shown.

and LiPH8 is well described and these isozymes are efficiently purified to homogeneity [Kirk et al., 1986; Gold and Alic, 1993; Gold et al., 2000], the purification of wtLiPH2 from standard HCLN cultures containing $MnSO_4$ is complicated by the presence of MnP. Several chromatographic methods were unable to completely separate LiPH2 from MnP as also observed in Fig. 1 of Khindaria et al. [1995]. In contrast, when grown in the absence of Mn^{II}, wtLiPH2 was efficiently purified from HCLN cultures and was apparently not contaminated by the MnP enzyme. SDS-PAGE and IEF showed that this purified wtLiPH2 is homogeneous and has a M_r and a *p*I which are very similar to those reported earlier [Farrell et al., 1989].

To obtain LiPH2 enzyme without possible contamination by MnP, rLiPH2 also was prepared and isolated. rLiPH2 was produced under the control of the *gpd* gene promoter during primary metabolic growth when endogenous LiP and MnP are not expressed [Mayfield et al., 1994; Sollewijn Gelpke et al., 1999a]. In contrast to heterologous expression in *E. coli*, homologous expression allows the production of recombinant peroxidases which are processed and modified in a manner essentially identical to the wild-type enzymes. This is especially important in the isolation of rLiPH2, where one phosphate, present as a mannose-6-phosphate, is part of an asparagine-linked oligosaccharide [Kuan and Tien, 1989]. A *P. chrysosporium* mannose-6-phosphate phosphatase is able to dephosphorylate LiPH2, resulting in its conversion to LiPH1 [Rothschild et al., 1999]. The observed increase in pI value when LiPH2 is converted to LiPH1 is consistent with the dephosphorylation of LiPH2 [Farrell et al., 1989; Kuan and Tien, 1989]. Recombinant expression of *lipH2* cDNA in *E. coli*, followed by refolding as described previously [Nie et al., 1998], would result in the isolation of a nonglycosylated, nonphosphorylated enzyme. Thus, the enzyme expressed in *E. coli* is probably a non-glycosylated form of LiPH1/LiPH2 and, therefore, is not the recombinant form of the glycosylated and phosphorylated wtLiPH2.

Purification of homologously expressed recombinant LiP by MonoQ ion-exchange chromatography resulted in the detection of two peaks with absorbance at 407 nm. The major and minor peaks were identified as rLiPH2 and rLiPH1,

respectively, by their chromatographic properties. This suggests that the recombinant expression of the *lipH2* gene results in production of both LiPH2 and LiPH1 isozymes, which is consistent with the observations that LiPH1 and LiPH2 differ by a posttranslational processing event [Rothschild et al., 1999]. The further purification of the protein in the major peak resulted in the isolation of active, heme-containing enzyme rLiPH2, which was essentially identical to wtLiPH2, indicating a similar heme environment and similar physical properties. Both SDS-PAGE and IEF analysis show that the wtLiPH2 and rLiPH2 were purified to homogeneity and that both proteins apparently undergo very similar posttranslational processing, including cleavage of leader sequences, folding, and most likely glycosylation. Steady-state kinetic analysis reveals that wtLiPH2 and rLiPH2 oxidize VA at similar rates. Furthermore, transient-state kinetic analysis indicates similar rates for compounds I and II reduction by VA.

Previously it was claimed that LiPH2 could efficiently oxidize Mn^{II} to Mn^{III} and that both compounds I and II of LiPH2 were reduced at higher rates by Mn^{II} than by VA [Khindaria et al., 1995]. However, there are discrepancies in these previous transient-state data analyses of LiPI an LiPII reduction by Mn^{II} (Figs. 2 and 3 in Khindaria et al. [1995]). For the specific Mn^{II} concentrations in the insets of both figures, the calculated k_{obs} are $\sim$10-fold lower than the k_{obs} in the graphs. Furthermore, there is probable contamination of their wtLiPH2 preparation with MnP (visible in Fig. 1 in Khindaria et al. [1995]). Reports from the same laboratory suggest that recombinant LiPH2 [Nie et al., 1998], which is probably recombinant nonglycosylated LiPH1/LiPH2 (as discussed above), can turn over with Mn^{II}. However, they claimed that wtLiPH1, a product of the same gene, cannot turn over with Mn^{II} as the sole reducing substrate [Sutherland et al., 1996]. These conflicting and unusual results require a reexamination of the kinetics of Mn^{II} oxidation by homogeneous preparations of LiPH2.

wtLiPH2, rLiPH2, and wtLiPH8 were used to examine both VA and Mn^{II} oxidation. Steady-state kinetic analysis showed that, while each enzyme was able to oxidize VA, none of the enzymes could turn over in the presence of Mn^{II} as the reducing substrate. The oxidation rates for VA were similar for wtLiPH2, rLiPH2,

and LiPH8 and were comparable to previous results [Farrell et al., 1989; Sollewijn Gelpke et al., 1999a], indicating that the isolated enzymes functioned normally. However, neither isozyme oxidized Mn^{II} under these conditions. This is in contrast to claims that wtLiPH2 can oxidize Mn^{II} at a rate similar to that of MnP [Khindaria et al., 1995] or that rLiPH2 expressed in *E. coli* can oxidize Mn^{II} at a rate only ~15-fold slower than MnP [Nie et al., 1998]. Spectral analysis of LiPH2 and LiPH8 with excess H_2O_2 and Mn^{II} in malonate buffer revealed the formation of LiP compounds III and III* [Wariishi and Gold, 1990], suggesting that the rate of LiPII reduction by Mn^{II} is nonexistent or slow compared to the conversion of LiPII to LiPIII by H_2O_2. This also demonstrates that neither LiPH2 nor LiPH8 was able to turn over with Mn^{II} as the sole reducing substrate.

The results of the transient-state kinetic analyses for the reduction of compounds I and II by VA were similar for LiPH2 and LiPH8 and were comparable to previous results [Wariishi et al., 1991; Sutherland et al., 1996]. The $k_{2,app}$ values for the reduction of LiPI by VA were ~8–10 × 10^5 and ~3–4 × 10^5 M^{-1} s^{-1} at pH 3.0 and 4.5, respectively. The apparent rates of LiPII reduction by VA were ~2–4 × 10^5 and ~5–6 × 10^4 M^{-1} s^{-1} at pH 3.0 and 4.5, respectively. The plots of the observed rate constants versus the Mn^{II} concentration for LiPI reduction were linearly proportional to the Mn^{II} concentrations for rLiPH2, wtLiPH2, and wtLiPH8, suggesting second-order kinetics. The apparent second-order rate ($k_{2,app}$) for LiPI reduction by Mn^{II} was ~1.5 × 10^2 M^{-1} s^{-1}, at pH 4.5. As shown in Fig. 5.4, the plots of the k_{obs} values versus the Mn^{II} concentrations did not pass through the origin. This probably occurs because the spontaneous rate of LiPI reduction without Mn^{II} is significant with respect to the k_{obs} values of LiPI reduction in the presence of Mn^{II}. Indeed, the spontaneous rates equal the k_{obs} values at the *y*-intercept of the plots of the observed rate constants versus the Mn^{II} concentration for LiPI reduction (Fig. 5.4). These results indicate that the rate for LiPI reduction at pH 4.5 by VA is ~2 × 10^3-fold higher than the rate of LiPI reduction by Mn^{II}, indicating that VA is a much better substrate for LiP under these conditions. Furthermore, we were not able to detect reduction of LiPH2 or LiPH8 compound II by Mn^{II} at pH 4.5. The low $k_{2,app}$ values for LiPI reduction by Mn^{II} and the absence of LiPII reduction by Mn^{II} are in

agreement with our steady-state results, where LiP is unable to turn over with Mn^{II} as the sole reducing substrate. These results for LiPI and LiPII reduction by Mn^{II} are in sharp contrast to the results reported earlier [Khindaria et al., 1995], where the LiP compound I and II apparent rates of reduction by Mn^{II} were reportedly $>10^7$ and 1.4×10^7 $M^{-1}s^{-1}$, respectively, which are comparable to the reduction rates of MnP compounds I and II by Mn^{II}. The differences in transient-state kinetic data for LiP compounds I and II reduction in the presence of Mn^{II}, reported here and previously, support our suspicion that the previously reported rates were determined with LiP enzyme preparations contaminated with MnP [Khindaria et al., 1995].

In contrast, we were able to obtain homogeneous enzyme preparations for our kinetic analyses. The adjustment of wtLiPH2 expression conditions, where $MnSO_4$ was omitted from the cultures, resulted in the isolation and purification of wtLiPH2, apparently not contaminated with MnP enzyme. In addition, the *P. chrysosporium* homologous expression system for LiP [Sollewijn Gelpke et al., 1999a] enabled the isolation and purification to homogeneity of rLiPH2. The steady-state kinetic parameters for LiPH2 and LiPH8 indicate that there is essentially no oxidation of Mn^{II} in malonate buffer and strongly suggest that Mn^{II} is not a productive substrate for LiP, indicating that VA is the preferred reducing substrate for LiP in the degradation of lignin substructures.

CHAPTER 6

LIGNIN PEROXIDASE OXIDATION OF VERATRYL ALCOHOL: EFFECTS OF THE MUTANTS H82A, Q222A, W171A AND F267L*

6.1 Introduction

The lignin-degrading basidiomycete *Phanerochaete chrysosporium* secretes two families of class II extracellular peroxidases: lignin peroxidase (LiP) and manganese peroxidase (MnP) [Welinder, 1992; Gold and Alic, 1993]. These enzymes, along with a H_2O_2-generating system, are the major components of the extracellular lignin-degrading system in this fungus [Buswell and Odier, 1987; Kirk and Farrell, 1987; Gold and Alic, 1993; Gold et al., 2000]. Lignin peroxidase isozyme H8 (LiPH8] from *P. chrysosporium* catalyzes the H_2O_2-dependent oxidation of nonphenolic lignin model compounds via formation of a substrate aryl cation radical, with subsequent nonenzymatic reactions yielding the final products [Kersten et al., 1985; Renganathan et al., 1986; Schoemaker, 1990; Joshi and Gold 1996]. Veratryl alcohol (VA), a secondary metabolite secreted by *P. chrysosporium* and a LiP substrate, stimulates the LiP-catalyzed oxidations of synthetic lignin [Hammel et al., 1993], proteins [Sheng and Gold, 1998, 1999], and a variety of lignin model compounds and aromatic pollutants [Hammel et al., 1986; Barr and Aust, 1994; Joshi and Gold, 1994; Tien and Ma, 1997].

LiPH8 is a monomeric heme protein with a molecular mass of 42 kDa and a pI of 3.3 [Kirk and Farrell, 1987; Leisola et al., 1987; Gold and Alic, 1993]. Early

---

* Originally published in this or similar form in *Biochemistry* and used here with permission of the American Chemical Society.

Sollewijn Gelpke, M. D., Lee, J., and Gold, M. H. (2002) Lignin peroxidase oxidation of veratryl alcohol: effects of the mutants H82A, Q222A, W171A, and F267L. *Biochemistry* **41,** in press.

spectroscopic studies indicated that the heme iron of native LiPH8 is ferric, high-spin, and pentacoordinate, with a histidyl fifth ligand [Andersson et al., 1985, 1987; de Ropp et al., 1991; Banci et al., 1993]. Analyses of the LiPH8 crystal structure [Piontek et al., 1993; Poulos et al., 1993] and amino acid sequence comparisons with other heme peroxidases [Ritch and Gold, 1992; Gold and Alic, 1993] demonstrate that important catalytic residues, including the proximal His176, the H-bonded Asp238, and the distal His47, Arg43, Phe46, and Asn84 residues, are all conserved within the heme pocket. These results indicate that the heme environment of LiP is similar to that of MnP and other fungal and plant peroxidases [Welinder, 1992; Gold and Alic, 1993].

Spectroscopic and kinetic studies of the LiP native enzyme and its oxidized intermediates demonstrate that the catalytic cycle of LiP is also similar to that of MnP, horseradish peroxidase (HRP), and other plant and fungal peroxidases [Renganathan and Gold, 1986; Marquez et al., 1988; Harvey et al., 1989; Dunford, 1999]. Native LiP undergoes a two-electron oxidation by H_2O_2, yielding compound I (LiPI) [Renganathan and Gold, 1986; Marquez et al., 1988]. The one-electron reduction of LiPI by reducing substrates such as veratryl alcohol (VA), yields compound II (LiPII) and a VA cation radical ($VA^{+\bullet}$). A second one-electron reduction returns the enzyme to the ferric oxidation state, completing the catalytic cycle [Renganathan and Gold, 1986; Marquez et al., 1988; Wariishi et al., 1991a]. In the absence of a reducing substrate, excess H_2O_2 converts native LiP to LiP compound III* (LiPIII*), an inactive form of the enzyme [Wariishi and Gold, 1990; Wariishi et al., 1990]. VA can convert LiPIII* back to the native enzyme, thus rescuing the inactive enzyme [Wariishi and Gold, 1990].

Recent detailed crystal structure analyses and structure–function studies of LiP indicate that Trp171 may be part of the VA interaction site of LiP. Mutation of the Trp171 residue, which is hydroxylated at the Cβ in wtLiP [Blodig et al., 1998], suggests Trp171 is involved in VA oxidation [Doyle et al., 1998]. An electron-transfer pathway from Trp171 to the heme was proposed [Blodig et al., 1998; Doyle et al., 1998]; however, the mechanism of this oxidation reaction remains unclear.

Previously, we developed a homologous expression system for LiPH8 [Sollewijn Gelpke et al., 1999a] in which the *P. chrysosporium* glyceraldehyde-3-phosphate dehydrogenase (*gpd*) gene promoter is used to drive the expression of the *lipH8* gene during primary metabolic growth when endogenous LiP and MnP are not expressed [Sollewijn Gelpke et al., 1999a]. In the present study, four site-directed mutants of LiPH8 (H82A, Q222A, W171A, and F267L) were produced using our homologous expression system. The variant enzymes were used to investigate the site of VA oxidation and the role of VA in the LiP catalytic cycle.

6.2 Materials and Methods

6.2.1 Organisms

P. chrysosporium wild-type strain OGC101 [Alic et al., 1987], auxotrophic strain OGC316-7 (Ura11) [Akileswaran et al., 1993], and prototrophic transformants where maintained as described previously [Alic and Gold, 1985]. *Escherichia coli* DH5α was used for subcloning plasmids.

6.2.2 Construction of Expression Plasmids

Site-directed mutations were introduced in the *lipH8* gene [Ritch and Gold, 1992] component of the recombinant LiPH8 homologous expression vector, pUGL [Sollewijn Gelpke et al., 1999a], using the Quikchange (Stratagene) protocol. pUGL contains 1.1 kb of the *P. chrysosporium gpd* gene promoter fused to the *P. chrysosporium lipH8* gene at their respective TATA box sites [Sollewijn Gelpke et al., 1999a]. The pUGL plasmid also contains the *Schizophyllum commune ura1* gene [Froeliger et al., 1989] as a selectable marker [Sollewijn Gelpke et al., 1999a]. Forward and reverse primers were designed to construct four expression plasmids containing the H82A, W171A, Q222A, or F267L mutations. The complete *lipH8* coding region, including the mutation sites, of each mutated expression plasmid was verified by double-stranded sequencing.

6.2.3 Transformation of the Uracil Auxotroph Ura11

Protoplasts of *P. chrysosporium* Ura11 were transformed with *Eco*RI-linearized mutant pUGL plasmids as described previously [Alic et al., 1991; Akileswaran et al., 1993]. Prototrophic transformants were transferred to minimal medium slants, and conidia from these slants were used to inoculate liquid stationary cultures as described previously [Mayfield et al., 1994; Sollewijn Gelpke et al., 1999a]. After 3 days of growth at 28°C, the extracellular medium was assayed for either LiP activity or protein, either using the 2,2′-azinobis(3-ethylbenzothiazoline-6-sulfonate) (ABTS) assay [Glenn and Gold, 1985] with 0.5 mM ABTS and 0.1 mM H_2O_2 or by western blotting using a polyclonal LiP antibody [Ritch and Gold, 1992]. Positive transformant clones, producing recombinant mutant LiP enzyme, were purified by isolating single basidiospores as described previously [Alic et al., 1987], followed by the final selection of the transformant strains.

6.2.4 Enzyme Production and Purification

The selected transformants were grown for 2 days at 37°C from conidial inocula as stationary cultures in 1-liter flasks, containing 80 ml of high-carbon, high-nitrogen (HCHN) medium, containing 2% glucose and 12 mM NH_4 tartrate, supplemented with 0.2% tryptone [Sollewijn Gelpke et al., 1999a]. Homogenized mycelial mats from the stationary cultures were used as inocula for 1-liter HCHN cultures in 2-liter flasks, supplemented with 3 mM VA and 0.1% Tween 80. The 1-liter cultures were incubated at 28°C for 4 days at 150 rpm on a rotary shaker [Sollewijn Gelpke et al., 1999a]. The extracellular medium of 14 1-liter HCHN cultures was harvested and subjected to successive steps of hollow-fiber ultrafiltration (10 kDa cutoff, Amicon), Phenyl-Sepharose chromatography, Sephadex G-100 size exclusion chromatography, and FPLC-MonoQ anion exchange column chromatography as described previously [Mayfield et al., 1994; Sollewijn Gelpke et al., 1999a]. Wild-type LiPH8 was produced and isolated as described previously [Gold et al., 1984; Wariishi and Gold, 1990].

6.2.5 SDS-PAGE and Isoelectric Focusing

SDS-PAGE was performed using a 10% Tris-glycine gel system and a Miniprotean II apparatus (BioRad); the BioRad SDS-PAGE Low Range marker mix was used. Isoelectric focusing (IEF) electrophoresis was performed using the Pharmacia Phastsystem with IEF Phastgels (pH 3–9) and the Sigma IEF Mix 3.6–6.6 marker kit. All gels were stained with Coomassie blue.

6.2.6 Enzyme Assays and Spectroscopic Procedures

Electronic absorption spectra of the various oxidation states of the LiP enzymes and steady-state kinetic data were collected at room temperature, using a Shimadzu UV-260 spectrophotometer. The wild-type or mutant LiP compound I oxidized state was prepared by mixing equimolar amounts of enzyme and H_2O_2 in water. The LiP compound II oxidized state was prepared by mixing equimolar amounts of enzyme and ferrocyanide in water followed by 1 equiv H_2O_2. Enzyme concentrations were determined at 407 nm using an extinction coefficient of 133 mM^{-1} cm^{-1} [Gold et al., 1984]. H_2O_2 concentrations were determined using ϵ_{240} = 43.6 M^{-1} cm^{-1} [Kulmacz, 1986].

VA and ABTS oxidation pH profiles by the wild-type and mutant enzymes were obtained by measuring the specific activity of the oxidation reactions conducted in 20 mM sodium succinate buffer at pH values from 3.0 to 6.0. For the oxidation of VA to veratrylaldehyde, the reaction mixture (1 ml) contained 2 μg of LiP, 2 mM VA, and 0.1 mM H_2O_2 in sodium succinate (20 mM); vertraldehyde formation was followed at 310 nm (ϵ_{310} = 9.3 M^{-1} cm^{-1}). The ABTS oxidation reactions (1 ml) contained 0.5 mM ABTS, 0.1 mM H_2O_2, and 2 μg of LiP, and were followed at 405 nm (ϵ_{405} = 36.6 M^{-1} cm^{-1}) [Glenn and Gold, 1985; Doyle et al., 1998].

Steady-state kinetic analysis for the oxidation of VA and ferrocyanide yielded apparent K_m and k_{cat} values which were calculated from linear double-reciprocal plots of the rates of oxidation versus varying substrate concentrations. VA oxidation was measured at 310 nm, and the initial rates were determined in the presence of 2 μg of enzyme/ml, in 20 mM sodium succinate (pH 3.0). The oxidation of ferrocyanide to ferricyanide was measured at 420 nm (ϵ_{420} = 1 mM^{-1} cm^{-1} [Cheddar et al., 1989]),

using various concentrations of ferrocyanide in the presence of 0.2 mM H_2O_2 and 2 mg/ml LiP.

6.2.7 Transient-State Kinetics

Transient-state kinetic measurements were conducted at 25 ± 0.1 °C using an Applied Photophysics stopped-flow reaction analyzer (SX.18MV) with sequential mixing and a diode array detector for rapid scanning spectroscopy. LiPI formation was measured at 397 nm, an isosbestic point between compounds I and II, by mixing 2 μM native enzyme in 20 mM sodium succinate (pH 3.0) with a 10–50-fold molar excess of H_2O_2 in the same buffer. LiPI reduction was measured at 417 nm in reaction mixtures containing 2 μM of compound I and at least a 10-fold molar excess of VA in 20 mM sodium succinate (pH 3.0 or 4.5). LiPI was first prepared by premixing equimolar amounts of enzyme and H_2O_2 in H_2O, and its formation was confirmed by diode array scanning. The reduction of LiPII was measured at 407 nm in reaction mixtures containing 2 μM LiPII and at least a 10-fold molar excess of VA in 20 mM sodium succinate (pH 3.0). LiPII was prepared by mixing equimolar amounts of enzyme and ferrocyanide in water, followed by 1 equiv of H_2O_2 in water; formation of LiPII was confirmed by diode array scanning. Typically, six substrate concentrations were used in triplicate measurements. Curve fitting was performed using the manufacturer's software.

6.2.8 UV-Vis Spectroscopic Analysis of Reactions of wtLiP and W171A

Stopped-flow diode array spectra were obtained for reactions of native wtLiP and W171A with excess H_2O_2, using a reaction mixture of ~4 μM enzyme and a 65-fold molar excess of H_2O_2 in 20 mM sodium succinate (pH 4.0). Absorption spectra were collected over 15.4 s. The stability of LiPI was investigated by incubation of ~2 μM compound I in 20 mM sodium succinate at pH 3.0, 4.0, 4.5, and 6.0. Compound I was first prepared by premixing equimolar amounts of enzyme and H_2O_2 in water. The spontaneous decay of compound I was followed at 417 nm.

Reactions of wtLiP and W171A with VA were also assessed using stopped-flow diode array scanning. Compound I was prepared as described above, using ~2

μM enzyme, and was incubated with a 10^3-fold molar excess of VA in 20 mM sodium succinate (pH 4.5). Absorption spectra were collected over 8 s. Absorption spectra were also collected for reactions of the W171A variant enzyme under steady-state conditions. Native W171A enzyme (4 μM) was incubated with 65-fold molar excess of H_2O_2 in 20 mM sodium succinate (pH 4.5), followed by the addition of 10^3-fold molar excess of VA, or the enzyme was incubated with 10^3-fold molar excess of VA in 20 mM sodium succinate (pH 4.5), followed by addition of 65-fold molar excess of H_2O_2.

6.2.9 Chemicals

Hydrogen peroxide 30% (w/w) solution was obtained from Sigma. VA was obtained from Aldrich and was purified by vacuum distillation. All other chemicals were reagent grade. Solutions were made in HPLC-grade water obtained from Aldrich.

6.3 Results

6.3.1 Expression and Purification of the Mutant Enzymes

The *P. chrysosporium* homologous expression system for LiP [Sollewijn Gelpke et al., 1999a] was used to express the mutant LiP enzymes H82A, Q222A, W171A, and F267L in the extracellular medium of HCHN-agitated shake cultures. The expression constructs for each of the variant enzymes were used to transform the uracil auxotrophic strain Ura11 (OGC316-7), resulting in the isolation of at least 20 transformants for each mutation. Twelve transformants of each mutation were grown in HCHN stationary cultures and screened for extracellular LiP activity using the ABTS assay or by identifying extracellular LiP enzyme using western blots. Selected transformants, which produced LiP enzyme in sufficient quantities, were further purified by isolating single basidiospores [Alic et al., 1987], and after rescreening, one isolate for each mutation was selected to obtain the strains H82A-T2:4, Q222A-T3:1, W171A-T6:1 and F267L-T8:1. Each of these transformant strains expressed extracellular recombinant LiP (rLiP) when grown in HCHN shake cultures at 28°C

for 4 days, conditions under which endogenous peroxidases are not expressed [Mayfield et al., 1994; Sollewijn Gelpke et al., 1999a]. The variant LiPs were purified to homogeneity as determined by SDS-PAGE and IEF. The molecular masses of the LiP variants (~42 kDa) and the pI values (~3.3) were similar to those of wtLiP (Fig. 6.1). The yields of expressed variant enzymes were 0.5–1.5 mg/l, which is comparable to that of recombinant wild-type LiPH8 [Sollewijn Gelpke et al., 1999a]. Typically, mutant enzymes were purified to R_z values of >3.

6.3.2 Spectral Properties of the LiP Mutant Enzymes

The electronic absorption spectra of the native enzyme and oxidized intermediates, compounds I and II, for each of the LiP variant enzymes were essentially identical to those of the wild-type enzyme, as shown in Fig. 6.2 for wtLiP and W171A, suggesting that substitutions of Ala for H82, Q222, and W171, and Leu for F267, do not significantly alter the heme environment of the protein.

6.3.3 Steady-State Kinetics

To assess the oxidation of VA by the wild-type and variant LiPs under steady-state conditions, linear double-reciprocal plots of initial oxidation rates were obtained over a range of H_2O_2 and VA concentrations. The apparent k_{cat} values for VA oxidation and the apparent K_m and k_{cat}/K_m values for VA and H_2O_2 are listed in Table 6.1. The apparent k_{cat} values for the H82A, Q222A, and F267L variants decreased only ~1.2-fold compared to that of wtLiP. In contrast, the W171A variant enzyme lost all VA oxidation activity. The apparent K_m values were similar between the H82A, Q222A, and wtLiP enzymes. However, the F267L variant exhibited a 3-fold increase in apparent K_m, suggesting that this residue may also be involved in the oxidation of VA by LiP. The $k_{cat\ app}$, $K_{m\ app}$, and k_{cat}/K_m values for ferrocyanide oxidation by wtLiP and variant LiPs were essentially identical for wtLiP and all LiP variants (Table 6.2).

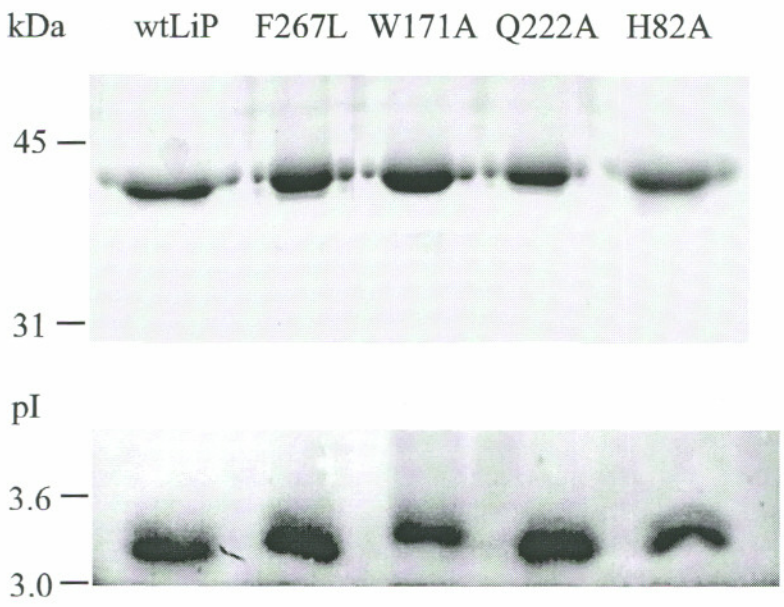

Fig. 6.1 Molecular mass and pI determination of wtLiP and the LiP variants F267L, W171A, Q222A, and H82A of LiP. (**A**) SDS-PAGE using a 10% Tris-glycine gel and (**B**) IEF using a Phastgel 3-9 of wild-type and LiP variants, showing similar M_r and pI for each enzyme.

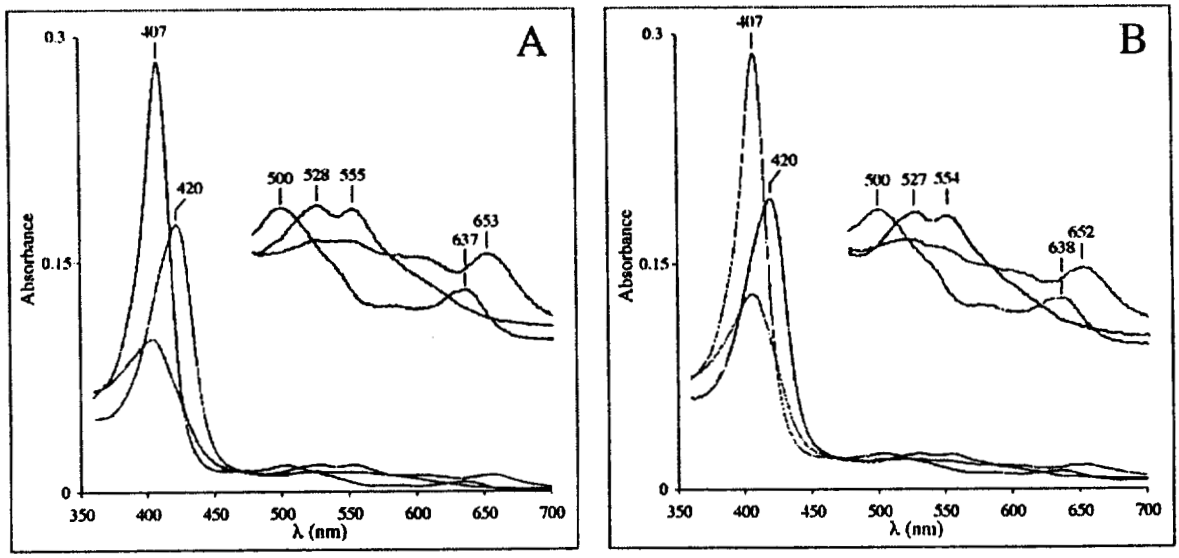

Fig. 6.2 Electronic absorption spectra of the native enzyme and oxidized intermediates, compounds I and II, are shown for wtLiP (**A**) and for the W171A variant enzyme (**B**). Samples contained ~2 μM enzyme, and the intermediates were produced as described in the text.

Table 6.1

Kinetic Parameters for the Steady-State Oxidation of VA by wtLiP and LiP Mutants[a]

Enzyme	k_{cat} (s^{-1})	VA		H_2O_2	
		K_m (μM)	k_{cat}/K_m ($M^{-1}s^{-1}$)	K_m (μM)	k_{cat}/K_m ($M^{-1}s^{-1}$)
wtLiP	19.9	102.9	2.5×10^5	48.6	4.8×10^5
W171A	na[b]	nr[c]	nr	nr	nr
Q222A	15.6	92.8	1.9×10^5	39.6	4.4×10^5
H82A	15.9	111.7	1.7×10^5	53.1	3.2×10^5
F267L	15.1	295.1	0.5×10^5	50.7	3.0×10^5

[a] Reactions were carried out in 20 mM potassium-succinate, pH 3.0. Apparent K_m and k_{cat} values for VA were determined using 0.1 mM H_2O_2, and apparent K_m and k_{cat} values for H_2O_2 were determined using 0.4 mM VA.
[b] na = no detectable activity.
[c] nr = no reaction.

Table 6.2

Steady-State Kinetic Parameters for the Oxidation of Ferrocyanide by Wild-Type and Variant LiP Enzymes[a]

Enzyme	k_{cat} (s^{-1})	K_m (μM)	k_{cat}/K_m ($M^{-1}s^{-1}$)
wtLiP	65.8	48.5	1.4×10^6
W171A	60.8	65.4	0.9×10^6
Q222A	53.2	71.8	0.7×10^6
H82A	76.4	64.0	1.2×10^6
F267L	61.5	57.1	1.1×10^6

[a] Reactions were carried out in 20 mM potassium succinate (pH 3.0). Apparent K_m and k_{cat} values for ferrocyanide oxidation were determined using 0.2 mM H_2O_2.

6.3.4 pH Profiles for the Oxidation of VA and ABTS

The specific activity for the oxidation of VA and ABTS was measured over a range of pH values for wtLiP and the LiP variant enzymes (Fig. 6.3). The specific activity for VA oxidation by wtLiP was highest at pH 3.0 and decreased gradually to $<1\ s^{-1}$ near pH 6.0. The H82A, Q222A, and F267L mutants exhibited a similar decrease in specific activities over the pH range of 3.0–6.0, while the W171A variant did not oxidize VA over this entire pH range. The specific activities for ABTS oxidation also exhibited a gradual decrease with increasing pH varying from $\sim$30–50 s^{-1} at pH 3.0 to $<2\ s^{-1}$ at pH 5.5, for wtLiP as well as the LiP mutants (Fig. 6.3).

6.3.5 Transient-State Kinetics

Transient-state kinetic rate constants were determined for each step in the LiP catalytic cycle. The kinetic traces for LiPI formation exhibited exponential character from which observed pseudo-first-order rate constants (k_{1obs}) were calculated. The k_{1obs} values were linearly proportional to H_2O_2 concentrations at 10–50-fold excess [data not shown]. The apparent second-order rate constants (k_{1app}) for LiPI formation were similar for the wild-type and mutant LiP enzymes (Table 6.3).

At pH 3.0 and 4.5, exponential kinetic traces were obtained for wtLiP, H82A, Q222A, and F267L compound I reduction, yielding observed pseudo-first-order rate constants (k_{2obs}) over a range of VA concentrations. The obtained k_{2obs} values were linearly proportional to the VA concentration for these enzymes, resulting in apparent second-order rate constants (k_{2app}) for LiPI reduction (Table 6.3). The k_{2app} values at pH 3.0 were very similar for H82A, Q222A, and wtLiP; however, the k_{2app} value for F267L was decreased by $\sim$2-fold. At pH 4.5, the k_{2app} values for H82A, Q222A, F267L, and wtLiP were similar but were slightly decreased compared to those at pH 3.0. The kinetic traces for the W171A compound I reduction in the presence of VA also exhibited exponential character at at various pHs, but the rates were in the range of the spontaneous rate of reduction. The k_{app} value was very low, suggesting that compound I reduction does not correlate with VA oxidation. The k_{2obs} values were

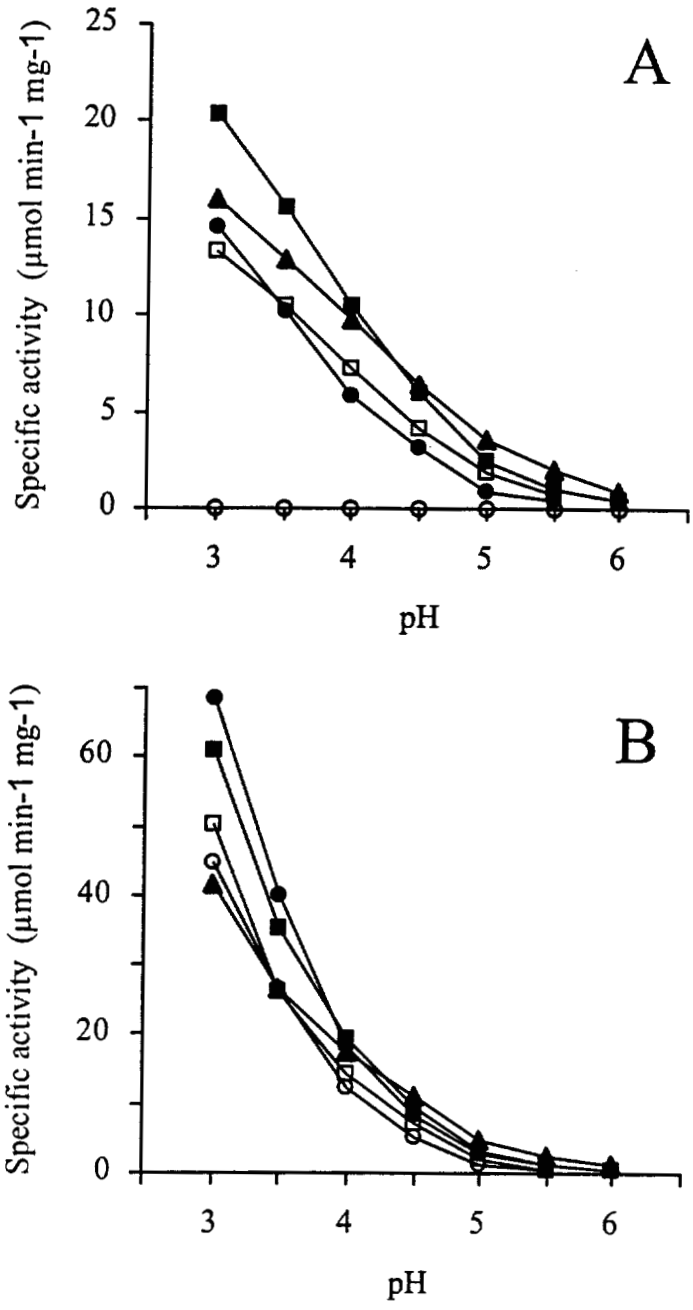

Fig. 6.3 pH profiles for the specific activities of VA (**A**) and ABTS (**B**) oxidation by the wild-type (■), H82A (•), Q222A (▲), F267L (□), and W171A (○) LiP variants. The oxidation reactions were performed in 20 mM sodium succinate buffer, using 2 μg of enzyme, 0.1 mM H_2O_2, and 2 mM VA or 0.5 mM ABTS.

Table 6.3

Kinetic Parameters for the Formation of LiP Compound I by H_2O_2 and Reduction of Compound I by VA in Wild-Type and Variant LiP Enzymes[a]

Enzyme	Compound I formation	Compound I reduction by VA	
	k_{1app} ($M^{-1}s^{-1}$)	k_{2app} ($M^{-1}s^{-1}$)	
		pH 3.0	pH 4.5
wtLiP	$(4.67 \pm 0.04) \times 10^5$	$(9.70 \pm 0.08) \times 10^5$	$(5.82 \pm 0.08) \times 10^5$
Q222A	$(4.58 \pm 0.08) \times 10^5$	$(8.82 \pm 0.11) \times 10^5$	$(4.12 \pm 0.07) \times 10^5$
H82A	$(4.39 \pm 0.06) \times 10^5$	$(8.70 \pm 0.07) \times 10^5$	$(5.71 \pm 0.04) \times 10^5$
F267L	$(4.42 \pm 0.04) \times 10^5$	$(4.20 \pm 0.07) \times 10^5$	$(3.75 \pm 0.05) \times 10^5$
W171A	$(4.83 \pm 0.06) \times 10^5$	nc[b]	nc

[a] Reactions were performed in 20 mM potassium succinate (pH 3.0 or pH 4.5) as indicated, using ~1 μM enzyme. The formation of compound I was monitored as the decrease of the native enzyme peak at 397 nm. The reduction of compound I in the presence of VA was monitored at 417 nm.

[b] nc = not calculated.

low and stayed in the range of the k_{2obs} value of the spontaneous decay of W171A LiPI to LiPII.

For LiP compound II reduction by VA, exponential kinetic traces were obtained for wtLiP and the H82A, Q222A, and F267L variants, yielding observed pseudo-first-order rate constants (k_{3obs}) for VA concentrations of 25 μM to 2 mM. The plots of k_{3obs} values versus the VA concentration were hyperbolic, indicating saturation kinetics [Wariishi et al., 1991a]. The first-order rate constants (k_3) and the dissociation constants (K_D) were calculated from the least-squares fit of k_{3obs} values versus the VA concentration, and are shown in Table 6.4. The k_3 values for H82A, Q222A, F267L, and wtLiP were similar. However, the K_D for the F267L variant increased $\sim$4-fold compared to the K_D of H82A, Q222A, and wtLiP. No W171A compound II reduction by VA was detected.

6.3.6 Spectroscopic Analysis of W171A

The reactions of both the wtLiP and W171A native enzyme with H_2O_2 were investigated. Stopped-flow diode array spectra of the enzymes in the presence of excess H_2O_2 clearly show the conversion of native enzyme to compound I and subsequent conversion to compound III*, evidenced by the shift in the Soret peak to 419 nm and the appearance of peaks at 545 and 578 nm in the visible region (Fig. 6.4). Addition of excess VA to wild-type LiPIII* results in the conversion of compound III* to native enzyme. This is followed by the catalytic turnover of VA oxidation, as shown previously [Wariishi and Gold, 1990]. In contrast, addition of excess VA to W171A compound III* did not result in its conversion to native enzyme or compound II. Instead, a slow decrease in absorbance intensity with no shift in the peaks occurred [data not shown].

The stability of compound I of wtLiP and of the W171A variant was assessed in 20 mM sodium succinate at pH 3.0, 4.0, 4.5, and 6.0. The single-wavelength traces (417 nm) of the spontaneous reduction of compound I were exponentials from which observed rate constants (k_{obs}) were calculated (Table 6.5). The k_{obs} values of

Table 6.4

Kinetic Parameters for LiP Compound II Reduction by VA in Wild-Type and Variant LiP Enzymes[a]

Enzyme	Compound II reduction by VA		
	k_3 (s^{-1})	K_D (μM)	k_{3app} ($M^{-1}s^{-1}$)
wtLiP	34.0 ± 0.2	(1.82 ± 0.05) × 10^2	1.85 × 10^5
Q222A	32.8 ± 0.5	(1.80 ± 0.08) × 10^2	1.82 × 10^5
H82A	26.4 ± 0.4	(1.60 ± 0.07) × 10^2	1.65 × 10^5
F267L	41.1 ± 0.5	(6.58 ± 0.13) × 10^2	0.63 × 10^5
W171A	na[b]	nr[c]	nr

[a] Reactions were performed in 20 mM potassium succinate (pH 3.0) using ~2 μM enzyme and were monitored at 407 nm.
[b] na = no detectable activity.
[c] nr = no reaction.

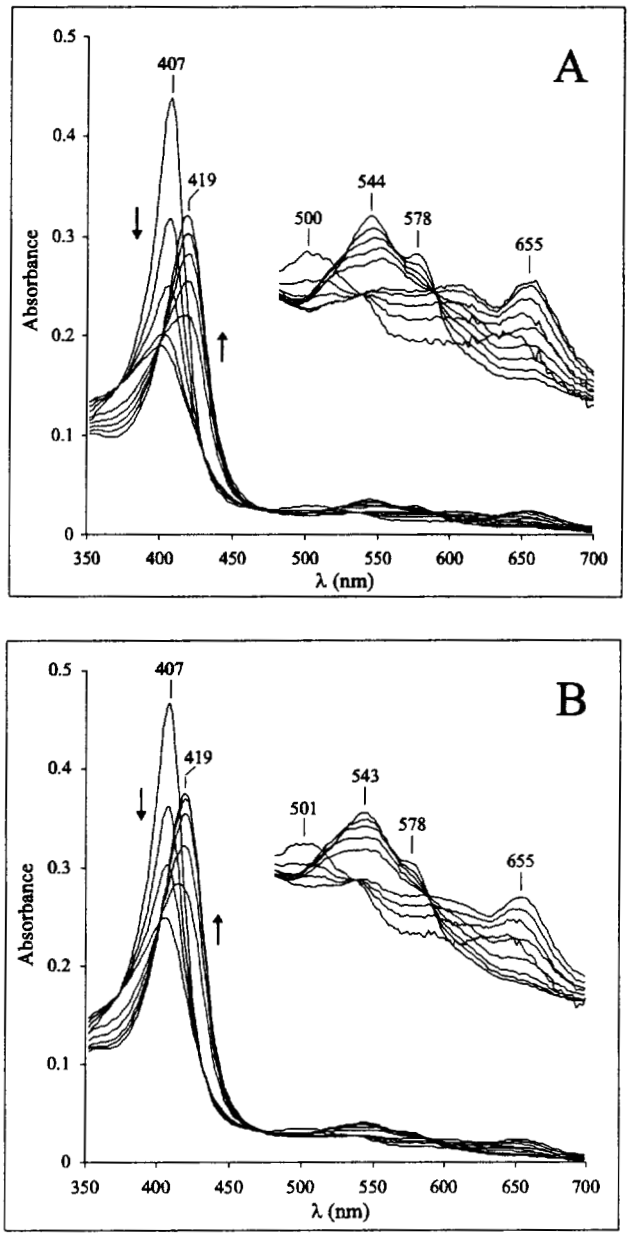

Fig. 6.4 Reaction of the wtLiP and W171A variant with H_2O_2. Stopped-flow spectra of the wtLiP (**A**) and the W171A variant (**B**) incubated with 65-fold molar excess of H_2O_2 in 20 mM sodium-succinate (pH 4.0), using ~ 4 μM of each enzyme. The arrows indicate decrease or increase of absorption values over time. The series of spectra were collected at logarithmic intervals between 3 ms and 15.4 s, starting with 5 spectra from 3 to 40 ms, followed by 5 spectra from 1.1 to 15.4 s (A), or starting with 4 spectra from 3 to 27 ms, followed by 5 spectra from 1.1 to 15.4 s (B).

Table 6.5

Observed Rates for Spontaneous Reduction of Compound I in the Wild-Type and W171A Variant[a]

pH	k_{obs} (s^{-1})	
	wtLiP	W171A
3.0	6.5 ± 0.4	6.0 ± 0.3
4.0	2.2 ± 0.3	2.9 ± 0.3
4.5	(8.0 ± 0.4) × 10^{-1}	(9.6 × 0.5) × 10^{-1}
6.0	(5.0 ± 0.5) × 10^{-2}	(2.0 ± 0.1) × 10^{-2}

[a] Equimolar amounts of enzyme and H_2O_2 were premixed to form compound I in 20 mM sodium succinate at the indicated pH.

spontaneous compound I reduction were similar for wtLiP and W171A at each assessed pH level.

Under steady-state VA oxidation conditions, the W171A variant formed compound III*. Native W171A enzyme was incubated with excess VA, followed by the addition of excess H_2O_2. Absorption spectra were collected from 3 ms to 32.4 s after the start of the reaction as a series of 15 spectra, distributed logarithmically (Fig. 6.5). The native W171A enzyme was rapidly oxidized to compound I by H_2O_2, which was followed by a conversion of compound I to compound II, and subsequent conversion of compound II to compound III*. The oxidized intermediates were identified by absorption maxima in the 480–700 nm range (Fig. 6.5).

6.3.7 Spectroscopic Analysis of Reactions with VA

Electronic absorption spectra of the W171A and wtLiP native enzymes and oxidized intermediates, compounds I and II were essentially identical (Fig. 6.2). Diode array absorption spectra of the incubation of W171A compound I with excess VA in buffer showed that W171A compound I is converted to compound II over ~8 s (Fig. 6.5A). In contrast, transient-state kinetic analysis shows that wild-type LiPI is reduced rapidly to native enzyme in the presence of excess VA, with a k_{2app} value for compound I reduction of 5.82×10^5 $M^{-1}s^{-1}$ and a k_{3app} value for LiPII reduction of $\sim 5.5 \times 10^4$ $M^{-1}s^{-1}$ [Wariishi et al., 1991a], under these conditions. Incubation of W171A compound II, prepared with equimolar amounts of ferrocyanide and H_2O_2, with excess VA did not alter the absorption spectrum [data not shown].

6.4 Discussion

Lignin peroxidase catalyses the one-electron oxidation of nonphenolic lignin model compounds with high redox potentials via the formation of a substrate aryl cation radical [Kersten et al., 1985; Renganathan et al., 1986; Buswell and Odier, 1987; Kirk and Farrell, 1987; Higuchi, 1990; Schoemaker, 1990]. However, the detailed mechanism by which LiP degrades polymeric lignin remains unclear. *P. chrysosporium* and other LiP-producing fungi secrete VA [Kirk and Farrell, 1987;

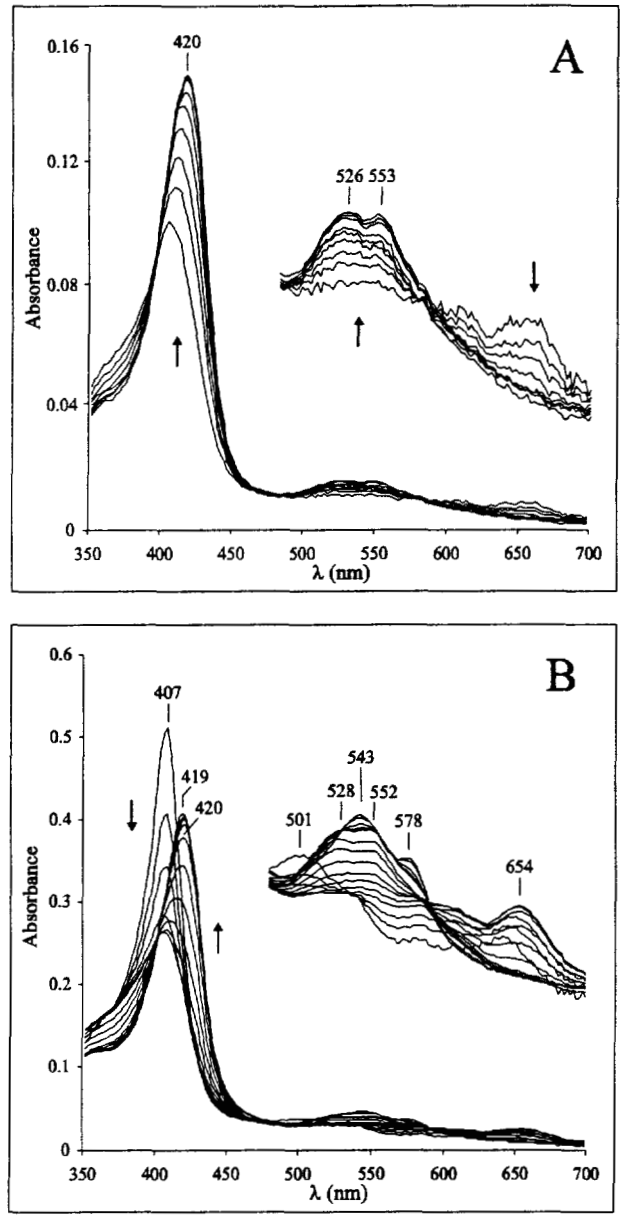

Fig. 6.5 Reactions of the W171A variant LiP with VA and H_2O_2. (**A**) Stopped-flow spectra of W171A compound I reduction by VA, using ~4 μM enzyme and 1000-fold molar excess of VA, in 20 mM sodium succinate (pH 4.5). Spectra were collected from 9 ms to 8 s with logarithmic intervals. (**B**) Stopped-flow spectra of the steady-state oxidation of VA by W171A in the presence of ~4 μM enzyme, a 65-fold molar excess of H_2O_2, and a 1000-fold molar excess of VA, in 20 mM sodium succinate (pH 4.5). A series of 15 spectra was collected from 3 ms to 32.4 s, distributed logarithmically. The arrows indicate a decrease or increase of absorption values at the wavelength indicated over time.

Hatakka, 1994], which has been found to stimulate the depolymerization of synthetic lignin and the oxidation of a variety of recalcitrant substrates by LiP [Harvey et al., 1986; Valli et al., 1990; Hammel and Moen, 1991; Sheng and Gold, 1999]. Several mechanisms have been proposed to account for the stimulation of LiP reactions by VA. Studies suggest that VA acts as a redox mediator in the oxidation of lignin and some model substrates [Harvey et al., 1986; Koduri and Tien, 1995; Tien and Ma, 1997; Sheng and Gold, 1999]. Other studies suggest that VA aids the enzyme in completing its catalytic cycle during the oxidation of at least some substrates [Valli et al., 1990; Koduri and Tien, 1994].

Previously, we developed a homologous expression system to produce active *P. chrysosporium* LiPH8 [Sollewijn Gelpke et al., 1999a]. This system was used to produce variant LiPs, which may be involved in the oxidation of VA and other substrates. The W171A mutant enzyme was used to reexamine a recently proposed site for VA oxidation [Doyle et al., 1998]. The F267L mutant was used to assess the role of this residue, which is in proximity to Trp171. The H82A and Q222A mutant enzymes were used to investigate the role of the heme access channel, another proposed site for VA oxidation [Poulos et al., 1993; Schoemaker et al., 1994] and possibly an alternative substrate oxidation site. The recombinant mutant enzymes all have a molecular mass, pIs, and absorption spectra similar to wtLiP, suggesting that the variant proteins are produced and secreted without significant changes in either the overall structure or the heme environment.

Crystal structure data show that the amino acids H82 and Q222 are located in the heme access channel of LiP [Piontek et al., 1993; Poulos et al., 1993], which is the apparent site of substrate oxidation for other peroxidases such as HRP, *Coprinus* peroxidase, and ascorbate peroxidase [Smith and Veitch, 1998]. A binding mode for VA involving H82 and Q222 was previously proposed, based on modeling studies [Poulos et al., 1993; Schoemaker et al., 1994]. A third amino acid residue at the heme access channel, E146, was mutated in previous studies, resulting in a ~2–3-fold reduced VA oxidation activity [Ambert-Balay et al., 1998; Doyle et al., 1998] and a significant increase in the pK_a for the oxidation of the small, negatively charged dye 4-[(3,5-difluoro-4-hydroxyphenyl)azo]benzenesulfonic acid (DFAD) [Doyle et al.,

1998]. The decrease in VA oxidation activity for these variants was minor compared to the large effect of the W171F and W171S mutations on VA oxidation [Doyle et al., 1998]. E146 does appear to control the low-pH optimum for the oxidation of DFAD, suggesting that the heme access channel may be the productive site for this particular substrate [Doyle et al., 1998]. However, E146 is conserved in both MnP and LiP enzymes, suggesting a function which is not specific for LiP.

Since both His82 and Q222 were originally proposed to be part of the VA binding site [Poulos et al., 1993; Schoemaker et al., 1994], we decided to examine the effects of mutations of these two residues on the oxidation of VA, ferrocyanide, and ABTS. Steady-state kinetic analyses of VA oxidation by LiP show that the apparent K_m values for these variants are similar to that of wtLiP, whereas the apparent k_{cat} values for these mutants are only slightly reduced compared to wtLiP. In addition, the pH profiles of VA oxidation were similar for H82A, Q222A and wtLiP enzymes. These results suggest that the H82A and Q222A mutations have little effect on VA oxidation and, therefore, are unlikely to be components of the VA binding site in LiP. Since Glu146 is also in the heme access channel, our results suggest that this residue is unlikely to affect VA oxidation directly. Thus, the decrease in VA oxidation in the E146G mutant reported earlier [Doyle et al., 1998] is probably due to an indirect effect such as a small change in enzyme structure or in an important salt bridge.

Transient-state kinetic analyses of the individual steps in the LiP catalytic cycle show that the H82A and Q222A mutations do not have a significant effect on the formation of LiPI by H_2O_2 or the reduction of the oxidized intermediates, LiPI and LiPII, by VA. Thus, residues His82 and Gln222, which are located at the heme access channel, do not affect the binding or oxidation of VA, suggesting that the heme access channel is an unlikely VA binding site in LiP. Analysis of the steady-state oxidation of ferrocyanide showed essentially identical k_{cat} and K_m values for wtLiP and the H82A and Q222A variant proteins. Furthermore, the pH profiles for the oxidation of ABTS by wtLiP and H82A and Q222A mutants were similar. Together, these results suggest that the residues His82 and Gln222 are not involved in the

Our results show that the incubation of native W171A or wild-type enzyme with excess H_2O_2 results in the rapid formation of compound I, followed by its conversion to compound III*, as clearly shown by the absorption peaks at 543 and 578 nm (Fig. 6.4). The latter conversion results from several reactions, including the decay of compound I to compound II, followed by conversion of compound II to compound III and compound III to compound III* by H_2O_2 [Wariishi and Gold, 1990; Wariishi et al., 1990]. In addition, the so-called rapid phase for compound I conversion was observed by Doyle et al. in a single-wavelength trace at 412 nm [Doyle et al., 1998], although the isosbestic point between LiP compounds I and II is located around 417 nm [Dunford, 1999], thereby further complicating the analysis of their kinetic traces. Moreover, the proposed rate for a spontaneous electron transfer of $\sim 2.3\ s^{-1}$ [Doyle et al., 1998] is much too slow to support the VA oxidation k_{cat} of around $20\ s^{-1}$.

Incubation of LiP compound I, prepared by mixing equimolar amounts of enzyme and H_2O_2, resulted in spontaneous decay for both wtLiP and W171A at several pH levels. The decay of compound I was exponential over time for wtLiP and W171A, and the rates of the decay were similar for both variants at each pH. These results indicate that the spontaneous decay of compound I may not be a result of the spontaneous electron transfer from amino acid Trp171 to the porphorin π-cation radical, suggesting that electron transfer does not occur in the absence of VA. The binding of VA to wtLiP probably initiates the transfer of electrons from VA via Trp171 to the heme edge, resulting in oxidized VA. A possible through-protein electron-transfer pathway will need to be determined. The direct pathway from Trp171 to the proximal histidine ligand of the heme, His176, via the protein backbone is approximately 21.5 Å. An alternative 12.7-Å-long pathway runs partly through the protein backbone and includes two hydrogen bonds. Mutation studies on the amino acids between Trp171 and His176 may indicate a possible shortcut through the side chain of one of these residues to the heme.

The local environment near Trp171, the apparent site of VA oxidation, is acidic and highly conserved (Fig. 6.6) [Poulos et al., 1993]. In addition to Trp171, the amino acids Asp165, Glu250, Lys260, and Phe267 are completely conserved

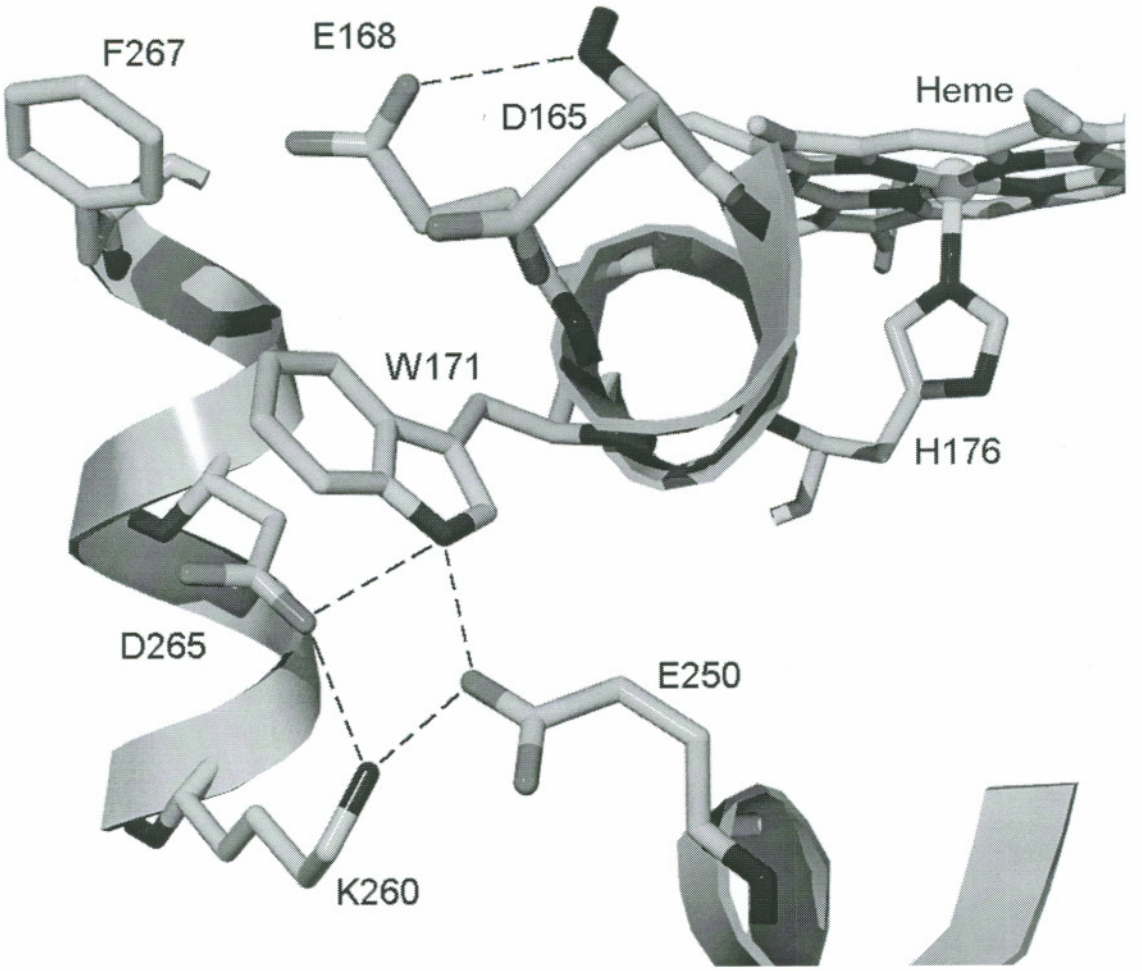

Fig. 6.6 View of the environment surrounding Trp171 of LiP [Piontek et al., 1993; Poulos et al., 1993].

among known LiP enzyme sequences, whereas Glu168 is only partly conserved. In LiPH8, Glu250, Asp264, and Lys260 appear to form a H-bonding network with the nitrogen of the Trp171 indole side chain, possibly orienting Trp171 in a fixed position (Fig. 6.6). On the other side of Trp171, the acidic residues, Asp165 and Glu168, may be involved in the composition of the acidic environment, which has been proposed to stabilize the $VA^{+\bullet}$ [Khindaria et al., 1996]. However, at lower pH, these carboxylic residues, which have a typical pK_a of 4.4, are most likely protonated, resulting in neutral side chains that are unable to stabilize the positively charged $VA^{+\bullet}$. Kinetic studies show that the activity for VA oxidation increases with decreasing pH from 6 to 3. Therefore, additional studies are required to elucidate the role of these acidic residues in LiP function.

The aromatic residue, Phe267, located near Trp171 (Fig. 6.6) may be involved in the binding and oxidation of VA by a stacking interaction of the electron-rich π-systems of Trp171, VA, and Phe267. The aromatic character of this Trp171-centered VA binding site is disturbed by introduction of the F267L mutation. Kinetic analysis indicates that the steady-state oxidation of VA by F267L exhibited a $\sim$3-fold increase in K_m. The transient-state kinetic analysis of F267L compound II reduction by VA exhibited a $\sim$4-fold increase in K_D with no change in k_3 compared to wtLiP. Thus, both kinetics studies indicate that he F267L mutation affects VA binding to the enzyme, while the rate of oxidation remains similar to that of wtLiP.

In conclusion, these results indicate that mutations at the His82 and Gln222 positions in the heme access channel have little effect on VA oxidation, while a mutation at Trp171 eliminates the VA oxidation ability of the enzyme, confirming that Trp171 is essential for VA oxidation and suggesting that VA is oxidized at this site during catalysis. The local environment of Trp171 is involved in the binding of VA to this site as indicated by our results with the F267 mutation. The detailed mechanism of electron transfer from VA to the heme and the nature of the electron-transfer pathway await further studies.

CHAPTER 7
CONCLUSIONS AND FUTURE DIRECTIONS

7.1 Manganese Peroxidase

7.1.1 The Mn^{II} Binding Site

The structure-function studies of MnP [Sundaramoorthy et al., 1994, 1997; Kusters-van Someren et al., 1995; Kishi et al., 1996] indicate there is a site for Mn^{II} binding and oxidation at the surface of MnP, where the enzyme bound Mn^{II} is hexacoordinate, with two water ligands and four carboxylate ligands from the sidechains of the essential amino acids Glu35, Glu39 and Asp179, and heme propionate 6. Mutagenesis studies have demonstrated that an additional residue, Arg177, is important for Mn^{II} binding to the Mn^{II} binding site. Breaking the Arg177-Glu35 salt bridge by mutation of this residue, is likely to affect the ability of the enzyme to undergo the conformational change from the open configuration in the absence of Mn^{II}, to the closed configuration upon Mn^{II} binding.

Analysis of the MnP crystal structure does not reveal any other amino acids which may be involved in the oxidation of Mn^{II} at this binding site. Future research on the Mn^{II} binding site may assess the role of the heme propionates in the oxidation of Mn^{II}. The role of propionate 6, which is a Mn^{II} ligand, and the role of propionate 7, which ligates to the Mn^{II} via a water molecule can be investigated by exchange of the iron protoporphyrin IX for a modified heme prosthetic group. Refolding procedures of denatured MnP are being used to obtain recombinant MnP from E.coli [Whitwam and Tien, 1996], but may need further optimization in order to introduce a modified heme.

An alternative approach to investigate essential ligands and ligand orientations for Mn^{II} oxidation is to introduce Mn^{II} oxidation activity to a different enzyme.

Structure-function information of MnP is being used to construct a Mn^{II} binding site in CcP by protein engineering [Yeung et al., 1997; Wilcox et al., 1998]. In an analogous experiment, LiP can be used as the template to build a Mn^{II} site. The overall structures of LiP and MnP are very similar (Fig. 5.5) and it is possible that a Mn^{II} binding site can be constructed with high Mn^{II} oxidation activity. An understanding of the essential ligand orientations may help the development of a synthetic molecule with Mn^{II} oxidation capacity but with much higher temperature stability and resistance to oxidative stress than the MnP enzyme. In addition, an engineered LiP enzyme with its original activity and with high Mn^{II} oxidation activity may be useful in industrial processes.

Comparison of the deduced amino acid sequences of several MnP and LiP enzymes shows that MnP enzymes have a conserved C-terminal region, which is 10 amino acids longer than in LiP [Gold et al., 2000] and is absent in HRP and CcP. The role of this C-terminal region in MnP on Mn^{II} binding and oxidation and especially on the stability of MnP, can be assessed by mutagenesis studies. There are indications from the crystal structure analysis of MnP with Cd^{II} that a Cd^{II} binding site is present, involving the last three C-terminal amino acids and amino acid Asp84. This site may be involved in the increased temperature stability of MnP when incubated with Mn^{II} and Cd^{II} [Youngs et al., 2000]. In addition, MnP isozymes from *D. squalens* contain a sequence of C-terminal Asp residues, suggesting a possible role in the increased temperature stability of these enzymes. Future research on the temperature stability of peroxidases should also include determination of the mechanism of inactivation. Is the inactivation a result of protein unfolding near the active site or at another local position, or is the loss of the heme prosthetic group the result of inactivation. Local unfolding may be inhibited by the addition of stabilizing metal ions, or by the introduction of additional disulfide bonds.

A new protein engineering approach with the objective to create enzymes with high temperature stability, high resistance to stress and a possible activity increase is directed evolution. The peroxidase from *C. cinereus* was optimized by directed evolution experiments, resulting in a peroxidase with increased temperature stability and resistance to oxidative stress while retaining its original substrate oxidation

activity levels [Cherry et al., 1999]. Random mutagenesis in combination with gene shuffling, followed by the screening of a large number of recombinant mutant enzymes can result in the isolation of significantly improved mutant enzymes, without knowing the specific mutations in advance. Mutations which lead to enzyme improvement can later increase understanding about the mechanism of substrate oxidation and factors involved in enzyme stability. The directed evolution of LiP or MnP may lead to improved enzyme characteristics and improved understanding of the enzyme mechanisms in a significantly shorter time than the 'traditional' approach. However, essential requirements for the directed evolution procedure are fast production of mutant enzymes and fast activity screening. Our current homologous expression system is not suitable to generate the large variety of mutant enzymes that are needed to generate and identify advantageous mutations. The development of a yeast expression system for MnP or LiP is an essential first step in this approach.

7.1.2 The Heme Environment and Peroxide Binding Site

Multiple structure-function studies of the heme environment in HRP and CcP [Vitello et al., 1992, 1993; Erman et al., 1993; Newmyer and Ortiz de Montellano, 1995; Smith and Veitch, 1998] indicate that the mechanism of binding and reduction of H_2O_2 by the enzymes, resulting in the formation of compound I, are similar among these peroxidases [Poulos and Kraut, 1980; Dunford, 1999]. The enzymes from the family of plant and fungal peroxidases all have similar heme environments in which the important amino acids and their orientations are conserved. It is likely that structure-function studies on amino acid residues in the MnP heme environment will result in similar effects on the different steps of the catalytic cycle as the homologous mutations in HRP and CcP, thereby demonstrating a mechanism for MnP compound I formation which is similar to that of HRP or CcP. Future structure function studies on amino acids in the MnP heme environment may be difficult. Preliminary studies have shown that the homologous expression of this class of mutants does not result in the production of active enzyme, indicating that the development of an alternative recombinant expression system needs to be considered.

7.2 Lignin Peroxidase

7.2.1 Oxidation of Mn^{II} by LiP

A homologous expression system for LiP in *P. chrysosporium* was successfully developed. This system is analogous to the previously developed expression system for recombinant MnP [Mayfield et al., 1994]. This enabled the production of active recombinant LiP enzyme in the extracellular medium under high-nitrogen conditions. Sufficient rLiP is produced for spectroscopic and kinetic analysis, which indicate that folding, heme insertion and post-translational modification of rLiP is essentially identical to that of wtLiP. This expression system was used to produce recombinant LiP isozymes H2 and H8 and site-directed mutants of LiPH8. The rLiPH2 enzyme was used, together with homogeneously purified wild-type LiPH2 and wtLiPH8, to investigate previous claims that LiP was able to oxidize Mn^{II} at higher rates than VA [Khindaria et al., 1995]. Our results demonstrate that LiPH2 and LiPH8 are unable to oxidize Mn^{II} and that Mn^{II} is not a productive substrate for LiP.

7.2.2 The VA Oxidation Site in LiP

A previously proposed binding mode for VA in heme access channel of LiP [Poulos et al., 1993; Schoemaker et al., 1994], incorporated several amino acid contacts, including His82 and Gln222. However, mutation of the residues, His82 and Gln222, have no effect on VA oxidation, indicating that these residues are not involved in this reaction. In contrast, mutation of the amino acid Trp171 in LiP, which is not near the heme access channel, eliminated VA oxidation by LiP and the reduction of both compound I and II by VA. These results confirm that Trp171 is essential for VA oxidation [Doyle et al., 1998], suggesting that LiP has two substrate oxidation sites of which the VA oxidation site at Trp171 appears most important for oxidation of substrates with higher redox potential. Mutation of residue Phe267 near Trp171, negatively affects VA binding by LiP, whereas rates of VA oxidation remained unchanged. The aromatic residue Phe267 may be involved in the binding of VA by a stacking interaction of the electron rich π-systems of Trp171, VA and Phe267.

To elucidate the mechanism of substrate oxidation by LiP, the electron transfer pathway needs to be examined. Upon reduction of LiPI or LiPII, one electron is transferred from the site of substrate oxidation, Trp171, to the heme, where the porphyrin π-cation radical is located. Future site-directed mutagenesis studies may demonstrate the pathway for through-protein electron transfer. A direct pathway from Trp171 to the proximal histidine ligand of the heme, His176, through the protein backbone covers a distance of 21.5 Å, and is difficult to investigate with mutation studies. An alternative pathway is 12.7 Å long and runs partly through the protein backbone and includes two hydrogen bonds. Mutation studies on the amino acids between Trp171 and His176 may indicate a possible shortcut from Trp171 through the sidechain of Met172 or Leu173 to the heme. The possible absence of an electron pathway in a mutant LiP may also result in the absence of β-hydroxylation of Trp171.

The electron transfer may occur prior to substrate binding, which would result in the formation of a Trp171 protein radical. This mechanism is somewhat analogous to that of CcP, where the protein radical is formed directly after the two electron oxidation of the enzyme. However, UV-vis spectroscopy shows that the two electron oxidation state of LiP compound I with a porphyrin π-cation radical is fairly stable and is not affected by the Trp171 mutation. In addition the existence of a LiP protein radical has not been demonstrated by spectroscopic methods, e.g., EPR. Thus, the electron transfer may be initiated by the binding of substrate, thereby oxidizing the substrate directly without the formation of other spectroscopic enzyme intermediates. Further site-directed mutagenesis studies may reveal to what extent the residues in the Trp171 environment are involved in substrate binding and in substrate oxidation. Mutation of residue Phe267 has been shown to affect VA binding by LiP, whereas rates of VA oxidation remained unchanged. The aromatic residue Phe267 may be involved in the binding of VA by a stacking interaction of the electron rich π-systems of Trp171, VA and Phe267. The VA cation radical is possibly stabilized by acidic residues, including Glu168, Asp165, Glu250 and D265, in the Trp171 environment, thereby promoting VA oxidation. However, kinetic studies show that the activity for VA oxidation increases with pH decreasing from 6 to 3, suggesting a possible a-typical pK_a for the carboxylate sidechains of these amino acids. The H-bonding

network of Trp171, Glu250, Asp264 and Lys260 may stabilize the negative charge of the carboxylate sidechains of Glu250 and Asp264, thereby lowering the pK_a of these sidechains.

The reconstruction of a LiP active site, using an other peroxidase as a template may increase understanding of the mechanism of oxidation. It has been claimed that a single mutation in MnP, which introduces a Trp residue at a similar position as Trp171 in LiP, gives MnP a VA oxidation activity [Timofeevski et al., 2000]. The introduction of other residues in the new Trp environment may increase understanding of important interactions between enzyme and VA or other substrate.

LITERATURE CITED

Adler, E. (1977) Lignin chemistry. Past, present and future. *Wood Sci. Technol.* **11**, 169–218.

Akileswaran, L., M. Alic, E. K. Clark, J. L. Hornick, and M. H. Gold (1993) Isolation and transformation of uracil auxotrophs of the lignin-degrading basidiomycete *Phanerochaete chrysosporium. Curr. Genet.* **23**, 351–356.

Alic, M., and M. H. Gold (1985) Genetic recombination in the lignin-degrading basidiomycete *Phanerochaete chrysosporium. Appl. Environ. Microbiol.* **50**, 27–30.

Alic, M., C. Letzring, and M. H. Gold (1987) Mating system and basidiospore formation in the lignin-degrading basidiomycete *Phanerochaete chrysosporium. Appl. Environ. Microbiol.* **53**, 1464–1469.

Alic, M., E. K. Clark, J. R. Kornegay, and M. H. Gold (1990) Transformation of *Phanerochaete chrysosporium* and *Neurospora crassa* with adenine biosynthetic genes from *Schizophyllum commune. Curr. Genet.* **17**, 305–311.

Alic, M., M. B. Mayfield, L. Akileswaran, and M. H. Gold (1991) Homologous transformation of the lignin-degrading basidiomycete *Phanerochaete chrysosporium. Curr. Genet.* **19**, 491–494.

Alic, M., L. Akileswaran, and M. H. Gold (1997) Characterization of the gene encoding manganese peroxidase isozyme 3 from *Phanerochaete chrysosporium. Biochim. Biophys. Acta* **1338**, 1–7.

Ambert-Balay, K., S. M. Fuchs, and M. Tien (1998) Identification of the veratryl alcohol binding site in lignin peroxidase by site-directed mutagenesis. *Biochem. Biophys. Res. Commun.* **251**, 283–286.

Ander, P., and K.-E. Eriksson (1976) The importance of phenol oxidase activity in lignin degradation by the white-rot fungus *Sporotrichum pulverulentum. Arch. Microbiol.* **109**, 1–8.

Ander, P., K.-E. Eriksson, and H. S. Yu (1984) Metabolism of lignin-derived aromatic acids by wood-rotting fungi. *J. Gen. Microbiol.* **130**, 63–68.

Ander, P., I. Stoytschev, and K.-E. Eriksson (1988) Cleavage and metabolism of methoxyl groups from vanillic and ferulic acids by brown-rot and soft-rot fungi. *Cellulose Chem. Technol.* **22**, 255–266.

Andersson, L. A., V. Renganathan, A. A. Chiu, T. M. Loehr, and M. H. Gold (1985) Spectral characterization of diarylpropane oxygenase, a novel peroxide-dependent, lignin-degrading heme enzyme. *J. Biol. Chem.* **260**, 6080–6087.

Andersson, L. A., V. Renganathan, T. M. Loehr, and M. H. Gold (1987) Lignin peroxidase: resonance Raman spectral evidence for compound II and for a temperature-dependent coordination-state equilibrium in the ferric enzyme. *Biochemistry* **26**, 2258–2263.

Asada, Y., Y. Kumura, T. Oka, and M. Kuwahara (1992) Characterization of a cDNA and gene encoding a lignin peroxidase from the lignin-degrading basidiomycete *Bjerkandera adusta*. In *Biotechnology in the Pulp and Paper Industry* (M. Kuwahara and M. Shimada, Eds.). Uni Publishers, Tokyo, pp. 421–426.

Ator, M. O., and P. R. Ortiz de Montellano (1987) Protein control of prosthetic heme reactivity. Reaction of substrates with the heme edge of horseradish peroxidase. *J. Biol. Chem.* **262**, 1542–1551.

Banci, L., I. Bertini, E. A. Pease, M. Tien, and P. Turano (1992) ^{1}H NMR investigation of manganese peroxidase from *Phanerochaete chrysosporium*. A comparison with other peroxidases. *Biochemistry* **31**, 10009–10017.

Banci, L., I. Bertini, I. C. Kuan, M. Tien, P. Turano, and A. J. Vila (1993) NMR investigation of isotopically labeled cyanide derivatives of lignin peroxidase and manganese peroxidase. *Biochemistry* **32**, 13483–13489.

Banci, L., I. Bertini, L. Dal Pozzo, R. Del Conte, and M. Tien (1998) Monitoring the role of oxalate in manganese peroxidase. *Biochemistry* **37**, 9009–9015.

Bao, W., Y. Fukushima, K. A. Jensen, Jr., M. A. Moen, and K. E. Hammel (1994) Oxidative degradation of non-phenolic lignin during lipid peroxidation by fungal manganese peroxidase. *FEBS Lett.* **354**, 297–300.

Barr, D. P., and S. D. Aust (1994) Mechanisms white-rot fungi use to degrade pollutants. *Environ. Sci. Technol.* **28**, 78A–87A.

Barr, D. P., M. M. Shah, T. A. Grover, and S. D. Aust (1992) Production of hydroxyl radical by lignin peroxidase from *Phanerochaete chrysosporium*. *Arch. Biochem. Biophys.* **298**, 480–485.

Baunsgaard, L., H. Dalbøge, G. Houen, E. M. Rasmussen, and K. G. Welinder (1993) Amino acid sequence of *Coprinus macrorhizus* peroxidase and cDNA sequence encoding *Coprinus cinereus* peroxidase. A new family of fungal peroxidases. *Eur. J. Biochem.* **213**, 605–611.

Beguin, P. (1990) Molecular biology of cellulose degradation. *Annu. Rev. Microbiol.* **44**, 219–248.

Blanchette, R. A. (1991) Delignification by wood-decay fungi. *Annu. Rev. Phytopathol.* **29**, 381–398.

Blanchette, R. A., E. W. Krueger, J. E. Haight, M. Akhtar, and D. E. Akin (1997) Cell wall alteration in loblolly pine wood decayed by the white-rot fungus, *Ceriporiopsis subvermispora*. *J. Biotechnol.* **53**, 203–213.

Blodig, W., W. A. Doyle, A. T. Smith, K. Winterhalter, T. Choinowski, and K. Piontek (1998) Autocatalytic formation of a hydroxy group at Cβ of Trp171 in lignin peroxidase. *Biochemistry* **37**, 8832–8838.

Blodig, W., A. T. Smith, K. Winterhalter, and K. Piontek (1999) Evidence from spin-trapping for a transient radical on tryptophan residue 171 of lignin peroxidase. *Arch. Biochem. Biophys.* **370**, 86–92.

Blumberg, W. E., J. Peisach, B. A. Wittenberg, and J. B. Wittenberg (1968) The electronic structure of protohemes. I. An electron paramagnetic resonance and optical study of horseradish peroxidase and its derivatives. *J. Biol. Chem.* **243**, 1854–1862.

Brown, J. A., J. K. Glenn, and M. H. Gold (1990) Manganese regulates expression of manganese peroxidase by *Phanerochaete chrysosporium*. *J. Bacteriol.* **172**, 3125–3130.

Bumpus, J. A., and S. D. Aust (1987a) Biodegradation of DDT [1,1,1-trichloro-2,2-bis(4-chlorophenyl)ethane] by the white rot fungus *Phanerochaete chrysosporium*. *Appl. Environ. Microbiol.* **53**, 2001–2008.

Bumpus, J. A., and S. D. Aust (1987b) Biodegradation of environmental pollutants by the white rot fungus *Phanerochaete chrysosporium*: involvement of the lignin-degrading system. *BioEssays* **6**, 166–170.

Burdsall, H. H., Jr., and W. E. Eslyn (1974) A new *Phanerochaete* with a *chrysosporium* imperfect state. *Mycotaxon* **1**, 123–133.

Buswell, J. A., and E. Odier (1987) Lignin biodegradation. *CRC Crit. Rev. Biotechnol.* **6**, 1–60.

Cancel, A. M., A. B. Orth, and M. Tien (1993) Lignin and veratryl alcohol are not inducers of the ligninolytic system of *Phanerochaete chrysosporium*. *Appl. Environ. Microbiol.* **59**, 2909–2913.

Candeias, L. P., and P. J. Harvey (1995) Lifetime and reactivity of the veratryl alcohol radical cation. Implications for lignin peroxidase catalysis. *J. Biol. Chem.* **270**, 16745–16748.

Carlile, M. J., and S. C. Watkinson (1994) *The Fungi*. Academic Press, San Diego.

Chance, B., L. Powers, Y. Ching, T. Poulos, G. R. Schonbaum, I. Yamazaki, and K. G. Paul (1984) X-ray absorption studies of intermediates in peroxidase activity. *Arch. Biochem. Biophys.* **235**, 596–611.

Cheddar, G., T. E. Meyer, M. A. Cusanovich, C. D. Stout, and G. Tollin (1989) Redox protein electron-transfer mechanisms: electrostatic interactions as a determinant of reaction site in *c*-type cytochromes. *Biochemistry* **28**, 6318–6322.

Chen, C.-L., and H.-M. Chang (1982) Aromatic acids produced during degradation of lignin in spruce wood by *Phanerochaete chrysosporium*. *Holzforschung* **36**, 3–9.

Cherry, J. R., M. H. Lamsa, P. Schneider, J. Vind, A. Svendsen, A. Jones, and A. H. Pedersen (1999) Directed evolution of a fungal peroxidase. *Nat. Biotechnol.* **17**, 379–384.

Choinowski, T., W. Blodig, K. H. Winterhalter, and K. Piontek (1999) The crystal structure of lignin peroxidase at 1.70 Å resolution reveals a hydroxy group on the C-β of tryptophan 171: a novel radical site formed during the redox cycle. *J. Mol. Biol.* **286**, 809–827.

Chung, N., and S. D. Aust (1995) Veratryl alcohol-mediated indirect oxidation of phenol by lignin peroxidase. *Arch. Biochem. Biophys.* **316**, 733-737.

Crawford, R. L. (1981) *Lignin Biodegradation and Transformation*. Wiley-Interscience, New York.

Critchlow, J. E., and H. B. Dunford (1972a) Studies on horseradish peroxidase. IX. Kinetics of the oxidation of *p*-cresol by compound II. *J. Biol. Chem.* **247**, 3703–3713.

Critchlow, J. E., and H. B. Dunford (1972b) Studies on horseradish peroxidase. X. The mechanism of the oxidation of *p*-cresol, ferrocyanide, and iodide by compound II. *J. Biol. Chem.* **247**, 3714–3725.

Cullen, D. (1997) Recent advances on the molecular genetics of lignolytic fungi. *J. Biotechnol.* **53**, 273–289.

Daniel, G., B. Pettersson, T. Nilsson, and J. Volc (1990) Use of immunogold cytochemistry to detect Mn(II)-dependent and lignin peroxidases in wood degraded by the white rot fungi *Phanerochaete chyrsosporium* and *Lentinula edodes*. *Can. J. Bot.* **68**, 920–933.

Dawson, J. H. (1988) Probing structure-function relations in heme-containing oxygenases and peroxidases. *Science* **240**, 433–439.

de Boer, H. A., Y. Z. Zhang, C. Collins, and C. A. Reddy (1987) Analysis of nucleotide sequences of two ligninase cDNAs from a white-rot filamentous fungus, *Phanerochaete chrysosporium*. *Gene* **60**, 93–102.

de Jong, E., J. A. Field, and J. A. M. de Bont (1994) Aryl alcohols in the physiology of lignolytic fungi. *FEMS Microbiol. Rev.* **13**, 153–188.

de Ropp, J. S., G. N. La Mar, H. Wariishi, and M. H. Gold (1991) NMR study of the active site of resting state and cyanide-inhibited lignin peroxidase from *Phanerochaete chrysosporium*. Comparison with horseradish peroxidase. *J. Biol. Chem.* **266**, 15001–15008.

Dolphin, D., A. Forman, D. C. Borg, J. Fajer, and R. H. Felton (1971) Compounds I of catalase and horseradish peroxidase: π-cation radicals. *Proc. Natl. Acad. Sci. U.S.A.* **68**, 614–618.

Doyle, W. A., and A. T. Smith. (1996) Expression of lignin peroxidase H8 in *Escherichia coli*: folding and activation of the recombinant enzyme with Ca^{2+} and haem. *Biochem. J.* **315**, 15–19.

Doyle, W. A., W. Blodig, N. C. Veitch, K. Piontek, and A. T. Smith (1998) Two substrate interaction sites in lignin peroxidase revealed by site-directed mutagenesis. *Biochemistry* **37**, 15097–15105.

Dunford, H. B. (1982) Peroxidases. *Adv. Inorg. Biochem.* **4**, 41–68.

Dunford, H. B. (1991) Horseradish peroxidase: structure and kinetic properties. In *Peroxidases in Chemistry and Biology*, Vol. 2 (K. E. Everse and M. B. Grisham, Eds.). CRC Press, Boca Raton, FL, pp. 1–24.

Dunford, H. B. (1999) *Heme Peroxidases*. John Wiley, New York.

Dunford, H. B., and J. S. Stillman. (1976) On the function and mechanism of action of peroxidase. *Coord. Chem. Rev.* **19**, 187–251.

Dutton, M. V., C. S. Evans, P. T. Atkey, and D. A. Wood (1992) Oxalate production by Basidiomycetes, including the white-rot species *Coriolus versicolor* and *Phanerochaete chrysosporium*. *Appl. Microbiol. Biotechnol.* **39**, 5–10.

Edwards, S. L., H. X. Nguyen, R. C. Hamlin, and J. Kraut (1987) Crystal structure of cytochrome *c* peroxidase compound I. *Biochemistry* **26**, 1503–1511.

Edwards, S. L., R. Raag, H. Wariishi, M. H. Gold, and T. L. Poulos (1993) Crystal structure of lignin peroxidase. *Proc. Natl. Acad. Sci. U.S.A.* **90**, 750–754.

English, A. M., and G. Tsaprailis (1995) Catalytic structure-function relationships in heme peroxidases. *Adv. Inorg. Chem.* **43**, 79–125.

Eriksson, K.-E. L., R. A. Blanchette, and P. Ander (1990) *Microbial and Enzymatic Degradation of Wood and Wood Components*. Springer-Verlag, Berlin.

Erman, J. E., L. B. Vitello, M. A. Miller, A. Shaw, K. A. Brown, and J. Kraut (1993) Histidine 52 is a critical residue for rapid formation of cytochrome *c* peroxidase compound I. *Biochemistry* **32**, 9798–9806.

Farrell, R. L., K. E. Murtagh, M. Tien, M. D. Mozuch, and T. K. Kirk (1989) Physical and enzymatic properties of lignin peroxidase isoenzymes from *Phanerochaete chrysosporium*. *Enzyme Microb. Technol.* **11**, 322–328.

Felton, R. H., A. Y. Romans, N. T. Yu, and G. R. Schonbaum (1976) Laser Raman spectra of oxidized hydroperoxidases. *Biochim. Biophys. Acta* **434**, 82–89.

Finzel, B. C., T. L. Poulos, and J. Kraut (1984) Crystal structure of yeast cytochrome *c* peroxidase refined at 1.7-Å resolution. *J. Biol. Chem.* **259**, 13027–13036.

Fishel, L. A., J. E. Villafranca, J. M. Mauro, and J. Kraut (1987) Yeast cytochrome *c* peroxidase: mutagenesis and expression in *Escherichia coli* show tryptophan-51 is not the radical site in compound I. *Biochemistry* **26**, 351–360.

Fishel, L. A., M. F. Farnum, J. M. Mauro, M. A. Miller, J. Kraut, Y. J. Liu, X. L. Tan, and C. P. Scholes (1991) Compound I radical in site-directed mutants of cytochrome *c* peroxidase as probed by electron paramagnetic resonance and electron-nuclear double resonance. *Biochemistry* **30**, 1986–1996.

Froeliger, E. H., R. C. Ullrich, and C. P. Novotny (1989) Sequence analysis of the URA1 gene encoding orotidine-5′-monophosphate decarboxylase of *Schizophyllum commune*. *Gene* **83**, 387–393.

Gajhede, M., D. J. Schuller, A. Henriksen, A. T. Smith, and T. L. Poulos (1997) Crystal structure of horseradish peroxidase C at 2.15 Å resolution. *Nat. Struct. Biol.* **4**, 1032–1038.

Gettemy, J. M., B. Ma, R. Alic, and M. H. Gold (1998) Reverse transcription-PCR analysis of the regulation of the manganese peroxidase gene family. *Appl. Environ. Microbiol.* **64**, 569–574.

Glenn, J. K., and M. H. Gold (1985) Purification and characterization of an extracellular Mn(II)-dependent peroxidase from the lignin-degrading basidiomycete, *Phanerochaete chrysosporium*. *Arch. Biochem. Biophys.* **242**, 329–341.

Glenn, J. K., M. A. Morgan, M. B. Mayfield, M. Kuwahara, and M. H. Gold (1983) An extracellular H_2O_2-requiring enzyme preparation involved in lignin biodegradation by the white rot basidiomycete *Phanerochaete chrysosporium*. *Biochem. Biophys. Res. Commun.* **114**, 1077–1083.

Glenn, J. K., L. Akileswaran, and M. H. Gold (1986) Mn(II) oxidation is the principal function of the extracellular Mn-peroxidase from *Phanerochaete chrysosporium*. *Arch. Biochem. Biophys.* **251**, 688–696.

Glumoff, T., P. J. Harvey, S. Molinari, M. Goble, G. Frank, J. M. Palmer, J. D. Smit, and M. S. Leisola (1990) Lignin peroxidase from *Phanerochaete chrysosporium*. Molecular and kinetic characterization of isozymes. *Eur. J. Biochem.* **187**, 515–520.

Godfrey, B. J., M. B. Mayfield, J. A. Brown, and M. H. Gold (1990) Characterization of a gene encoding a manganese peroxidase from *Phanerochaete chrysosporium*. *Gene* **93**, 119–124.

Godfrey, B. J., L. Akileswaran, and M. H. Gold (1994) A reporter gene construct for studying the regulation of manganese peroxidase gene expression. *Appl. Environ. Microbiol.* **60**, 1353–1358.

Gold, M. H., and M. Alic (1993) Molecular biology of the lignin-degrading basidiomycete *Phanerochaete chrysosporium*. *Microbiol. Rev.* **57**, 605–622.

Gold, M. H., and T. M. Cheng (1978) Induction of colonial growth and replica plating of the white rot basidiomycete *Phanerochaete chrysosporium*. *Appl. Environ. Microbiol.* **35**, 1223–1225.

Gold, M. H., M. Kuwahara, A. A. Chiu, and J. K. Glenn (1984) Purification and characterization of an extracellular H_2O_2-requiring diarylpropane oxygenase from the white rot basidiomycete, *Phanerochaete chrysosporium*. *Arch. Biochem. Biophys.* **234**, 353–362.

Gold, M. H., H. Wariishi, and K. Valli (1989) Extracellular peroxidases involved in lignin degradation by the white rot basidiomycete *Phanerochaete chrysosporium*. In *Biocatalysis in Agricultural Biotechnology* (J. R. Whittaker and P. E. Sonnet, Eds.). ACS Symp. Ser. 389, American Chemical Society, Washington, DC, pp. 127-140.

Gold, M. H., H. L. Youngs, and M. D. Sollewijn Gelpke (2000) Manganese peroxidase. In *Metal Ions in Biological Systems, Vol. 37: Manganese and Its Role in Biological Processes* (A. Sigel and H. Sigel, Eds.). Marcel Dekker, New York, pp. 559-586.

Goodin, D. B., A. G. Mauk, and M. Smith (1986) Studies of the radical species in compound ES of cytochrome *c* peroxidase altered by site-directed mutagenesis. *Proc. Natl. Acad. Sci. U.S.A.* **83**, 1295–1299.

Grisebach, H. (1981) *The Biochemistry of Plants*. Academic Press, New York.

Hames, B. D., and D. Rickwood (1981) *Gel Electrophoresis of Proteins: A Practical Approach*. IRL Press, Oxford.

Hammel, K. E. (1989) Organopollutant degradation by ligninolytic fungi. *Enzyme Microb. Technol.* **11**, 776–777.

Hammel, K. E. (1992) Oxidation of aromatic pollutants by lignin-degrading fungi and their extracellular peroxidases. In *Metal Ions in Biological Systems, Vol. 28: Degradation of Environmental Pollutants by Microorganisms and Their Metalloenzymes* (H. Sigel and A. Sigel, Eds.). Marcel Dekker, New York, pp. 41-60.

Hammel, K. E., and M. A. Moen (1991) Depolymerization of a synthetic lignin *in vitro* by lignin peroxidase. *Enzyme Microb. Technol.* **13**, 15–18.

Hammel, K. E., M. Tien, B. Kalyanaraman, and T. K. Kirk (1985) Mechanism of oxidative Cα-Cβ cleavage of a lignin model dimer by *Phanerochaete chrysosporium* ligninase. Stoichiometry and involvement of free radicals. *J. Biol. Chem.* **260**, 8348–8353.

Hammel, K. E., B. Kalyanaraman, and T. K. Kirk (1986) Oxidation of polycyclic aromatic hydrocarbons and dibenzo[*p*]-dioxins by *Phanerochaete chrysosporium* ligninase. *J. Biol. Chem.* **261**, 16948–16952.

Hammel, K. E., K. A. Jensen, Jr., M. D. Mozuch, L. L. Landucci, M. Tien, and E. A. Pease (1993) Ligninolysis by a purified lignin peroxidase. *J. Biol. Chem.* **268**, 12274–12281.

Harkin, J. M., and J. R. Obst (1973) Demethylation of 2,4,6-trimethoxyphenol by phenol oxidase. *Science* **180**, 296–298.

Harris, R. Z., H. Wariishi, M. H. Gold, and P. R. Ortiz de Montellano (1991) The catalytic site of manganese peroxidase. Regiospecific addition of sodium azide and alkylhydrazines to the heme group. *J. Biol. Chem.* **266**, 8751–8758.

Harvey, P. J., and L. P. Candeias (1995) Radical cation cofactors in lignin peroxidase catalysis. *Biochem. Soc. Trans.* **23**, 262–267.

Harvey, P. J., H. E. Schoemaker, and J. M. Palmer (1986) Veratryl alcohol as a mediator and the role of radical cations in lignin biodegradation by *Phanerochaete chrysosporium*. *FEBS Lett.* **195**, 242–246.

Harvey, P. J., J. M. Palmer, H. E. Schoemaker, H. L. Dekker, and R. Wever (1989) Pre-steady-state kinetic study on the formation of compound I and II of ligninase. *Biochim. Biophys. Acta* **994**, 59–63.

Hashimoto, S., Y. Tatsuno, and T. Kitagawa (1986) Resonance Raman evidence for oxygen exchange between the Fe(IV)=O heme and bulk water during enzymic catalysis of horseradish peroxidase and its relation with the heme-linked ionization. *Proc. Natl. Acad. Sci. U.S.A.* **83**, 2417–2421.

Hatakka, A. (1994) Lignin-modifying enzymes from selected white-rot fungi: production and role in lignin degradation. *FEMS Microbiol. Rev.* **13**, 125–135.

Henriksen, A., D. J. Schuller, K. Meno, K. G. Welinder, A. T. Smith, and M. Gajhede (1998a) Structural interactions between horseradish peroxidase C and the substrate benzhydroxamic acid determined by X-ray crystallography. *Biochemistry* **37**, 8054–8060.

Henriksen, A., K. G. Welinder, and M. Gajhede (1998b) Structure of barley grain peroxidase refined at 1.9-Å resolution. A plant peroxidase reversibly inactivated at neutral pH. *J. Biol. Chem.* **273**, 2241–2248.

Higuchi, T. (1989) Mechanisms of lignin degradation by lignin peroxidase and laccase of white-rot fungi. In *Plant Cell Wall Polymers* (N. G. Lewis and M. G. Paice, Eds.). ACS Symp. Ser. 399, American Chemical Society, Washington, DC, pp. 482–502.

Higuchi, T. (1990) Lignin biochemistry: biosynthesis and biodegradation. *Wood Sci. Technol.* **24**, 23–63.

Higuchi, T. (1993) Biodegradation mechanism of lignin by white-rot basidiomycetes. *J. Biotechnol.* **30**, 1–8.

Homolka, L., F. Nerud, O. Kofronová, E. Novotná, and V. Machurová (1994) Degradation of wood by the basidiomycete *Coriolopsis occidentalis*. *Folia Microbiol. (Praha)* **39**, 37–43.

Howes, B. D., J. N. Rodriguez-Lopez, A. T. Smith, and G. Smulevich (1997) Mutation of distal residues of horseradish peroxidase: influence on substrate binding and cavity properties. *Biochemistry* **36**, 1532–1543.

Itakura, H., Y. Oda, and K. Fukuyama (1997) Binding mode of benzhydroxamic acid to *Arthromyces ramosus* peroxidase shown by X-ray crystallographic analysis of the complex at 1.6 Å resolution. *FEBS Lett.* **412**, 107–110.

Jin, L., T. P. Schultz, and D. D. Nicholas (1990) Structural characterization of brown rotted lignin. *Holzforschung* **44**, 133–138.

Johansson, T., and P. O. Nyman (1996) A cluster of genes encoding major isozymes of lignin peroxidase and manganese peroxidase from the white-rot fungus *Trametes versicolor*. *Gene* **170**, 31–38.

Johansson, T., K. G. Welinder, and P. O. Nyman (1993) Isozymes of lignin peroxidase and manganese(II) peroxidase from the white-rot basidiomycete *Trametes versicolor*. II. Partial sequences, peptide maps, and amino acid and carbohydrate compositions. *Arch. Biochem. Biophys.* **300**, 57–62.

Johnson, F., G. H. Loew, and P. Du (1994) Homology models of two isozymes of manganese peroxidase: prediction of a Mn(II) binding site. *Proteins* **20**, 312–319.

Jonsson, L., H. G. Becker, and P. O. Nyman (1994) A novel type of peroxidase gene from the white-rot fungus *Trametes versicolor*. *Biochim. Biophys. Acta* **1207**, 255–259.

Joshi, D. K., and M. H. Gold (1993) Degradation of 2,4,5-trichlorophenol by the lignin-degrading basidiomycete *Phanerochaete chrysosporium*. *Appl. Environ. Microbiol.* **59**, 1779–1785.

Joshi, D. K., and M. H. Gold (1994) Oxidation of dibenzo-*p*-dioxin by lignin peroxidase from the basidiomycete *Phanerochaete chrysosporium*. *Biochemistry* **33**, 10969–10976.

Joshi, D. K., and M. H. Gold (1996) Oxidation of dimethoxylated aromatic compounds by lignin peroxidase from *Phanerochaete chrysosporium*. *Eur. J. Biochem.* **237**, 45–57.

Kersten, P. J., and T. K. Kirk (1987) Involvement of a new enzyme, glyoxal oxidase, in extracellular H_2O_2 production by *Phanerochaete chrysosporium*. *J. Bacteriol.* **169**, 2195-2201.

Kersten, P. J., M. Tien, B. Kalyanaraman, and T. K. Kirk (1985) The ligninase of *Phanerochaete chrysosporium* generates cation radicals from methoxybenzenes. *J. Biol. Chem.* **260**, 2609-2612.

Kersten, P. J., B. Kalyanaraman, K. E. Hammel, B. Reinhammar, and T. K. Kirk (1990) Comparison of lignin peroxidase, horseradish peroxidase and laccase in the oxidation of methoxybenzenes. *Biochem. J.* **268**, 475-480.

Khindaria, A., D. P. Barr, and S. D. Aust (1995) Lignin peroxidases can also oxidize manganese. *Biochemistry* **34**, 7773-7779.

Khindaria, A., I. Yamazaki, and S. D. Aust (1996) Stabilization of the veratryl alcohol cation radical by lignin peroxidase. *Biochemistry* **35**, 6418-6424.

Kirk, T. K. (1975) Lignin-degrading enzyme system. *Biotechnol. Bioeng. Symp.* **5**, 139-150.

Kirk, T. K., and E. Adler (1970) Methoxyl-deficient structural elements in lignin of sweetbum decayed by a brown-rot fungus. *Acta Chem. Scand.* **24**, 3379-3390.

Kirk, T. K., and H.-M. Chang (1974) Decomposition of lignin by white-rot fungi. I. Isolation of heavily degraded lignins from decayed spruce. *Holzforschung* **28**, 217-222.

Kirk, T. K., and H.-M. Chang (1975) Decomposition of lignin by white-rot fungi. II. Characterization of heavily degraded lignins from decayed spruce. *Holzforschung* **29**, 56-64.

Kirk, T. K., and E. B. Cowling (1984) The chemistry of solid wood. In *Advances in Chemistry*, Vol. 207 (R. M. Rowell, Ed.). American Chemical Society, Washington, DC, pp. 435-487.

Kirk, T. K., and R. L. Farrell (1987) Enzymatic "combustion": the microbial degradation of lignin. *Annu. Rev. Microbiol.* **41**, 465-505.

Kirk, T. K., E. Schultz, W. J. Connors, L. F. Lorenz, and J. G. Zeikus (1978) Influence of culture parameters on lignin metabolism by *Phanerochaete chrysosporium*. *Arch. Microbiol.* **117**, 277-285.

Kirk, T. K., M. Tien, S. C. Johnsrud, and K.-E. Eriksson (1986a) Lignin degrading activity of *Phanerochaete chrysosporium* Burds.: comparison of cellulase-negative and other strains. *Enzyme Microb. Technol.* **8**, 75–80.

Kirk, T. K., M. Tien, P. J. Kersten, M. D. Mozuch, and B. Kalyanaraman (1986b) Ligninase of *Phanerochaete chrysosporium*. Mechanism of its degradation of the non-phenolic arylglycerol β-aryl ether substructure of lignin. *Biochem. J.* **236**, 279–287.

Kishi, K., H. Wariishi, L. Marquez, H. B. Dunford, and M. H. Gold (1994) Mechanism of manganese peroxidase compound II reduction. Effect of organic acid chelators and pH. *Biochemistry* **33**, 8694–8701.

Kishi, K., M. Kusters-van Someren, M. B. Mayfield, J. Sun, T. M. Loehr, and M. H. Gold (1996) Characterization of manganese(II) binding site mutants of manganese peroxidase. *Biochemistry* **35**, 8986–8994.

Kishi, K., D. P. Hildebrand, M. Kusters-van Someren, J. Gettemy, A. G. Mauk, and M. H. Gold (1997) Site-directed mutations at phenylalanine-190 of manganese peroxidase: effects on stability, function, and coordination. *Biochemistry* **36**, 4268–4277.

Kjalke, M., M. B. Andersen, P. Schneider, B. Christensen, M. Schülein, and K. G. Welinder (1992) Comparison of structure and activities of peroxidases from *Coprinus cinereus*, *Coprinus macrorhizus* and *Arthromyces ramosus*. *Biochim. Biophys. Acta* **1120**, 248–256.

Kobayashi, K., M. Tamura, K. Hayashi, H. Hori, and H. Morimoto (1980) Electron paramagnetic resonance and optical absorption spectrum of the pentacoordinated ferrihemoproteins. *J. Biol. Chem.* **255**, 2239–2242.

Koduri, R. S., and M. Tien (1994) Kinetic analysis of lignin peroxidase: explanation for the mediation phenomenon by veratryl alcohol. *Biochemistry* **33**, 4225–4230.

Koduri, R. S., and M. Tien (1995) Oxidation of guaiacol by lignin peroxidase. Role of veratryl alcohol. *J. Biol. Chem.* **270**, 22254–22258.

Kuan, I. C., and M. Tien (1989) Phosphorylation of lignin peroxidases from *Phanerochaete chrysosporium*. Identification of mannose 6-phosphate. *J. Biol. Chem.* **264**, 20350–20355.

Kuan, I. C., and M. Tien (1993) Stimulation of Mn peroxidase activity: a possible role for oxalate in lignin biodegradation. *Proc. Natl. Acad. Sci. U.S.A.* **90**, 1242–1246.

Kuan, I. C., K. A. Johnson, and M. Tien (1993) Kinetic analysis of manganese peroxidase. The reaction with manganese complexes. *J. Biol. Chem.* **268**, 20064-20070.

Kulmacz, R. J. (1986) Prostaglandin H synthase and hydroperoxides: peroxidase reaction and inactivation kinetics. *Arch. Biochem. Biophys.* **249**, 273-285.

Kunishima, N., K. Fukuyama, H. Matsubara, H. Hatanaka, Y. Shibano, and T. Amachi (1994) Crystal structure of the fungal peroxidase from *Arthromyces ramosus* at 1.9 Å resolution. Structural comparisons with the lignin and cytochrome *c* peroxidases. *J. Mol. Biol.* **235**, 331-344.

Kusters-van Someren, M., K. Kishi, T. Lundell, and M. H. Gold (1995) The manganese binding site of manganese peroxidase: characterization of an Asp179Asn site-directed mutant protein. *Biochemistry* **34**, 10620-10627.

Kuwahara, M., J. K. Glenn, M. A. Morgan, and M. H. Gold (1984) Separation and characterization of two extracellular H_2O_2-dependant oxidases from ligninolytic cultures of *Phanerochaete chrysosporium*. *FEBS Lett.* **169**, 247-250.

La Mar, G. N., J. S. de Ropp, K. M. Smith, and K. C. Langry (1981) Proton nuclear magnetic resonance investigation of the electronic structure of compound I of horseradish peroxidase. *J. Biol. Chem.* **256**, 237-243.

La Mar, G. N., J. S. de Ropp, L. Latos Grazynski, A. L. Balch, R. B. Johnson, K. M. Smith, D. W. Parish, and R. Chang (1983) Proton NMR characterization of the ferryl group in model heme complexes and hemoproteins: evidence for the Fe(IV)=O group in ferryl myoglobin and compound II of horseradish peroxidase. *J. Am. Chem. Soc.* **105**, 782-787.

La Mar, G. N., M. J. Chatfield, D. H. Peyton, J. S. de Ropp, W. S. Smith, R. Krishnamoorthi, J. D. Satterlee, and J. E. Erman (1988) Solvent isotope effects on NMR spectral parameters in high-spin ferric hemoproteins: an indirect probe for distal hydrogen bonding. *Biochim. Biophys. Acta* **956**, 267-276.

Laemmli, U. K. (1970) Cleavage of structural proteins during the assembly of the head of bacteriophage T4. *Nature (London)* **227**, 680-685.

Leisola, M. S. A., B. Kozulic, F. Meussdoerffer, and A. Fiechter (1987) Homology among multiple extracellular peroxidases from *Phanerochaete chrysosporium*. *J. Biol. Chem.* **262**, 419-424.

Li, D., N. Li, B. Ma, M. B. Mayfield, and M. H. Gold (1999) Characterization of genes encoding two manganese peroxidases from the lignin-degrading fungus *Dichomitus squalens*. *Biochim. Biophys. Acta* **1434**, 356-364.

Limongi, P., M. Kjalke, J. Vind, J. W. Tams, T. Johansson, and K. G. Welinder (1995) Disulfide bonds and glycosylation in fungal peroxidases. *Eur. J. Biochem.* **227**, 270–276.

Lundell, T., H. Schoemaker, A. Hatakka, and G. Brunow (1993) New mechanism of the Cα-Cβ cleavage in non-phenolic arylglycerol β-aryl ether lignin substructures catalyzed by lignin peroxidase. *Holzforschung* **47**, 219–224.

Marquez, L., H. Wariishi, H. B. Dunford, and M. H. Gold (1988) Spectroscopic and kinetic properties of the oxidized intermediates of lignin peroxidase from *Phanerochaete chrysosporium. J. Biol. Chem.* **263**, 10549–10552.

Mauk, M. R., K. Kishi, M. H. Gold, and A. G. Mauk (1998) pH-Linked binding of Mn(II) to manganese peroxidase. *Biohemistry* **37**, 6767–6771.

Mauro, J. M., L. A. Fishel, J. T. Hazzard, T. E. Meyer, G. Tollin, M. A. Cusanovich, and J. Kraut (1988) Tryptophan-191—phenylalanine, a proximal-side mutation in yeast cytochrome *c* peroxidase that strongly affects the kinetics of ferrocytochrome *c* oxidation. *Biochemistry* **27**, 6243–6256.

Mayfield, M. B., B. J. Godfrey, and M. H. Gold (1994a) Characterization of the mnp2 gene encoding manganese peroxidase isozyme 2 from the basidiomycete *Phanerochaete chrysosporium. Gene* **142**, 231–235.

Mayfield, M. B., K. Kishi, M. Alic, and M. H. Gold (1994b) Homologous expression of recombinant manganese peroxidase in *Phanerochaete chrysosporium. Appl. Environ. Microbiol.* **60**, 4303-4309.

Miki, K., V. Renganathan, and M. H. Gold (1986) Mechanism of β-aryl ether dimeric lignin model compound oxidation by lignin peroxidase of *Phanerochaete chrysosporium. Biochemistry* **25**, 4790–4796.

Mino, Y., H. Wariishi, N. J. Blackburn, T. M. Loehr, and M. H. Gold (1988) Spectral characterization of manganese peroxidase, an extracellular heme enzyme from the lignin-degrading basidiomycete, *Phanerochaete chrysosporium. J. Biol. Chem.* **263**, 7029–7036.

Mylrajan, M., K. Valli, H. Wariishi, M. H. Gold, and T. M. Loehr (1990) Resonance Raman spectroscopic characterization of compound III of lignin peroxidase. *Biochemistry* **29**, 9617–9623.

Nagano, S., M. Tanaka, K. Ishimori, Y. Watanabe, and I. Morishima (1996) Catalytic roles of the distal site asparagine-histidine couple in peroxidases. *Biochemistry* **35**, 14251–14258.

Neri, F., C. Indiani, K. G. Welinder, and G. Smulevich (1998) Mutation of the distal arginine in *Coprinus cinereus* peroxidase—structural implications. *Eur. J. Biochem.* **251**, 830–838.

Neri, F., C. Indiani, B. Baldi, J. Vind, K. G. Welinder, and G. Smulevich (1999) Role of the distal phenylalanine 54 on the structure, stability, and ligand binding of *Coprinus cinereus* peroxidase. *Biochemistry* **38**, 7819–7827.

Newmyer, S. L., and P. R. Ortiz de Montellano (1995) Horseradish peroxidase His-42→Ala, His-42→Val, and Phe-41→Ala mutants. Histidine catalysis and control of substrate access to the heme iron. *J. Biol. Chem.* **270**, 19430-19438.

Newmyer, S. L., J. Sun, T. M. Loehr, and P. R. Ortiz de Montellano (1996) Rescue of the horseradish peroxidase His-170→Ala mutant activity by imidazole: importance of proximal ligand tethering. *Biochemistry* **35**, 12788-12795.

Nie, G., N. S. Reading, and S. D. Aust (1998) Expression of the lignin peroxidase H2 gene from *Phanerochaete chrysosporium* in *Escherichia coli*. *Biochem. Biophys. Res. Commun.* **249**, 146–150.

Niku-Paavola, M. L., E. Karhunen, P. Salola, and V. Raunio (1988) Ligninolytic enzymes of the white-rot fungus *Phlebia radiata*. *Biochem. J.* **254**, 877–884.

Orth, A. B., D. J. Royse, and M. Tien (1993) Ubiquity of lignin-degrading peroxidases among various wood-degrading fungi. *Appl. Environ. Microbiol.* **59**, 4017–4023.

Orth, A. B., M. Rzhetskaya, D. Cullen, and M. Tien (1994) Characterization of a cDNA encoding a manganese peroxidase from *Phanerochaete chrysosporium*: genomic organization of lignin and manganese peroxidase-encoding genes. *Gene* **148**, 161–165.

Ortiz de Montellano, P. R. (1992) Catalytic sites of hemoprotein peroxidases. *Annu. Rev. Pharmacol. Toxicol.* **32**, 89–107.

Paszczyński, A., V. B. Huynh, and R. Crawford (1986) Comparison of ligninase-I and peroxidase-M2 from the white-rot fungus *Phanerochaete chrysosporium*. *Arch. Biochem. Biophys.* **244**, 750–765.

Pease, E. A., and M. Tien (1992) Heterogeneity and regulation of manganese peroxidases from *Phanerochaete chrysosporium*. *J. Bacteriol.* **174**, 3532–3540.

Pease, E. A., A. Andrawis, and M. Tien (1989) Manganese-dependent peroxidase from *Phanerochaete chrysosporium*. Primary structure deduced from cDNA sequence. *J. Biol. Chem.* **264**, 13531–13535.

Pelaez, F., M. J. Martinez, and A. T. Martinez (1995) Screening of 68 species of basidiomycetes for enzymes involved in lignin degradation. *Mycol. Res.* **99**, 37–42.

Penner-Hahn, J. E., K. S. Eble, T. J. McMurry, M. Renner, A. L. Balch, J. T. Groves, J. H. Dawson, and K. O. Hodgson (1986) Structural characterization of horseradish peroxidase using EXAFS spectroscopy. Evidence for Fe(IV)=O ligation in compound I and II. *J. Am. Chem. Soc.* **108**, 7819–7925.

Périé, F. H., and M. H. Gold (1991) Manganese regulation of manganese peroxidase expression and lignin degradation by the white rot fungus *Dichomitus squalens*. *Appl. Environ. Microbiol.* **57**, 2240–2245.

Petersen, J. F., J. W. Tams, J. Vind, A. Svensson, H. Dalboge, K. G. Welinder, and S. Larsen (1993) Crystallization and X-ray diffraction analysis of recombinant *Coprinus cinereus* peroxidase. *J. Mol. Biol.* **232**, 989–991.

Petersen, J. F., A. Kadziola, and S. Larsen (1994) Three-dimensional structure of a recombinant peroxidase from *Coprinus cinereus* at 2.6 Å resolution. *FEBS Lett.* **339**, 291–296.

Piontek, K., T. Glumoff, and K. Winterhalter (1993) Low pH crystal structure of glycosylated lignin peroxidase from *Phanerochaete chrysosporium* at 2.5 Å resolution. *FEBS Lett.* **315**, 119–124.

Poulos, T. L., and R. E. Fenna (1994) Peroxidases: structure, function, and engineering. In *Metals Ions in Biological Systems, Vol. 30: Metalloenzymes Involving Amino Acid-Residue and Related Radicals* (H. Sigel and A. Sigel, Eds.). Marcel Dekker, New York, pp. 25–75.

Poulos, T. L., and B. C. Finzel (1984) Heme enzyme structure and function. In *Peptide and Protein Reviews*, Vol. 4. Marcel Dekker, New York, pp. 115–171.

Poulos, T. L., and J. Kraut (1980) The stereochemistry of peroxidase catalysis. *J. Biol. Chem.* **255**, 8199–8205.

Poulos, T. L., S. L. Edwards, H. Wariishi, and M. H. Gold (1993) Crystallographic refinement of lignin peroxidase at 2 Å. *J. Biol. Chem.* **268**, 4429–4440.

Pribnow, D., M. B. Mayfield, V. J. Nipper, J. A. Brown, and M. H. Gold (1989) Characterization of a cDNA encoding a manganese peroxidase, from the lignin-degrading basidiomycete *Phanerochaete chrysosporium*. *J. Biol. Chem.* **264**, 5036–5040.

Reddy, G. V. B., M. D. Sollewijn Gelpke, and M. H. Gold (1998) Degradation of 2,4,6-trichlorophenol by *Phanerochaete chrysosporium*: involvement of reductive dechlorination. *J. Bacteriol.* **180**, 5159-5164.

Renganathan, V., and M. H. Gold (1986) Spectral characterization of the oxidized states of lignin peroxidase, an extracellular heme enzyme from the white-rot basidiomycete *Phanerochaete chrysosporium*. *Biochemistry* **25**, 1626–1631.

Renganathan, V., K. Miki, and M. H. Gold (1986) Role of molecular oxygen in lignin peroxidase reactions. *Arch. Biochem. Biophys.* **246**, 155–161.

Renganathan, V., K. Miki, and M. H. Gold (1987) Haloperoxidase reactions catalyzed by lignin peroxidase, an extracellular enzyme from the basidiomycete *Phanerochaete chrysosporium*. *Biochemistry* **26**, 5127–5132.

Ritch, T. G., Jr., and M. H. Gold (1992) Characterization of a highly expressed lignin peroxidase-encoding gene from the basidiomycete *Phanerochaete chrysosporium*. *Gene* **118**, 73–80.

Ritch, T. G., Jr., V. J. Nipper, L. Akileswaran, A. J. Smith, D. G. Pribnow, and M. H. Gold (1991) Lignin peroxidase from the basidiomycete *Phanerochaete chrysosporium* is synthesized as a preproenzyme. *Gene* **107**, 119–126.

Roberts, J. B., B. M. Hoffman, R. Rutter, and L. P. Hager (1981a) 17O ENDOR of horseradish peroxidase compound I. *J. Am. Chem. Soc.* **103**, 7654–7656.

Roberts, J. B., B. M. Hoffman, R. Rutter, and L. P. Hager (1981b) Electron-nuclear double resonance of horseradish peroxidase compound I. Detection of the porphyrin π-cation radical. *J. Biol. Chem.* **256**, 2118–2121.

Rothschild, N., A. Levkowitz, Y. Hadar, and C. Dosoretz (1999) Extracellular mannose-6-phosphate of *Phanerochaete chrysosporium*: a lignin peroxidase-modifying enzyme. *Arch. Biochem. Biophys.* **372**, 107–111.

Saloheimo, M., V. Barajas, M.-L. Niku-Paavola, and J. K. C. Knowles (1989) A lignin peroxidase-encoding cDNA from the white-rot fungus *Phlebia radiata*: characterization and expression in *Trichoderma reesei*. *Gene* **85**, 343–351.

Schmidt, H. W. H., S. D. Haemmerli, H. E. Schoemaker, and M. S. A. Leisola (1989) Oxidative degradation of 3,4-dimethoxybenzyl alcohol and its methyl ether by the lignin peroxidase of *Phanerochaete chrysosporium*. *Biochemistry* **2**, 1776–1783.

Schoemaker, H. E. (1990) On the chemistry of lignin biodegradation. *Recl. Trav. Chim. Pays-Bas* **109**, 255–272.

Schoemaker, H. E., and M. S. A. Leisola (1990) Degradation of lignin by *Phanerochaete chrysosporium*. *J. Biotechnol.* **13**, 101–110.

Schoemaker, H. E., T. K. Lundell, A. I. Hatakka, and K. Piontek (1994) The oxidation of veratryl alchol, dimeric lignin models and lignin by lignin peroxidase: The redox cycle revisted. *FEMS Microbiol. Rev.* **13**, 321–332.

Schuller, D. J., N. Ban, R. B. Huystee, A. McPherson, and T. L. Poulos (1996) The crystal structure of peanut peroxidase. *Structure* **4**, 311–321.

Schultz, C. E., R. Rutter, T. J. Sage, T. G. Debrunner, and L. P. Hager (1984) Mossbauer and electron paramagnetic resonance studies of horseradish peroxidase and its catalytic intermediates. *Biochemistry* **23**, 4743–4754.

Sheng, D., and M. H. Gold (1997) Haloperoxidase activity of manganese peroxidase from *Phanerochaete chrysosporium*. *Arch. Biochem. Biophys.* **345**, 126–134.

Sheng, D., and M. H. Gold (1998) Irreversible oxidation of ferricytochrome *c* by lignin peroxidase. *Biochemistry* **37**, 2029–2036.

Sheng, D. W., and M. H. Gold (1999) Oxidative polymerization of ribonuclease A by lignin peroxidase from *Phanerochaete chrysosporium*—role of veratryl alcohol in polymer oxidation. *Eur. J. Biochem.* **259**, 626–634.

Sitter, A. J., C. M. Reczek, and J. Terner (1985) Observation of the Fe(IV)=O stretching vibration of ferryl myoglobin by resonance Raman spectroscopy. *Biochim. Biophys. Acta* **828**, 229–235.

Smith, A. T., and N. C. Veitch (1998) Substrate binding and catalysis in heme peroxidases. *Curr. Opin. Chem. Biol.* **2**, 269–278.

Smith, A. T., N. Santama, S. Dacey, M. Edwards, R. C. Bray, R. N. F. Thornely, and J. F. Burke (1990) Expression of a synthetic gene for horseradish peroxidase C in *Escherichia coli* and folding and activation of the recombinant enzyme with Ca^{2+} and heme. *J. Biol. Chem.* **265**, 13335–13343.

Smith, A. T., S. A. Sanders, R. N. Thorneley, J. F. Burke, and R. R. Bray (1992) Characterisation of a haem active-site mutant of horseradish peroxidase, Phe41→Val, with altered reactivity towards hydrogen peroxide and reducing substrates. *Eur. J. Biochem.* **207**, 507–519.

Smulevich, G., F. Neri, M. P. Marzocchi, and K. G. Welinder (1996) Versatility of heme coordination demonstrated in a fungal peroxidase. Absorption and resonance Raman studies of *Coprinus cinereus* peroxidase and the Asp245→Asn mutant at various pH values. *Biochemistry* **35**, 10576–10585.

Sollewijn Gelpke, M. D., M. Mayfield-Gambill, G. P. Lin Cereghino, and M. H. Gold (1999a) Homologous expression of recombinant lignin peroxidase in *Phanerochaete chrysosporium*. *Appl. Environ. Microbiol.* **65**, 1670–1674.

Sollewijn Gelpke, M. D., P. Moënne-Loccoz, and M. H. Gold (1999b) Arginine 177 is involved in Mn(II) binding by manganese peroxidase. *Biochemistry* **38**, 11482-11489.

Spadaro, J. T., and V. Renganathan (1994) Peroxidase-catalyzed oxidation of azo dyes: mechanism of Disperse Yellow 3 degradation. *Arch. Biochem. Biophys.* **312**, 301–307.

Spiro, T. G. (Ed.) (1988) *Biological Applications of Raman Spectroscopy, Vol. 3: Resonance Raman Spectra of Hemes and Metalloproteins*. John Wiley & Sons, New York.

Spiro, T. G., J. D. Stong, and P. Stein (1979) Porphyrin core expansion and doming in heme proteins. New evidence from resonance Raman spectra of six-coordinate high-spin iron(III) hemes. *J. Am. Chem. Soc.* **101**, 2648–2655.

Stewart, P., P. Kersten, A. Vanden Wymelenberg, J. Gaskell, and D. Cullen (1992) Lignin peroxidase gene family of *Phanerochaete chrysosporium*: complex regulation by carbon and nitrogen limitation and identification of a second dimorphic chromosome. *J. Bacteriol.* **174**, 5036–5042.

Stewart, P., R. E. Whitwam, P. J. Kersten, D. Cullen, and M. Tien (1996) Efficient expression of a *Phanerochaete chrysosporium* manganese peroxidase gene in *Aspergillus oryzae*. *Appl. Environ. Microbiol.* **62**, 860–864.

Sundaramoorthy, M., K. Kishi, M. H. Gold, and T. L. Poulos (1994) The crystal structure of manganese peroxidase from *Phanerochaete chrysosporium* at 2.06-Å resolution. *J. Biol. Chem.* **269**, 32759–32767.

Sundaramoorthy, M., K. Kishi, M. H. Gold, and T. L. Poulos (1997) Crystal structures of substrate binding site mutants of manganese peroxidase. *J. Biol. Chem.* **272**, 17574–17580.

Sutherland, G. R., A. Khindaria, and S. D. Aust (1996) The effect of veratryl alcohol on manganese oxidation by lignin peroxidase. *Arch. Biochem. Biophys.* **327**, 20–26.

Tamura, M., T. Asakura, and T. Yonetani (1972) Heme-modification studies on horseradish peroxidase. *Biochim. Biophys. Acta* **268**, 292–304.

Tanaka, M., S. Nagano, K. Ishimori, and I. Morishima (1997) Hydrogen bond network in the distal site of peroxidases: spectroscopic properties of Asn70→Asp horseradish peroxidase mutant. *Biochemistry* **36**, 9791–9798.

Tanaka, M., K. Ishimori, and I. Morishima (1998) Structural roles of the highly conserved Glu residue in the heme distal site of peroxidases. *Biochemistry* **37**, 2629–2638.

ten Have, R., S. Hartmans, P. J. M. Teunissen, and J. A. Field (1998) Purification and characterization of two lignin peroxidase isozymes produced by *Bjerkandera* sp. strain BOS55. *FEBS Lett.* **422**, 391–394.

Tien, M., and T. K. Kirk (1983) Lignin-degrading enzyme from the hymenomycete *Phanerochaete chrysosporium* Burds. *Science* **221**, 661-663.

Tien, M., and D. Ma (1997) Oxidation of 4-methoxymandelic acid by lignin peroxidase. Mediation by veratryl alcohol. *J. Biol. Chem.* **272**, 8912–8917.

Timofeevski, S. L., G. Nie, N. S. Reading, and S. D. Aust (1999) Addition of veratryl alcohol oxidase activity to manganese peroxidase by site-directed mutagenesis. *Biochem. Biophys. Res. Commun.* **256**, 500–504.

Timofeevski, S. L., G. Nie, N. S. Reading, and S. D. Aust (2000) Substrate specificity of lignin peroxidase and a S168W variant of manganese peroxidase. *Arch. Biochem. Biophys.* **373**, 147–153.

Tonon, F., and E. Odier (1988) Influence of veratryl alcohol and hydrogen peroxide on ligninase activity and ligninase production by *Phanerochaete chrysosporium*. *Appl. Environ. Microbiol.* **54**, 466–472.

Tuor, U., H. Wariishi, H. E. Schoemaker, and M. H. Gold (1992) Oxidation of phenolic arylglycerol β-aryl ether lignin model compounds by manganese peroxidase from *Phanerochaete chrysosporium*: oxidative cleavage of an α-carbonyl model compound. *Biochemistry* **31**, 4986–4995.

Umezawa, T., and T. Higuchi (1989) Cleavages of aromatic ring and β-O-4 bond of synthetic lignin (DHP) by lignin peroxidase. *FEBS Lett.* **242**, 325–329.

Valli, K., and M. H. Gold (1991) Degradation of 2,4-dichlorophenol by the lignin-degrading fungus *Phanerochaete chrysosporium*. *J. Bacteriol.* **173**, 345–352.

Valli, K., H. Wariishi, and M. H. Gold (1990) Oxidation of monomethoxylated aromatic compounds by lignin peroxidase: role of veratryl alcohol in lignin biodegradation. *Biochemistry* **29**, 8535–8539.

Valli, K., H. Wariishi, and M. H. Gold (1992) Degradation of 2,7-dichlorodibenzo-*p*-dioxin by the lignin-degrading basidiomycete *Phanerochaete chrysosporium*. *J. Bacteriol.* **174**, 2131–2137.

Veitch, N. C., J. W. Tams, J. Vind, H. Dalbøge, and K. G. Welinder (1994) NMR studies of recombinant *Coprinus* peroxidase and three site-directed mutants. Implications for peroxidase substrate binding. *Eur. J. Biochem.* **222**, 909–918.

Vitello, L. B., J. E. Erman, M. A. Miller, J. M. Mauro, and J. Kraut (1992) Effect of Asp-235→Asn substitution on the absorption spectrum and hydrogen peroxide reactivity of cytochrome *c* peroxidase. *Biochemistry* **31**, 11524–11535.

Vitello, L. B., J. E. Erman, M. A. Miller, J. Wang, and J. Kraut (1993) Effect of arginine-48 replacement on the reaction between cytochrome *c* peroxidase and hydrogen peroxide. *Biochemistry* **32**, 9807–9818.

von Heijne, G. (1985) Signal sequences. The limits of variation. *J. Mol. Biol.* **184**, 99–105.

Wang, J. M., M. Mauro, S. L. Edwards, S. J. Oatley, L. A. Fishel, V. A. Ashford, N. H. Xuong, and J. Kraut (1990) X-ray structures of recombinant yeast cytochrome *c* peroxidase and three heme-cleft mutants prepared by site-directed mutagenesis. *Biochemistry* **29**, 7160–7173.

Wariishi, H., and M. H. Gold (1989) Lignin peroxidase compound III: formation, inactivation and conversion to native enzyme. *FEBS Lett.* **243**, 165–168.

Wariishi, H., and M. H. Gold (1990) Lignin peroxidase compound III. Mechanism of formation and decomposition. *J. Biol. Chem.* **265**, 2070–2077.

Wariishi, H., L. Akileswaran, and M. H. Gold (1988) Manganese peroxidase from the basidiomycete *Phanerochaete chrysosporium*: spectral characterization of the oxidized states and the catalytic cycle. *Biochemistry* **27**, 5365–5370.

Wariishi, H., H. B. Dunford, I. D. MacDonald, and M. H. Gold (1989a) Manganese peroxidase from the lignin-degrading basidiomycete *Phanerochaete chrysosporium*. Transient state kinetics and reaction mechanism. *J. Biol. Chem.* **264**, 3335–3340.

Wariishi, H., K. Valli, V. Renganathan, and M. H. Gold (1989b) Thiol-mediated oxidation of nonphenolic lignin model compounds by manganese peroxidase of *Phanerochaete chrysosporium*. *J. Biol. Chem.* **264**, 14185-14191.

Wariishi, H., L. Marquez, H. B. Dunford, and M. H. Gold (1990) Lignin peroxidase compounds II and III. Spectral and kinetic characterization of reactions with peroxides. *J. Biol. Chem.* **265**, 11137–11142.

Wariishi, H., J. Huang, H. B. Dunford, and M. H. Gold (1991a) Reactions of lignin peroxidase compounds I and II with veratryl alcohol. Transient-state kinetic characterization. *J. Biol. Chem.* **266**, 20694–20699.

Wariishi, H., K. Valli, and M. H. Gold (1991b) *In vitro* depolymerization of lignin by manganese peroxidase of *Phanerochaete chrysosporium*. *Biochem. Biophys. Res. Commun.* **176**, 269–275.

Wariishi, H., K. Valli, and M. H. Gold (1992) Manganese(II) oxidation by manganese peroxidase from the basidiomycete *Phanerochaete chrysosporium*. Kinetic mechanism and role of chelators. *J. Biol. Chem.* **267**, 23688–23695.

Wariishi, H., D. Sheng, and M. H. Gold (1994) Oxidation of ferrocytochrome *c* by lignin peroxidase. *Biochemistry* **33**, 5545–5552.

Welinder, K. G. (1991) The plant peroxidase superfamily. In *Biochemical, Molecular and Physiological Aspects of Plant Peroxidases* (J. Lobarzewski, H. Greppin, C. Penel, and T. Gaspar. Eds.). University of Geneva, Geneva, Switzerland, pp. 3-14.

Welinder, K. G. (1992) Superfamily of plant, fungal and bacterial peroxidases. *Curr. Opin. Struct. Biol.* **2**, 388–393.

Welinder, K. G., B. Bjornholm, and H. B. Dunford (1995) Functions of electrostatic potentials and conserved distal and proximal His-Asp H-bonding networks in haem peroxidases. *Biochem. Soc. Trans.* **23**, 257–262.

Whitwam, R., and M. Tien (1996) Heterologous expression and reconstitution of fungal Mn peroxidase. *Arch. Biochem. Biophys.* **333**, 439–446.

Whitwam, R. E., I. G. Gazarian, and M. Tien (1995) Expression of fungal Mn peroxidase in *E. coli* and refolding to yield active enzyme. *Biochem. Biophys. Res. Commun.* **216**, 1013–1017.

Whitwam, R. E., K. R. Brown, M. Musick, M. J. Natan, and M. Tien (1997) Mutagenesis of the Mn^{2+}-binding site of manganese peroxidase affects oxidation of Mn^{2+} by both compound I and compound II. *Biochemistry* **36**, 9766–9773.

Wilcox, S. K., C. D. Putnam, M. Sastry, J. Blankenship, W. J. Chazin, D. E. McRee, and D. B. Goodin (1998) Rational design of a functional metalloenzyme: introduction of a site for manganese binding and oxidation into a heme peroxidase. *Biochemistry* **37**, 16853–16862.

Xu, F. (1996) Oxidation of phenols, anilines, and benzenethiols by fungal laccases: correlation between activity and redox potentials as well as halide inhibition. *Biochemistry* **35**, 7608–7614.

Yeung, B. K., X. Wang, J. A. Sigman, P. A. Petillo, and Y. Lu (1997) Construction and characterization of a manganese-binding site in cytochrome *c* peroxidase: towards a novel manganese peroxidase. *Chem. Biol.* **4**, 215–221.

Youngs, H. L., M. Sundaramoorthy, and M. H. Gold (2000) Effects of cadmium on manganese peroxidase: competitive inhibition of Mn^{II} oxidation and thermal stabilization of the enzyme. *Eur. J. Biochem.* **267**, 1761–1769.

Youngs, H. L., M. D. Sollewijn Gelpke, D. Li, M. Sundaramoorthy, and M. H. Gold (2001) The role of E39 in Mn^{II} binding and oxidation by manganese peroxidase from *Phanerochaete chrysosporium*. *Biochemistry* **40**, 2243–2250.

BIOGRAPHICAL SKETCH

Maarten D. Sollewijn Gelpke was born in Amersfoort, The Netherlands, on July 14, 1967. He graduated from Wageningen Agricultural University in 1993, and worked as a research assistant in the Department of Molecular Genetics of Industrial Microorganisms of Wageningen Agricultural University until he joined the laboratory of Professor Michael H. Gold in the Department of Biochemistry and Molecular Biology of the Oregon Graduate Institute in 1995, where he successfully defended his dissertation in May, 2000. He began his postdoctoral research in August, 2000, in the Department of Molecular and Cell Biology at the University of California, Berkeley.

List of Publications

Middelhoven, W. J., Coenen, A., Kraakman, B., and Sollewijn Gelpke, M. D. (1992) Degradation of some phenols and hydroxybenzoates by the imperfect ascomycetous yeasts *Candida parapsilosis* and *Arxula adeninivorans*: evidence for an operative gentisate pathway. *Antonie van Leeuwenhoek* **62,** 181–187.

Middelhoven, W. J., and Gelpke, M. D. (1995) Partial conversion of cinnamic acid into styrene by growing cultures and cell-free extracts of the yeast *Cryptococcus elinovii*. *Antonie van Leeuwenhoek* **67,** 217–219.

van den Hombergh, J. P., Sollewijn Gelpke, M. D., van de Vondervoort, P. J., Buxton, F. P., and Visser, J. (1997) Disruption of three acid proteases in *Aspergillus niger*—effects on protease spectrum, intracellular proteolysis, and degradation of target proteins. Eur. J. Biochem. **247,** 605–613.

MacCabe, A. P., Vanhanen, S., Sollewijn Gelpke, M. D., van de Vondervoort, P. J., Arst, H. N. J., and Visser. J. (1998) Identification, cloning and sequence of the *Aspergillus niger* area wide domain regulatory gene controlling nitrogen utilisation. *Biochim. Biophys. Acta* **1396,** 163–168.

Reddy, G. V., Gelpke, M. D., and Gold, M. H. (1998) Degradation of 2,4,6-trichlorophenol by *Phanerochaete chrysosporium*: involvement of reductive dechlorination. *J. Bacteriol.* **180,** 5159–5164.

Sollewijn Gelpke, M. D., Mayfield-Gambill, M., Lin Cereghino, G. P., and Gold, M. H. (1999) Homologous expression of recombinant lignin peroxidase in *Phanerochaete chrysosporium*. *Appl. Environ. Microbiol.* **65,** 1670–1674.

Sollewijn Gelpke, M. D., Moënne-Loccoz, P., and Gold, M. H. (1999) Arginine 177 is involved in Mn(II) binding by manganese peroxidase. *Biochemistry* **38,** 11482–11489.

Sollewijn Gelpke, M. D., Youngs, H. L., and Gold, M. H. (2000) Role of arginine 177 in the Mn^{II} binding site of manganese peroxidase: studies with R177D, R177E, R177N and R177Q mutants. *Eur. J. Biochem.* **267,** 7038–7045.

Gold, M. H., Youngs, H. L., and Sollewijn Gelpke, M. D. (2000) Manganese peroxidase. In *Metal Ions in Biological Systems, Vol. 37: Manganese and Its Role in Biological Processes* (Sigel, H. and Sigel, A., eds.). Marcel Dekker, New York, pp. 559-589.

Sollewijn Gelpke, M. D., Sheng, D., and Gold, M. H. (2000) Mn^{II} is not a productive substrate for wild-type or recombinant lignin peroxidase isozyme H2. *Arch. Biochem. Biophys.* **381,** 16–24.

Sollewijn Gelpke, M. D., Lee, J., and Gold, M. H. (2002) Lignin peroxidase oxidation of veratryl alcohol: effects of the mutants H82A, Q222A, W171A and F267L. *Biochemistry* **41,** in press.